Model Fitting for Electric Arc Furnace Refining

by

Letsane Paul Rathaba

Submitted in partial fulfillment of the requirements for the degree

Master of Engineering (Electronic Engineering)

in the

Faculty of Engineering, the Built Environment and

Information Technology

UNIVERSITY OF PRETORIA

November 2004

Summary

Title:	Model Fitting for Electric Arc Furnace Refining
By:	Letsane Paul Rathaba
Supervisor:	Professor I.K. Craig
Co-supervisor:	Professor P.C. Pistorius
Department:	Department of Electrical, Electronic and Computer Engineering
Degree:	Master of Engineering(Electronic Engineering)

The dissertation forms part of an ongoing project for the modelling and eventual control of an electric arc furnace (EAF) process. The main motivation behind such a project is the potential benefits that can result from automation of a process that has largely been operator controlled, often with results that leave sufficient room for improvement. Previous work in the project has resulted in the development of a generic model of the process. A later study concentrated on the control of the EAF where economic factors were taken into account. Simulation results from both studies clearly demonstrate the benefits that can accrue from successful implementation of process control. A major drawback to the practical implementation of the results is the lack of a model that is proven to be an accurate depiction of the specific plant where control is to be applied. Furthermore, the accuracy of any process model can only be verified against actual process data.

There lies the *raison d'etre* for this dissertation: to take the existing model from the simulation environment to the real process. The main objective is to obtain a model that is able to mimic a selected set of process outputs. This is commonly a problem of system identification (SID): to select an appropriate model then fit the model to plant input/output data until the model response is similar to the plant under the same inputs (and initial conditions). The model fitting is carried out on an existing EAF model primarily by estimation of the model parameters for the EAF refining stage. Therefore the contribution of this dissertation is a model that is able to depict the EAF refining stage with reasonable accuracy.

An important aspect of model fitting is experiment design. This deals with the selection of inputs and outputs that must be measured in order to estimate the desired parameters. This constitutes the problem of identifiability: what possibilities exist for estimating parameters using available I/O data or, what additional data is necessary to estimate desired parameters. In the dissertation an analysis is carried out to determine which parameters are estimable from available data. For parameters that are not estimable recommendations are made about additional measurements required to remedy the situation.

Additional modelling is carried out to adapt the model to the particular process. This includes modelling to incorporate the oxyfuel subsystem, the bath oxygen content, water cooling and the effect of foaming on the arc efficiency.

Keywords: Electric arc furnace, identifiability, model fitting, parameter estimation.

Acknowledgements

I would like to thank my supervisors Prof Craig and Prof Pistorius for their guidance and valuable insights throughout my research; also for their support and patience when things were not going well. This dissertation would not have been possible without the generosity of the staff at Cape Gate, Vanderbijlpark for availing their time and resources to enable collection of the necessary plant data. I also owe a debt of gratitude to my my friend Lungile Mdlazi and my colleagues in the Control Lab for their fruitful inputs and friendship. More importantly, I want to express my gratitude to my mother and family for their support and understanding throughout my research.

Contents

Chapter 1

Introduction

This introductory chapter outlines the motivation for the dissertation, the objectives and contribution to furnace modelling. The objectives give a clear definition of focus of the dissertation; an overview of the dissertation organization is also given.

1.1 Motivation

With the increasing concern in the world for the depletion of natural resources, iron ore supplies are no exception; they too will invariably run low. A fitting solution to this challenge is recycling. And the electric arc furnace (EAF) is an appropriate long term solution. Its versatility lies in its facility for melting hot metal with any proportions of scrap or iron ore. It is commonly used to melt charges made up solely of scrap with no need for the often costly hot metal. Hence the preference for EAFs in mini mills that can be set up with minimal infrastructure costs.

There is a gradual but steady worldwide trend where basic oxygen furnaces (BOF) are being replaced by EAFs. The World Steel Organization reports a 34 % worldwide adoption of EAFs in 2002 [1]. An adoption of 50 % is predicted for 2020. A similar, albeit slower, trend is predicted for the South African industry.

The EAF remains one of the most poorly automated processes in the steel production line where all automation has only an indirect effect on the critical process outputs. Important outputs such as steel temperature and composition are still heavily dependent on operator control. With operator control, there abounds the accompanying disadvantages of poor response to disturbances and inconsistent outputs, leading to poor product quality. The increasing complexity of the process also renders it difficult for efficient operator control. Indeed, other factors such as material variations, production stoppages etc. will have an inevitable negative influence on the process variables.

However real benefits can be achieved by implementation of process control on the

EAF. It has the advantage of allowing good set-point following and rejection of disturbances, where the outputs can be precisely controlled within tight margins - this translates to safer and profitable operation [2, 3]. The potential benefits from process control have been demonstrated by simulation studies carried out by Bekker *et al.* [4, 5] and Oosthuizen *et al.* [6, 7]. In both cases modelling was carried out and the model assumed to be an adequate representation of the process based on qualitative grounds: the model was assumed valid based on expected model response to typical process inputs; however, only limited plant data was used.

Most control systems rely on the existence of an adequate process model. This adequacy depends on the intended use of the model but can ultimately only be tested using real process data. The EAF model used in [5, 7], can only be meaningfully adjusted using plant input-output data so that the model response coincides with the process response under similar conditions. This is typically a problem of system identification (SID) where plant data is used in a procedure to improve model accuracy.

Save for unscheduled process stoppages, under normal operation, the furnace refining stage operates intermittently because of the need for operator intervention when measurements are taken (and to execute control actions). Therefore, the adjustment for bath temperature and carbon content is an intermittent process, requiring measurement then control action based on the newly arrived information. This cycle can repeat several times during refining until adequate bath conditions are reached.

The direct problem of the above scenario is that various losses arise. Every measurement requires the use of an appropriate probe that is typically not reusable. The delays required for a measurement to be taken and then acted upon can be significant. Furthermore, to take a temperature measurement, arc power must be reduced, lowering the efficiency of the arc and thus increasing losses. The solution is to minimize the number of measurements required in order to obtain reliable information about the plant states, particularly temperature and carbon. An appropriate model for refining is a possible solution to the problem: apply an initial measurement of the plant states and use the model to predict future plant behaviour based on the subsequent inputs and knowledge of the process response (which is implicit in the model).

The motivation for the current work is the ability to use the model as an accurate representation of the plant refining stage. At a minimum it must be able to match the input-output relationships that prevail in the furnace; this is achieved mainly by proper adjustment of the model parameters. The physically based modelling approach of the process demands that while being able to reproduce the process I/O relationships the model variables must maintain a physical significance that is governed by the process metallurgy. This requirement (and necessary adjustment) will apply to the inputs, the

states, outputs and the parameters - more emphasis will be placed on the latter.

Controller design is typically based on linear models. Any inaccuracy in the linear models will be corrected by the use of feedback. However, some outputs, such as temperature and composition are expensive to measure - in time or direct instrumentation costs - and only a few measurements are available per tap. An accurate nonlinear model that serves as a good predictor of the plant can then be used to supplement these measurements. Any newly obtained measurements can be used to update the model prediction and thus improve the accuracy. In essence, the model will serve as a stand-in for the actual plant, extrapolating variables for which only limited measurements are available. The combination of measured values and predictions from the nonlinear model can then be used as feedback in a control system; a similar approach was followed by Oosthuizen [7].

1.2 Background

A notable contribution to EAF modelling was made by Morales *et al.* [8]. An initial contribution was the study of the slag foaming where extensive slag data was collected and analyzed; the practical benefits of slag foaming by reduced electrical consumption and improved yield were reported from continued use of foaming on a plant [9]. Later work focused on the development of an EAF simulator where emphasis was placed on the slag behaviour, particularly FeO and the effect of the properties of direct reduced iron (DRI) on the process; the behaviour of carbon and temperature were treated, albeit not in detail [8]. The results on slag foaming and EAF modelling were combined into a single model where again the emphasis was on slag chemistry; a new concept of dynamic foaming index was advanced - this adapts the foaming of the slag to the changing furnace conditions [10]. A detailed comparison of the model prediction and plant data is given for the static case but only data from 2 taps were used for comparison of results in the dynamic case (as a function of time).

A comprehensive model for a materials refining process of ALZ^{TM} (MRPA) - essentially a BOF process - was developed by Vercruyssen *et al.* [11]. The model provided a broad coverage of components dissolved in both the slag and the bath. The model results were compared to the limited plant data with reasonable accuracy; however, only data from 1 tap were used. The influence of adjustable parameters on the model outputs was also studied. A refining simulator for the EAF was developed by Oltmann and Pretorius [12]; in the work, emphasis was placed on the tradeoff between the benefits of foaming and yield losses that can result from excessive bath oxidation. Possible yield improvements and reduction in O_2 injection can accrue from injecting sufficient graphite to sustain a foamy slag and injecting oxygen without over-oxidizing the bath - it is possible to decrease the O_2

injection rate once the critical carbon has been reached and the bath is more susceptible to over-oxidation.

Nyssen *et al.* [13] developed an essentially static model of the EAF that serves as an operator aid. Off-line calculations for the process operating scheme are performed prior to furnace startup. Online adjustments are made to the model during the tap to take into account the deviations from the precalculated values - these also include heat losses through the water cooling system. Energy and productivity savings have been reported from adoption of the model on an industrial process. Further work by the same authors resulted in a dynamic model of the EAF, this has been implemented on two furnaces where it functions as an operator aid, providing estimates of the progress of raw material melting, foam height, bath temperature and composition [14].

The model originally developed by Bekker *et al.* [5] forms the basis for the current dissertation. The model is derived from the energy and mass balances of the EAF. The focus was on the use of off-gas variables to control the temperature, composition, pressure and other outputs of interest. Extensive modelling was carried out for the scrap and solid slag additives; the freeboard gases, including pressure; and the bath temperature and composition. Model predictive control (MPC) was employed and it was shown that the off-gas variable set can be successfully used primarily for control of the furnace pressure (to minimize heat loss through air entrainment) and indirectly, the bath temperature.

Using the above model, MPC design was carried out where economic objectives were used to formulate the cost function to be minimized by the controller [7, 15]; this is a variation on the traditional approach of using functional objectives on the controlled variables. Comparison with manual control reveals significant potential benefits from implementation of the controller. A Monte Carlo type of simulation was carried out where the effect of variations in model variables on the controller performance is simulated - this provides a reliable evaluation of the controller design.

Another study focused on the economic aspects of EAF operation was carried out by de Vos [16]. A static model of the EAF was developed and the objective was to optimize slag additives in order to reduce costs.

The use of static models is a popular approach for the modelling of the EAF; [17, 18, 19, 20]. This has largely been inherited from the oxygen processes. Conceptually, it is a straightforward approach that calculates the bulk mass and energy additions that are necessary to achieve desired final steel properties such as temperature and composition. This is done off-line before EAF operation; and sometimes re-tuned (during a tap) to compensate for deviations as up-to-date tap data is made available. This latter step is called the trim calculation, and it typically occurs at the early stages of oxygen blow to adjust for the final oxygen blow.

Dynamic control of the BOF process has been successfully implemented where a sublance is lowered into the bath to sample the temperature and carbon composition [18,19]. This data is used in conjunction with off-gas analysis to calculate (on-line) corrections to the blow. Other methods such as the use of laser sampling for carbon levels, drop-in thermocouples, and sonic analysis (for decarburization and foaming estimates) have been used with varying degrees of success.

Sonic analysis has been successfully adopted in EAF operation for the control of foaming [21, 22, 23]. Analysis of audible signals generated in the vicinity of the slag is used to control graphite injection (and thus foaming). The audible signals can however be prone to extraneous interference.

Significant research effort has been carried out on the effects of the various subsystems on the EAF as a whole. Common cases are: the oxyfuel subsystem, foaming and the electrical subsystem. Experimental work was carried out to demonstrate the advantages of the oxyfuel subsystem and the increased use of oxygen in the furnace [19, 24, 25, 26]. Online off-gas analysis results are used to implement a feedback control system to optimize the operation of the oxyfuel lances. Foaming is accepted as one of the methods to minimize heat loss, improve arc efficiency and prolong refractory life. It has been studied extensively with positive results [6, 27, 9, 28, 29, 30, 31].

More research was carried out into the electrical subsystem of the process. A popular approach is the use of neural networks, favoured for its facility in dealing with the stochastic nature of the current and voltage signals: it was used in King and Nyman [32] to predict the future arc behaviour and Raisz *et al.* [33] to predict the state of the furnace (meltdown, flat bath of foaming) based on analysis of electrical signals. A notable contribution was from Billings and Nicholson [34] where system identification of the derived 3-phase arc model was carried out based on arc voltage and current relationships. An important result is the evaluation of impedance and current control and the need for a strategy that employs both approaches to improve power transfer to the melt. Later work by the same authors [35] incorporates modelling of some metallurgical processes in the refining stage of the furnace such as bath temperature and composition. Significant drawbacks to good model performance were identified as process complexity, standard or unscheduled process interruptions, poor instrumentation and availability of process data; however, positive results were reported.

The current work builds on the modelling results of mainly Bekker *et al.* [5] and additional modelling work by Oosthuizen *et al.* [6] to estimate the adjustable parameters and determine the prevailing conditions so that the model can be used as an adequate representation of the EAF refining stage. Input-output data and initial conditions collected from an EAF plant will be used to carry out the model fit.

1.3 Contribution

The main contribution of the dissertation is to bridge the gap between the previously simulation-based model of the EAF and the actual process. Process data is used to carry out SID on the model. By adjustment of the model parameters it has been shown that the model is a good representation of the EAF refining stage. The following is a list of the various dissertation contributions:

- A verified EAF model
- Experimental data of EAF slag and bath chemistry and other properties
- Identifiability analysis of the EAF model
- A model of the furnace oxyfuel subsystem
- Additional modelling to adapt the existing model to the actual EAF being studied
- An extensive model fitting exercise using real plant data over several taps to fit the model, instead of the maximum of two[1] taps used in the open literature [10].

1.4 Dissertation approach

The work carried out in this dissertation makes a clear distinction between the meltdown stage and refining. Model fitting will be done separately for refining and meltdown. There is a strong bias towards the refining stage due to higher availability of plant data - it is standard practice to obtain carbon and temperature measurements so that these will not entail additional costs. The meltdown stage will be used mainly to provide initial conditions for the subsequent refining stage; however, some limited fitting will be carried out.

As previously discussed, the problem addressed by the dissertation is to determine important model parameters based on plant data. The model provides a representation of the EAF process. As a preliminary verification of the adequacy of this representation, it is important to ensure that the model response matches the plant behaviour under the same conditions. This means the model must depict expected plant behaviour such as (among others) decarburization, melting or temperature increase when the furnace is subjected to heat input, pressure increases when adequate gas generation takes place. Therefore the initial step in this process is to obtain an understanding of the practical EAF operation. This is then followed by a description of the model, and additional modelling to accommodate process routes that may not be adequately represented. Using

[1]Much research has been carried out in order to obtain an overall fit for the model slag chemistry [18, 36]; in these cases more extensive tap data was used.

measured plant data as inputs and initial conditions, it will be shown that the model is able to depict the main process variables with reasonable accuracy.

The estimation of model parameters is essentially a SID process [37, 38]. The various steps in the process are also followed in the dissertation. These begin with process understanding, experiment design and data collection, modelling, model fitting and, finally, the validation of the numerical accuracy of the final model (or parameter values). This part of the dissertation summarizes the tools commonly used for SID and that will also applied to the problem of parameter estimation.

Once an adequate understanding of the model and the process is arrived at, the next step is the collection of plant data. A preliminary step to this process is the experiment design. For the dissertation this entails the determination of the conditions under which plant measurements would be best obtained. However, due to the limitations placed by production schedules and cost, the measurement process was not allowed to force much deviation to normal process operation. Therefore, much of the measurements were obtained under normal plant operating conditions.

The parameter values are determined by nonlinear cost minimization applied to the nonlinear model. The cost is formulated in terms of the difference between the model and plant responses under similar initial conditions and inputs. The total mean squared error over all taps is used as the cost function in an essentially batch estimation process. Once this cost is sufficiently low, the parameters are deemed adequate. Further tests used to assess the model quality are the variance of the parameters, the magnitude of the model residuals and the sensitivity of the model to outliers or bad data.

One set of data was used to determine the parameter values - this was the test or estimation data. Once a satisfactory set of parameter values was obtained, the model was simulated using data from a new data set (called validation data) that was not previously used for estimation. The model output was then compared to the corresponding measured plant data. This final step of model validation was used to test whether the model can adequately reproduce plant output behaviour.

1.5 Organization

Chapter 2 of this dissertation present a brief overview of the EAF process as well as the practices that are particular to the plant under study. A brief simulation of a heat cycle using plant data is presented with explanations of the operating practices that occur along the tap.

Chapter 3 provides an outline of the problem and the solution steps which also motivate the later chapters. It will include a summary of SID theory and some tools used to obtain

the dissertation results.

Chapter 4 sets out the experiment design and data collection process. An analysis of the data is presented with comment on its significance for the actual process. Some plots are given - these relate the collected data to others in literature, with a view to test the veracity of the data.

In chapter 5 identification is carried out on the modified EAF model. The performance of the model is discussed in relation to EAF practice.

In chapter 6 a brief model validation is carried out.

The dissertation concludes with recommendations for future work and conclusions in chapter 7. As recommendation for future work, the chapter reassesses the control issues related with the specific plant under study. Possibilities for control are discussed with particular reference to previous work [5, 7].

Some process-specific detail, measured data and model variables are given in the appendix. It also outlines some implementation details concerning the model simulation and parameter estimation.

Chapter 2

Process modelling

This chapter presents an overall description of the EAF process under study. While the main emphasis of this dissertation is on the refining stage, a discussion of the overall process is given since many of the processes that precede refining also have a direct effect on it. A description of the melting process is given, followed by the refining stage; several plots from plant data are presented to illustrate the sequence of events.

This chapter also presents a modification to the original model to allow the use of the ratio of O_2 to fuel gas as manipulated inputs. An extended freeboard gas model is presented. For refining, a simplified model is derived from approximations based on the original model. The relationship between bath carbon content and oxygen activity is discussed and the relevant equations presented.

2.1 Process description

While a broad description of the EAF process will be given, some emphasis will be placed on the practice as studied at a local steel producer. All plant data used in this dissertation was obtained from this 80 ton EAF installation, and will serve as a benchmark to test the results of subsequent chapters. In general, the practice is similar to those followed in other EAF melt shops [17, 19].

Each tap in the furnace operation begins with the charging (into the furnace) of a mixture of mainly scrap, other metallic elements and slag formers. The furnace roof swings to the side, leaving the entire furnace open. A crane is then positioned above the open furnace, the bottom of the charge basket opens, depositing the charge into the furnace.

Some melt shops charge scrap at the beginning of a tap and then make continuous additions of DRI and slag formers [39]. These are deposited in chutes at the roof of the furnace using conveyer belts. This practice relies on an abundant and cost-effective supply

of DRI. It also requires infrastructure such as conveyor belts to transport the material to the furnace and chutes through which they can be deposited into the furnace.

A systematic layering of materials is followed when the charge is prepared in the basket. A layer of shredded scrap is placed at the bottom of the basket; first to act as a cushion to prevent damage when larger scrap pieces are dropped into the basket and secondly, because it is soft and melts rapidly, it is able to create a metal pool at the bottom of the furnace soon after arcing begins.

Most EAF melt shops follow a hot heel practice. At the end of each tap the furnace is not emptied completely. A pool of hot metal varying between 5 and 15 ton remains at the end of each tap. At the beginning of the next tap the hot heel is the first to initiate melting of the soft shredded scrap. This creates a large pool of molten metal that expedites subsequent melting of larger scrap pieces once arcing commences.

Once the furnace is fully charged, the roof swings into position to close the furnace and the slag door is closed. The roof also mounts the three graphite electrodes; these are lowered closer to the scrap and with the furnace practically sealed arcing begins. The arc bores deep into the scrap directly below it. This has several consequences. A growing pool of molten metal is created below the solid scrap. Significantly, the arc is shielded by the surrounding scrap so that most of the heat energy is retained within the vicinity of the scrap; otherwise the heat would be radiated to the water cooled panels and lost unused. This effectively increases the arc efficiency. Furthermore, damage to the refractory linings by the intense radiation from the arcs is reduced.

The arc is generated by the ends of three graphite electrodes that form an equilateral triangle above the metal, centred about the vertical axis of the furnace. This means most of the heat energy is concentrated near the centre of the furnace - energy transfer to regions further from the centre is limited. Bore-in will ensure that the arc penetrates deep enough into the scrap to shield the refractory above the scrap. On the other hand, it is essential that a molten pool is formed early enough to protect the furnace bottom from the arc [17]. At the early stage of bore-in the scrap will melt from below, by heat from the arc, radiation and conduction from the pool and resistive heating; the scrap not directly exposed to the arc or in direct contact with the molten pool will not melt as readily.

Therefore oxyfuel burners are used to heat the cold areas of the furnace. Composite lances that mix fuel gas and O_2 at the exit of the nozzle are placed strategically so that heat energy from the flame is transferred to the cold areas in the furnace. Figure 2.1 shows the configuration of the oxyfuel lances in the furnace. The burners are a highly efficient supplementary heat source since the flame is able to reach larger areas of the scrap. The high temperatures prevalent in the furnace and the abundance of O_2 - it is kept higher than stoichiometric - ensure that the combustion of the fuel gas is nearly complete [21].

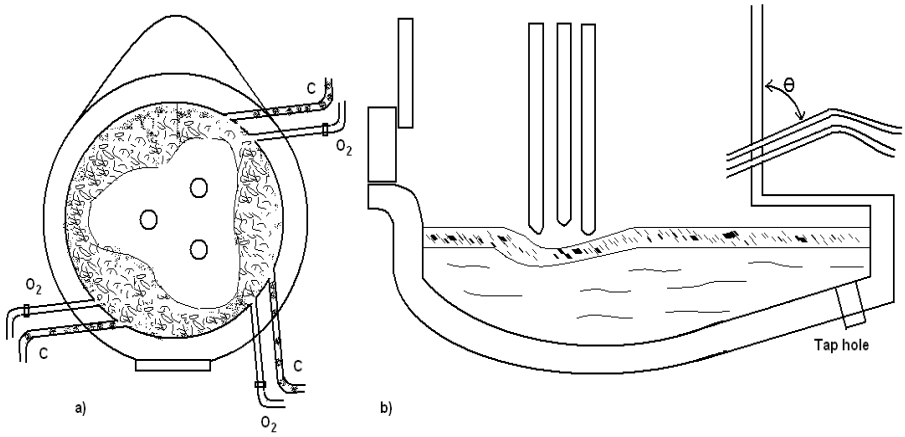

Figure 2.1: Placement of the oxyfuel lances in the furnace. Figure a) shows the top view and b) the cross-sectional view. All the oxygen lances are inclined at a fixed angle of approximately $\theta = 45\,^{\circ}$, while the graphite lances are at $\theta = 60\,^{\circ}$.

While the oxyfuel lances are strategically placed to transfer heat to all the regions in the furnace, cold spots will always exist. These are depicted in figure 2.1, as regions of solid raw material. These cold spots are also a source of scrap cave-ins and late melt-ins. When a flat bath has been reached (typically near refining), solid scrap that may be lodged in these cold spots has been observed to fall into the flat bath [17]. This can happen especially with heavier pieces of scrap that are not easily melted by flame heat. Some late melt-ins can also result when heavy scrap pieces remain suspended in the bath well into the refining stage [22]. Some cave-ins that occur during meltdown can break the electrodes as the scrap falls against the electrodes [17]. This is a catastrophic breakdown: the bath carbon content will be inflated by partial dissolution of the graphite electrode, the removal of which from the furnace will lead to long delays.

Different grades of scrap require varying levels of energy to melt [17]. This can be explained in terms of the specific surface area available for heat transfer and the efficiency of heat transfer between the scrap and the molten steel. A charge made up of metal sheets or plates will melt rapidly due a large surface area available for heat transfer - and all molten scrap will readily flow away from the heat source, leaving room for more scrap to melt. Heavy scrap is denser and generally has a lower specific area for heat transfer. It can be too solid and closely packed - tending to localize the arc - and slow melting while preventing free access of arc heat to other regions of the melt. This has the effect of reducing the effective melting power of the arc.

Light scrap (such as plates and turnings) is rapidly melted to form a pool of metal at the furnace bottom while heavy scrap (such as butts and ingots) is placed directly

below the arc to receive maximum arc power. In this location the heavy scrap will also prevent the arc from boring into the furnace bottom while allowing sufficient depth to the electrodes for effective heat transfer to the scrap surrounding it.

An added advantage of using high density scrap is the reduced charging time. With heavy scrap two basket charges are sufficient, while lighter scrap will necessitate up to three charges in order to fulfill the requirements for the meltdown mass - this is time-consuming. On the other hand a heavy piece of scrap will likely break an electrode if it happens to roll against it as the melt settles [17] and will be less susceptible to melting by the oxyfuel burners. Therefore, the charge will always maintain a balance between heavy scrap and light scrap.

Silicon is removed nearly completely during the decarburization period; in fact it is removed well before the carbon, this typically happens early in the melting period [19]. In the refining period after t_1 the bath silicon content is at an average value of 0.025 % and a standard deviation of 0.0074 % ; it can be assumed to be the minimum composition. This value will be taken as the silicon content at the asymptotic stage. Despite its small quantities, silicon oxidation is also one of the most exothermic reactions.

2.1.1 The oxyfuel subsystem

The efficiency of the oxyfuel system depends on the ability of the combustion products to transfer heat energy to the scrap. The heat transfer occurs mainly by convection and radiation from the flame products; and, to a lesser extent, by conduction when excess oxygen reacts with the charge [19].

As in the case of arc heat transfer, a large specific area of the scrap will favour effective heat transfer. This follows since a large surface area will be exposed to the flame [19]. As scrap melts, the overall efficiency generally decreases since less scrap will be in contact with the flame. The molten steel will present a poor medium for heat transfer due to its high temperature and small surface area.

The efficiency of the oxyfuel system also depends on the temperature of the scrap [19]. A low scrap temperature allows a higher degree of transfer of oxyfuel flame energy to the scrap. A practical indication of the efficiency is obtained by monitoring the off-gas temperature. A high off-gas temperature means that more of the freeboard heat is removed with the off-gas, and less is transferred to the scrap. This typically occurs at the late melting stage where the little scrap that remains is already at a high temperature and the flat bath is receiving virtually none of the heat from the freeboard. Plant trials reveal that the freeboard temperature ranges from 800 to 1200 °C (see subsection 4.3.4.2) while the flat bath will be at a minimum 1520 °C, the melting temperature of steel [19];

however, the average temperature of the total furnace charge will be lower due to the presence of unmelted scrap.

At refining the operation of the oxyfuel burners follow three main preset programs, depending on the desired steel carbon content. A low desired carbon content is generally accompanied by high volumes of injected oxygen, while the highest desired carbon content will have little oxygen lancing. Table 2.1 shows the settings for the volume of injected oxygen and gas for the three grades of steel based on the desired bath carbon.

Table 2.1: Injection programs used for refining.

Grade	Low C	Medium C	High C
Bath carbon	%C < 0.2%	0.2 < %C < 0.4%	%C > 0.4%
Operating mode	lancing	lancing	burner
O_2 flow rate [Nm^3/h]	1500	1200	900
fuelgas flow [Nm^3/h]	200	200	200

An adequate condition for effective results from auxiliary burners is good heat transfer with (usually) light scrap that has a large specific area for heat transfer. The flue gas can contain high levels of CO and H_2 due to incomplete combustion. While the flame is in contact with the charge, the flue gas (CO and H_2) will tend to react with the scrap, producing CO_2 and H_2O and oxidizing the iron. The resulting FeO leads to severe iron slagging i.e. accumulation of FeO on the scrap surface. This can limit the degree of heat transfer. However, a high carbon content in the charge can reduce the slagging [40]. Furthermore, the CO and H_2 must be combusted downstream, and so placing higher demands on the off-gas system. Yield losses have also been reported due to oxidation of the molten steel by CO_2, made possible by the high temperatures at the bath-gas interface [19]. Therefore, to minimize bath oxidation, the burners must be operated only when sufficient scrap is available and when the molten steel can flow rapidly away from the flame area.

Once most of the scrap has melted, the use of oxyfuel burners can lead to yield losses and lower efficiencies. The amount of scrap in contact with the flame decreases as its overall temperature increases, leading to poor heat transfer. A rise in the off-gas temperature is a good indicator of when oxygen burners should be stopped. Alternatively, the temperature of the panels adjacent to the burners will begin to rise because of poor heat transfer to the charge and the consequent heat build-up in the vicinity of the burners. A general recommendation is that burner operation should be discontinued after 50% of meltdown [19].

An alternative operating mode of the oxyfuel burners is oxygen injection. Once suffi-

cient meltdown is achieved, the burners operate as high efficiency oxygen lances. Intensive injection of oxygen into the bath begins by cutting the scrap under high temperatures. Once a flat bath is attained carbon levels in the bath are generally high. The oxidation of this bath carbon provides an efficient energy source: for every Nm^3 of oxygen injected $0.75\,\mathrm{Nm}^3$ reacts with carbon [19]. Reduction of slag FeO by bath carbon is another route by which decarburization takes place [5], and becomes more predominant with sufficient stirring [41] and at lower carbon levels.

2.1.2 Deslagging

Deslagging is the process by which the slag layer above the steel is removed from the furnace. It is important for removing impurities from the furnace and to limit the slag height. Most furnaces are equipped with an opening above the slag line, used specifically for deslagging. As foaming proceeds, the slag can increase to such a level that it begins to overflow this slag door. Otherwise by tilting the furnace in the direction of the slag door, the slag can be poured out of the furnace. In a typical refining stage, the furnace may be deslagged several times - the first substantial mass will be removed before an initial bath sample and temperature are taken. Then foaming, followed by deslagging will take place several times as continuous sampling and adjustment of bath properties proceeds.

Phosphorus is transferred to the slag early in the heat while the temperature is relatively low[1]. The first deslagging (at the start of refining) removes a substantial portion of the phosphorus (as P_2O_5), thus preventing its reversion into the steel. It is also important that the slag is removed before it reaches the refractories to prevent slag attack, in spite of the favourable slag properties that may exist. A further (practical) motivation for deslagging is to remove the thick layer above the bath so that measurement probes can be inserted into the bath without contamination from the slag. Therefore, it is advantageous to limit the number of temperature (and carbon and oxygen) measurements as this will limit the number of times the furnace is deslagged, and thus reduce losses by maintaining a foamy slag layer for longer.

2.1.3 The off-gas system

There are two main routes by which the exhaust fumes can be removed from the furnace. The direct evacuation system is the main route, consisting of an induced draft that withdraws freeboard gases through a hole (called the fourth hole) in the furnace roof [17].

[1]Other slag conditions that favour phosphorus removal such as high basicity, high FeO content and high slag volume are typically in place: the CaO-SiO_2 ratio (basicity) is always greater than the minimum 2.2 suggested by Taylor [17]; FeO can be found in high volumes and the slag volume is assumed sufficient.

Alternatively, gases that escape through other openings (such as electrode ports, openings between furnace panels and slag door) are collected by the secondary emission control system. This is made up of a canopy hood installed in the roof work area directly above the furnace; it withdraws all gases that are in the immediate environment of the furnace. This secondary system makes the operation of the furnace under a slight positive pressure less detrimental. This positive pressure operation will typically take place during the first few minutes of melting when volatile materials burn, and significant flame and flash-off are observed at all the furnace openings [19].

Significant volumes of air are entrained into the off-gas system as the gases are being transported away from the furnace. This serves two roles: to cool the gas and to combust the CO. The entrained air itself will increase the total volume of the gas as will the combustion of CO. As a result, the off-gas system is usually designed to remove four times as much gas as leaves the furnace [19], the rest being contributed directly or indirectly by the entrained air. For the EAF being studied, the off-gas system operates at a mass flow rate of 66000 Nm^3/h [22].

Some metal has been known to vaporize under the influence of oxygen injection [18]. The oxygen and the vaporized metal will react to form a gaseous oxide. This accounts for the presence of oxide fumes that will report to the off-gas system. In the EAF the effect will be lowered by the presence of anthracite and fuel gas. Under oxygen lancing the abundance of oxygen will make the effect inevitable, but it may be offset by the presence of a slag layer that helps to cover the steel. Therefore, some limited iron losses through the off-gas can be expected.

2.1.4 Process delays/interruptions

Several unscheduled interruptions are experienced by the process. Their direct effect on the process is to introduce delays. These will typically increase the total energy losses per tap and consequently the energy required to achieve the aimed bath temperature.

The prolonged application of arc energy will also increase the consumption of electrodes. This in turn translates to an increase in bath carbon, although this is in small quantities: on average, electrode consumption occurs at a rate of 147 kg/tap, based on the number of electrodes replaced over a data record of 78 taps. The majority of this consumption takes place during meltdown [19].

Another delay that is typically encountered during the furnace operation is maximum demand power-off. This is used to prevent exceeding the maximum power limit as prescribed by the power utility.[2]

[2]This delay occurs several minutes to the hour every hour during peak times from 11 AM to 3 PM.

2.1.5 Charge constituents

Of the total scrap charged, a typical yield of about 90 % is reported [42]. The other 10 % is lost as oxides to the slag, and to the off-gas system as vaporized iron, gaseous products of oxidation and dust.

In the case of the current process, the total of the 2 to 3 charges consists mainly of scrap, cast iron and slag formers. Table 2.2 shows the breakdown of the average composition over 18 taps[3]. In a total charge of 80.5 ton, scrap makes up 69.4 ton; a significant portion of the anthracite and slag formers is lost as dust to the off-gas system[4]. This is approximated to up to 50% of all anthracite and 20 to 30 % of all slag formers [22]; the remaining anthracite is dissolved as carbon into the melting bath. The total slag removed from the furnace is estimated to be approximately 20 ton (see subsection 4.3.4.3). Bales, cut scrap and liquid iron are sometimes charged with the scrap.[5]

Table 2.2: Average charge constituents per tap.

Constituent	Mass [ton]	% composition
General scrap	69.37	73.61
Shredded scrap	3.65	3.87
Sponge iron	4.21	4.47
Pool iron	7.37	7.82
Cast iron	3.02	3.21
Lime	4.52	4.79
Dolomitic lime	1.15	1.22
Anthracite	0.96	1.02

The iron-based constituents - scrap, sponge iron, pool iron, cast iron - provide the main raw materials that will melt into steel. Cast iron contributes to the bath carbon composition with its relatively high carbon content of 2 to 5 %. Similarly, pool iron, sourced from a blast furnace, contributes to the bath about 5 % carbon and smaller amounts of silicon, manganese, phosphorus and sulphur. Further details about the composition of the various charge constituents are given in table 2.3. Most scrap units are assumed to have a 100 % iron content since their composition is not measured. In any event impurities

[3]This is the number of taps for which data were collected and used throughout the dissertation.

[4]No information of this loss is available since the off-gas composition, or the resulting dust are not measured.

[5]Some excess hot metal may be obtained from continuous casting operations - as happened for one of the taps from the recorded data. But this is rare, and may be due to failure in casting operations which necessitated that the hot metal be returned to the EAF. Only 17 ton of hot metal was charged for one tap from a total of 78 taps (the total of all taps over 3 days, including the 18 monitored taps) - it is expected that even less hot metal charging is used in general; the only source of hot metal in the EAF is the hot heel.

in the scrap will normally appear in trace quantities. Other constituents such as ash, sulphur and phosphorus are not shown but may be found in varying quantities.

Table 2.3: Approximate composition of charge constituents.

Constituent	% Fe	% C	% Si	% CaO	% MgO	% SiO_2	% Al_2O_3
General scrap	100	0	0	0	0	0	0
Shredded scrap	100	0	0	0	0	0	0
Cut scrap	100	0	0	0	0	0	0
DRI/Sponge iron[6]	78	0	1	0	0	3	3
Pool iron	95	4-4.4	1	0	0	0	0
Cast iron	95	2-5	0	0	0	0	0
Bales	100	0	0	0	0	0	0
Liquid iron	100	0	0	0	0	0	0
Lime	0	0	0	90.5	1.3	3	3
Doloma	0	0	0	63	37	0	0
Anthracite [7]	0	80.3	0	0	0	0	0

Unlike BOF practices where the main hot metal charge is high in carbon, most scrap input used for the EAF is generally low in carbon and so will the resulting molten steel. Therefore, anthracite is charged into the furnace mainly to facilitate carbon pickup in the bath. In practice, for medium carbon steel, carbon is charged at 2-12 kg/ton of molten steel, depending on the projected oxygen injection and the desired end carbon [19]. In the current process, on average 0.96 ton anthracite is charged for 87.6 ton of metallic charge, giving 17 kg/ton. However, the effective carbon added to the bath will be lower since the recovery rate from anthracite is less than 100 %: some anthracite is combusted during burner operation and some is lost as dust to the off-gas. During melting, most of the anthracite dissolves into the melting steel. Once a flat bath is reached, exothermic energy is generated by decarburization of the high bath carbon. Given the right slag conditions, the generation of CO will also improve slag foaming at early meltdown. While most of the carbon is introduced into the bath only to be removed, its main role is foaming and to supply chemical energy to the bath.

The other advantage of melting steel at a higher carbon content than specified is the vigorous carbon boil that occurs as the temperature rises [17]. This effectively stirs the bath, thus increasing the interfacial area between the steel and slag, and homogenizing the temperature and composition. The evolution of CO also leads to removal of nitrogen and hydrogen.

Direct reduced iron (DRI) is processed iron ore with a high metallization (i.e. a high proportion of iron to oxides) - so called clean or virgin iron [19]. Its main advantage is

[6] At 88 % total Fe and 78 % metallic Fe.

[7] Other components to be found in anthracite are: ash - 11.1 %, volatiles - 7 %, H_2O - 1.6 % and sulphur - 1.3 %.

its low levels of tramp elements that are otherwise commonly found in scrap (Cu, Sn, Ni, Cr, Zn, Pb). In the EAF, no practical refining method exists for removing these elements from the steel. When the only available scrap is high in these tramp elements, the pure DRI is used to neutralize the steel, effectively diluting the tramp elements [17]. The high levels of oxides in the DRI will also contribute towards slag foaming.

The composition of the charge is also chosen based on the desired composition of the melt. Table 2.4 shows the compositions of charge basket one and two as a function of the desired end point carbon[8]. Pool iron and DRI are the only constituents that vary as the desired carbon content of the bath changes. Pool iron is high in carbon and is increased as the desired end carbon increases - because of the slow melt-in of the pool iron, a high carbon level will be ensured at the end of tap. On the other hand the DRI is decreased so that less FeO from the DRI will reduce bath decarburization.

Table 2.4: Basket composition [ton] for desired grade of steel (carbon composition).

	Basket 1			Basket 2		
Desired grade	Low C	Medium C	High C	Low C	Medium C	High C
C composition	%C < 0.2%	0.2 < %C < 0.4%	%C > 0.4%	%C < 0.2%	0.2 < %C < 0.4%	%C > 0.4%
Shredded scrap	10	10	10	5	5	5
Pool iron	2.0	4.0	6.0	0	0	0
Lime	2.0	2.0	2.0	2.0	2.0	2.0
Doloma	1.0	1.0	1.0	1.0	1.0	1.0
Anthracite	0.75	0.75	0.75	0.75	0.75	0.75
DRI	4.0	3.0	2.0	4.0	3.0	2.0
General scrap[9]	75	75	75	75	75	75

2.1.6 Refining

Once flat bath conditions have been reached the next important step in EAF operation is refining. During this stage, the final adjustment of steel properties is carried out: the bath composition and temperature are controlled to meet the final steel specifications. In particular, the refining stage involves the removal of phosphorus, sulphur, aluminium, silicon, manganese and carbon; with the latter being more important. With the increasing use of oxygen, the control of the final oxygen content (and other gases such as nitrogen and hydrogen) is also important. In all cases the final composition is generally controlled to be lower than specification - alloying additions can be made in the ladle to raise the composition to desired levels.

Once the charge is fully melted, the temperature and composition of the bath are determined. A sample of the steel is extracted and processed for laboratory chemical

[8]This is the typical charge composition as used in practice [22].

[9]The scrap is chosen to fulfil final bath mass requirements, and may be slightly different from 75 ton.

analysis. The sample chemical composition can be reported within 3 minutes from extraction to analysis [22] in the absence of any operator delays or equipment malfunction. The bath temperature is measured using a disposable thermocouple that is inserted into the bath and reports the result instantaneously. A composite probe is also employed - this gives instantaneous measurements of temperature, oxygen activity and calculated bath carbon. It avoids the long delays involved in obtaining a detailed sample analysis at the latter stages of refining.

Much of the removal of undesired elements from the bath occurs by oxidation. Oxygen injection begins well before flat bath conditions are reached. As a result, some of the refining reactions will take place before operator control (after a bath analysis and temperature have been secured). For the purposes of this dissertation, the refining period will be taken as the time from the first bath analysis to tapping; the preceding period is pre-refining and generally overlaps with the late melting stage.

Removal of phosphorus, manganese, silicon and carbon occur mainly by oxidation. Phosphorus is oxidized as P_2O_5 and transferred to the slag. The phosphate capacity of the slag is controlled by CaO and MgO components of the slag [19]. Other factors such as temperature, FeO and basicity are important for phosphorus retention in the slag i.e. low temperature, high slag FeO and basicity. Therefore the first deslagging is important for removal of large quantities of the phosphorus - this typically occurs at early refining before the temperature is raised to a level that may cause phosphorus reversion into the bath [17]. The slag additives are chosen to maintain sufficient basicity - a minimum of 2.2 CaO/SiO_2 - and high levels of FeO are generally maintained (see table A.1 in the appendix).

Manganese is oxidized from the bath as MnO and transported to the slag. Retention in the slag is ensured by some of the conditions that apply for phosphorus: high FeO, low temperature and lime-silica ratio less that 2.2. A lime-silica ratio of 2.2 will ensure optimal conditions for retention of both manganese and phosphorus - this is generally not possible. A good solution is to begin with a charge that is low in manganese or to increase the proportion of DRI. Or, consistent oxygen injection will ensure a high rate of manganese oxidation despite suboptimal conditions for its retention in the slag.

Sulphur has a detrimental effect on the steel surface quality as well as the mechanical properties. It is also one of the more difficult elements to control: at most only half the total sulphur introduced with the charge can be removed from the bath [17]. Some (20 to 30 %) desulphurization can be achieved during oxidation. Conditions that favour successful removal of sulphur are: high basicity, low FeO, high slag fluidity and low bath oxygen. Temperature and chemistry of the bath and slag are also important variables in desulphurization. The sum of the acidic oxides, $\%\,SiO_2$ and $\%\,P_2O_5$, has a negative effect

on the sulphide capacity of the slag [19]. Lime additions can also improve desulphurization but they must be accompanied by flux additives to maintain slag fluidity. Generally, the reducing phase is favourable for effective desulphurization. However steel EAF operations are oxidizing, so that desulphurization is deferred for the ladle metallurgy where reducing conditions can be maintained [19].

Silicon is oxidized well before carbon. The reaction is highly exothermic, transferring significant amount of energy to the bath and SiO_2 to the slag. Its control is generally simple and presents few challenges - in fact all silicon is removed completely during decarburization [17]. Therefore the bath is normally tapped with much lower silicon than specified. Then ferrosilicon is added to raise the silicon level to specification.

Decarburization is the most important reaction in steelmaking [19]: it determines the process time, slag FeO levels and consequently the yield and refining. Experimental results reveal two routes by which decarburization takes place [20, 36, 43]. Above the critical carbon content ($\%\,C_{crit}$), the removal of carbon is proportional to the rate of oxygen injection - it is also independent of the carbon content. The $\%\,C_{crit}$ lies in the range $0.1 - 0.6\,\%$, established by the corresponding oxygen volume flow rates of $1 - 4.5\,m^3/(t.min)$. Below $\%\,C_{crit}$, the decarburization is proportional to the carbon content. Specifically, the rate of decarburization is proportional to the difference between the current carbon content and the equilibrium carbon content (see subsection 2.2.1 for details) - this is effectively decarburization by FeO reduction [5, 19, 41].

The latter reactions are:

$$\mathrm{Fe} + \frac{1}{2}\mathrm{O_2} = \mathrm{FeO} \qquad (2.1a)$$

$$\mathrm{FeO} + \mathrm{C} = \mathrm{Fe} + \mathrm{CO} \qquad (2.1b)$$

$$\text{net:} \quad \mathrm{C} + \frac{1}{2}\mathrm{O_2} = \mathrm{CO} \qquad (2.1c)$$

Both patterns of decarburization result in the same net reaction (2.1c), so that either will suffice. The original model derivation models decarburization by FeO reduction [39], this will be retained in the current dissertation. Any deviation can be corrected by adjustment of the appropriate rate constant (k_{dC}).

2.1.7 Differences between original and current EAF

With the preceding discussion of the process under study, a discussion about the original model derivation and how it relates to the current process is in order. The model derived in Bekker [5] and later used by Oosthuizen [7] was based on a 150 ton process with a

significant hot metal charge, continuous DRI and slag feeds and oxygen injection from the beginning to the end of tap. The following differences are observed:

- Only a relatively small hot heel is used at the beginning of tap and no hot metal charge is made.
- All carbon and silicon originate from the scrap and other metallic charge. Their composition in the molten steel will increase only as the solid metal melts. In the original derivation, these impurities are dissolved in the liquid metal charge and decrease progressively.
- The generation of slag FeO and SiO_2 will not occur until well into the tap when sufficiently flat bath conditions have been reached and oxygen injection commences.
- This means decarburization and desiliconization will only occur once proper slag conditions are in place, not from the beginning of tap.
- Oxyfuel burners serve as an additional source of heat energy during early meltdown. Once most of the metal is melted they operate as high efficiency oxygen lances to inject oxygen - cutting the remaining scrap, oxidizing impurities from the bath and increasing the slag metal-interaction by vigorous bath stirring - this oxygen injection occurs throughout the tap for the original model.
- There are no continuous feeds of slag or DRI; these are introduced into the furnace as part of the charge.
- There are relatively low levels of carbon in the scrap with limited contributions from cast iron and pool iron - bath carbon levels are increased by carbon pickup from the charge anthracite.

With the above discussion, the model decarburization, desiliconization and bath oxidation cannot proceed as originally derived. Decarburization is given by the difference between the current (X_C) and equilibrium (X_C^{eq}) carbon concentrations:

$$\dot{x}_3 = -k_{dC}(X_{\mathrm{C}} - X_{\mathrm{C}}^{eq}). \tag{2.2}$$

For successful decarburization, $(X_{\mathrm{C}} - X_{\mathrm{C}}^{eq}) > 0$, made possible by the availability of FeO, liquid slag and a high bath carbon. At initial melting some liquid slag is developed, but no FeO or SiO_2. A situation can result with low FeO, finite liquid slag (increasing the equilibrium point) and low bath carbon where $X_{\mathrm{C}} < X_{\mathrm{C}}^{eq}$. This will lead to an increase in bath carbon - impossible since there is no source for this additional carbon. To circumvent this problem, the initial FeO, SiO_2 and liquid slag are deliberately exaggerated (in practice

the magnitudes of these states are negligible until near-flat bath conditions have been reached). The same values are used for each tap so that their effect is consistent from one tap to the next and will not violate the resulting mass and heat balances. This maintains the necessary conditions where bath carbon and silicon are always higher than their equilibrium concentrations.

Only small initial values of dissolved carbon and silicon will be used; a major portion is introduced as solids - carbon as anthracite and silicon in the scrap. Therefore, over the entire tap simulation, the dissolved carbon and silicon will increase gradually in proportion to the scrap melting rate.

2.2 The process model

2.2.1 The EAF model

A detailed description of the model is given in Bekker [5]; it was later updated by Oosthuizen *et al.* [6]. In this subsection, only a listing of the important equations will be given. The non-linear model has the form

$$\Sigma_\theta : \begin{cases} \dot{\mathbf{x}} = \mathbf{f}(\mathbf{x}, \theta, \mathbf{u}) \\ \mathbf{y} = \mathbf{h}(\mathbf{x}, \theta, \mathbf{u}) \\ \mathbf{x}(\mathbf{0}, \theta) = \mathbf{x}_0 \end{cases} \tag{2.3}$$

where $x \in \Re^n$, $u \in \Re^m$, $y \in \Re^p$ and $\theta \in \Re^q$ are the state, input, output and parameters of the system.

The following definitions are used to describe the current masses of carbon and silicon at time t relative to their equilibrium concentrations with the FeO in the slag. At steady state, the concentration of carbon and silicon in the bath will be at equilibrium with the FeO in the slag. That is, their current concentrations will change so as to reach equilibrium, hence the following equations.

$$X_{\mathrm{C}} = \frac{x_3/M_{\mathrm{C}}}{x_2/M_{\mathrm{Fe}} + x_3/M_{\mathrm{C}} + x_4/M_{\mathrm{Si}}} \tag{2.4}$$

$$X_{\mathrm{FeO}} = \frac{x_7/M_{\mathrm{FeO}}}{x_6/M_{slag} + x_7/M_{\mathrm{FeO}} + x_8/M_{\mathrm{SiO_2}}} \tag{2.5}$$

$$X_{\mathrm{C}}^{eq} = k_{XC}\left(\frac{x_6 M_{\mathrm{FeO}}}{x_7 M_{slag}} + \frac{x_8 M_{\mathrm{FeO}}}{x_7 M_{\mathrm{SiO_2}}} + 1\right) \tag{2.6}$$

$$X_{\mathrm{Si}} = \frac{x_3/M_{\mathrm{Si}}}{x_2/M_{\mathrm{Fe}} + x_3/M_{\mathrm{Si}} + x_4/M_{\mathrm{Si}}} \tag{2.7}$$

$$X_{\mathrm{Si}}^{eq} = k_{XSi}\left(\frac{x_6 M_{\mathrm{FeO}}}{x_7 M_{slag}} + \frac{x_8 M_{\mathrm{FeO}}}{x_7 M_{\mathrm{SiO_2}}} + 1\right)^2 \tag{2.8}$$

where X_i and M_i are (respectively) the molar fraction and molar mass of element or compound i. The equilibrium concentrations for carbon (X_{C}^{eq}) and silicon (X_{Si}^{eq}) are based on the concentrations of the slag-based constituents FeO (x_7), SiO_2 (x_8) and the composite slag which is made up mainly of the CaO and MgO parts of the slag (x_6); the corresponding equilibrium concentration constants are given by

$$\begin{aligned} k_{XC} &= X_{\mathrm{FeO}} X_{\mathrm{C}} = 491 \cdot 10^{-6} \\ k_{XSi} &= X_{\mathrm{FeO}}^2 X_{\mathrm{Si}} = 8.08 \cdot 10^{-8} \end{aligned} \tag{2.9}$$

A listing describing the variables used above and in the rest of the model is given in section A.1 of the Appendix.

The heat energy derived from the chemical reactions in the bath is given by:

$$\begin{aligned} p_1 &= (\Delta H_{C(S)} + \Delta H_{\mathrm{FeO}} - \Delta H_{\mathrm{CO}}) k_{dC} / M_{\mathrm{C}} (X_{\mathrm{C}} - X_{\mathrm{C}}^{eq}) \\ p_2 &= (-2\Delta H_{\mathrm{FeO}} d_1 / M_{\mathrm{O_2}}) \eta_{\mathrm{FeO}} \\ p_3 &= ((\Delta H_{\mathrm{CO_2}} - \Delta H_{\mathrm{CO}}) 2 k_{air_1} k_{PR} x_{14}) \\ p_4 &= (\Delta H_{\mathrm{Si\_S}} - \Delta H_{\mathrm{SiO_2}} - \Delta H_{\mathrm{SiO_2\_S}}) \frac{k_{dSi}}{M_{\mathrm{Si}}} (X_{\mathrm{Si}} - X_{\mathrm{Si}}^{eq}) \\ p_5 &= \frac{d_1}{M_{\mathrm{O_2}}} (x_{12} - T_{\mathrm{O_2}}) C_{p(\mathrm{O_2})} \\ p_6 &= k_{air_1} k_{PR} x_{14} (x_{12} - T_{AIR}) C_{p(\mathrm{O_2})} \\ p_7 &= k_{air_2} k_{PR} x_{14} (x_{12} - T_{AIR}) C_{p(\mathrm{N_2})} \\ p_8 &= -2 d_3 C_{p(Slag_{(S)})} (x_{12} - T_{slag}) / M_{slag} \\ p_9 &= \frac{-\%_{met} d_2 (\lambda_{\mathrm{Fe}} + C_{p(\mathrm{Fe}_{(s)})}) (x_{12} - T_{DRI})}{M_{\mathrm{Fe}}} \\ p_{10} &= -k_{therea_1} x_1 \frac{x_2}{x_1 + x_2} (x_{12} - x_{13}) - k_{therea_5} x_5 \frac{x_6}{x_5 + x_6} (x_{12} - x_{13}) \\ p_{11} &= \frac{x_7 k_{gr} d_5 (\Delta H_{\mathrm{FeO}} - \Delta H_{\mathrm{CO}})}{(x_6 + x_7 + x_8) M_{\mathrm{C}}} \end{aligned}$$

p_3, p_6 and p_7 relate to heat energy interactions due to air entrainment. p_6 and p_7 are heating losses to entrained O_2 and N_2; p_3 is the heat input from combustion of freeboard CO by entrained O_2. These contributions only apply under negative furnace pressure, otherwise they have no influence on the heat balance. Since the model is based on simple heat balance, the different modes of heat transfer - radiation, convection and conduction - are not explicitly handled. That is, all the energy input (via some efficiency constants) is transferred to the furnace without regard to the specific mode of transfer. This simplifies modelling without violating the heat balance. The total energy from chemical reactions is $p_t = p_1 + ... + p_{12}$, where p_{12} is defined in the next subsection (2.2.2)

The model state equations are given by:

$$\begin{aligned}
\dot{x}_1 &= \frac{-M_{\mathrm{Fe}}k_{therea_1}(x_1)(x_{12}-x_{13})\sqrt{(x_{13}/x_{12})}}{(\lambda_{\mathrm{Fe}}+C_{p(\mathrm{Fe}_{(S)})}(x_{12}-x_{13}))} \\
&\quad + \frac{M_{\mathrm{Fe}}k_{therea_1}(x_1)\max(T_l-x_{12},0)}{\lambda_{\mathrm{Fe}}} \qquad (2.10)\\
\dot{x}_2 &= \frac{M_{\mathrm{Fe}}k_{therea_1}(x_1)(x_{12}-x_{13})\sqrt{(x_{13}/x_{12})}}{\lambda_{\mathrm{Fe}}+C_{p(\mathrm{Fe}_{(S)})}(x_{12}-x_{13})} + \frac{x_7k_{gr}M_{\mathrm{Fe}}d_5}{(x_6+x_7+x_8)M_C} \\
&\quad + \frac{M_{\mathrm{Fe}}}{M_{\mathrm{C}}}k_{d\mathrm{C}}(X_{\mathrm{C}}-X_{\mathrm{C}}^{eq}) + \frac{2M_{\mathrm{Fe}}}{M_{\mathrm{Si}}}k_{dSi}(X_{\mathrm{Si}}-X_{\mathrm{Si}}^{eq}) - \frac{2M_{\mathrm{Fe}}d_1}{M_{O_2}} + 0.825d_2 \\
&\quad - \frac{M_{\mathrm{Fe}}k_{therea_1}(x_1)\max(T_l-x_{12},0)}{\lambda_{\mathrm{Fe}}} \qquad (2.11)\\
\dot{x}_3 &= -k_{d\mathrm{C}}(X_{\mathrm{C}}-X_{\mathrm{C}}^{eq}) \qquad (2.12)\\
\dot{x}_4 &= -k_{dSi}(X_{\mathrm{Si}}-X_{\mathrm{Si}}^{eq}) \qquad (2.13)\\
\dot{x}_5 &= \frac{-M_{slag}k_{therea_5}(x_5)(x_{12}-x_{13})\sqrt{(x_{13}/x_{12})}}{\lambda_{Slag}+C_{p(Slag_{(S)})}(x_{12}-x_{13})} + d_3 \\
&\quad + \frac{M_{slag}k_{therea_5}(x_5)\max(T_l-x_{12},0)}{\lambda_{Slag}} \qquad (2.14)\\
\dot{x}_6 &= \frac{M_{slag}k_{therea_5}(x_5)(x_{12}-x_{13})\sqrt{(x_{13}/x_{12})}}{\lambda_{Slag}+C_{p(Slag_{(S)})}(x_{12}-x_{13})} \\
&\quad - \frac{M_{slag}k_{therea_5}(x_5)\max(T_l-x_{12},0)}{\lambda_{Slag}} \qquad (2.15)\\
\dot{x}_7 &= \frac{2M_{\mathrm{FeO}}d_1}{M_{\mathrm{O_2}}}\eta_{\mathrm{FeO}} - \frac{M_{\mathrm{FeO}}}{M_{\mathrm{C}}}k_{d\mathrm{C}}(X_{\mathrm{C}}-X_{\mathrm{C}}^{eq}) - \frac{2M_{\mathrm{FeO}}}{M_{\mathrm{Si}}}k_{dSi}(X_{\mathrm{Si}}-X_{\mathrm{Si}}^{eq}) \\
&\quad - \frac{x_7k_{gr}M_{\mathrm{Fe}}d_5}{(x_6+x_7+x_8)M_C} + 0.13d_2 \qquad (2.16)\\
\dot{x}_8 &= \frac{M_{\mathrm{SiO_2}}}{M_{\mathrm{Si}}}k_{dSi}(X_{\mathrm{Si}}-X_{\mathrm{Si}}^{eq}) + 0.045d_2 \qquad (2.17)\\
\dot{x}_{12} &= (p_t+\eta_{ARC}d_4-k_{VT}(x_{12}-T_{air}))/\left[\frac{x_2C_{p(\mathrm{Fe}_L)}}{M_{\mathrm{Fe}}} + \frac{x_3C_{p(C)}}{M_C} + \frac{x_4C_{p(\mathrm{Si})}}{M_{\mathrm{Si}}}\right. \\
&\quad \left. + \frac{2x_6+2x_7+3x_8}{M_{slag}}C_{p(Slag_{(L)})}\right] \qquad (2.18)\\
\dot{x}_{13} &= \frac{k_{therea_1}(x_1)(x_{12}-x_{13})x_2/(x_1+x_2)}{x_1C_{p(\mathrm{Fe}_{(S)})}/M_{\mathrm{Fe}}+2x_5C_{p(Slag_{(S)})}/M_{slag}} \\
&\quad + \frac{k_{therea_5}(x_5)(x_{12}-x_{13})(1-\sqrt{(x_{13}/x_{12})})x_6/(x_5+x_6)}{x_1C_{p(\mathrm{Fe}_{(S)})}/M_{\mathrm{Fe}}+2x_5C_{p(Slag_{(S)})}/M_{slag}} \qquad (2.19)
\end{aligned}$$

$$\dot{x}_{14} = \left(\frac{x_9}{M_{CO}} + \frac{x_{10}}{M_{CO_2}} + \frac{x_{11}}{M_{N_2}} + \frac{x_{18}}{M_{\mathrm{H_2O}}} + \frac{x_{19}}{M_{\mathrm{CH_4}}} + \frac{x_{20}}{M_{\mathrm{C_3H_8}}} + \frac{x_{21}}{M_{\mathrm{H_2}}} + \frac{x_{22}}{M_{\mathrm{O_2}}}\right)\frac{R\dot{x}_{12}}{Vol} + \frac{Rx_{12}}{Vol}\left(\dot{x}_9 + \dot{x}_{10} + \dot{x}_{11} + \dot{x}_{18} + \dot{x}_{19} + \dot{x}_{20} + \dot{x}_{21} + \dot{x}_{22}\right) \quad (2.20)$$

$$\dot{x}_{15} = x_{16} \quad (2.21)$$

$$\dot{x}_{16} = x_{17} \quad (2.22)$$

$$\dot{x}_{17} = -\frac{2}{t_d\tau_1\tau_2}x_{15} - \frac{2\tau_1 + 2\tau_2 + t_d}{t_d\tau_1\tau_2}x_{16} - \left(\frac{1}{\tau_1} + \frac{1}{\tau_2} + \frac{2}{t_d}\right)x_{17} + u_1 \quad (2.23)$$

Under negative pressure, equations for the freeboard gas masses are given by

$$\dot{x}_9 = -\Pi x_9 + \frac{M_{\mathrm{CO}}}{M_C}k_{d\mathrm{C}}(X_{\mathrm{C}} - X_{\mathrm{C}}^{eq}) + 2M_{\mathrm{CO}}k_{air_1}k_{PR}x_{14} + \frac{M_{\mathrm{CO}}d_5}{M_{\mathrm{C}}} \quad (2.24)$$

$$\dot{x}_{10} = -\Pi x_{10} - 2M_{\mathrm{CO_2}}k_{air_1}k_{PR}x_{14} \quad (2.25)$$

$$\dot{x}_{11} = -\Pi x_{11} - M_{N_2}k_{air_2}k_{PR}x_{14} + \frac{d_5}{150} \quad (2.26)$$

$$\dot{x}_{18} = -\Pi x_{18} + d_{\mathrm{H_2O}} - 2M_{\mathrm{CH_4}}k_{air_1}k_{PR}x_{14} - 0.4M_{\mathrm{C_3H_8}}k_{air_1}k_{PR}x_{14} - 2M_{\mathrm{H_2}}k_{air_1}k_{PR}x_{14} \quad (2.27)$$

$$\dot{x}_{19} = -\Pi x_{19} + d_{\mathrm{CH_4}} + 0.5M_{\mathrm{CH_4}}k_{air_1}k_{PR}x_{14} \quad (2.28)$$

$$\dot{x}_{20} = -\Pi x_{20} + d_{\mathrm{C_3H_8}} + 0.1M_{\mathrm{C_3H_8}}k_{air_1}k_{PR}x_{14} \quad (2.29)$$

$$\dot{x}_{21} = -\Pi x_{21} + d_{\mathrm{H_2}} + 2M_{\mathrm{H_2}}k_{air_1}k_{PR}x_{14} \quad (2.30)$$

$$\dot{x}_{22} = -\Pi x_{22} + d_1(1 - \eta_{PC}) \quad (2.31)$$

The above equations for $\dot{x}_i$, $i = 9, \ldots, 11$ and $i = 19, \ldots, 22$ are valid for $x_{14} < 0$ (i.e. negative pressure). Under positive pressure they are given by

$$\dot{x}_9 = -\Pi x_9 + \frac{M_{\mathrm{CO}}d_5}{M_{\mathrm{C}}} + \frac{M_{\mathrm{CO}}}{M_{\mathrm{C}}}k_{d\mathrm{C}}(X_{\mathrm{C}} - X_{\mathrm{C}}^{eq}) - \frac{k_{PR}x_{14}x_9}{\zeta} \quad (2.32)$$

$$\dot{x}_{10} = -\Pi x_{10} - \frac{k_{PR}x_{14}x_{10}}{\zeta} \quad (2.33)$$

$$\dot{x}_{11} = -\Pi x_{11} - \frac{k_{PR}x_{14}x_{11}}{\zeta} + \frac{d_5}{150} \quad (2.34)$$

$$\dot{x}_{18} = -\Pi x_{18} + d_{\mathrm{H_2O}} - \frac{k_{PR}x_{14}x_{18}}{\zeta} \quad (2.35)$$

$$\dot{x}_{19} = -\Pi x_{19} + d_{\mathrm{CH_4}} - \frac{k_{PR}x_{14}x_{19}}{\zeta} \quad (2.36)$$

$$\dot{x}_{20} = -\Pi x_{20} + d_{\mathrm{C_3H_8}} - \frac{k_{PR}x_{14}x_{20}}{\zeta} \quad (2.37)$$

$$\dot{x}_{21} = -\Pi x_{21} + d_{\mathrm{H_2}} - \frac{k_{PR}x_{14}x_{21}}{\zeta} \quad (2.38)$$

$$\dot{x}_{22} = -\Pi x_{22} + d_1(1 - \eta_{PC}) - \frac{k_{PR}x_{14}x_{21}}{\zeta} \quad (2.39)$$

where

$$\Pi = \frac{[(2K_M/(t_d\tau_1\tau_2))x_{15} - (K_M/(\tau_1\tau_2))x_{16}]h_d}{(k_U u_2 + h_d)(\zeta)} \quad (2.40)$$

and

$$\zeta = (x_9 + x_{10} + x_{11} + x_{18} + x_{19} + x_{20} + x_{21} + x_{22}), \tag{2.41}$$

the total freeboard gas mass, and $T_l \approx 1500\,^{\circ}\mathrm{C}$ is the melting temperature of the steel.

2.2.2 The oxyfuel subsystem

A further contributor to furnace heating is the oxyfuel system [44]. In the current implementation it consists of 3 composite oxygen-and-fuel gas lances placed at an angle of 120^{o} adjacent from one another, at a 45^{o} pitch. The central core of each lance carries a stream of oxygen while the outer rim injects fuel gas. In one mode the lance acts solely for injection of oxygen in which case, some fuel gas is still injected for cooling the lance. In burner mode, the pressure and flow of oxygen are significantly reduced, allowing for efficient mixing with the fuel gas.

The inputs to the combustion reaction are fuel gas and O_2, both of which are approximately at room temperature. In this study the fuel gas has the following volume composition: 45.5% H_2, 27% CH_4, 19% CO, 4.7% CO_2, 1.8% C_3H_8 and 1.6% N_2.

The net enthalpy of the combustion reactions is given, in general, by:

$$\begin{aligned} \Delta H_{\mathrm{r,T}} &= (\Delta H_{\mathrm{T}})_P - (\Delta H^{\mathrm{o}})_R \\ &= (\Delta H_{\mathrm{T}} + \Delta H_f^o)_P - (\Delta H_f^o)_R \\ &= \Delta H_{\mathrm{r}}^o + (\Delta H_{\mathrm{T}})_P, \end{aligned} \tag{2.42}$$

where R and P refer to reactants and products; the reactants enter at room temperature. ΔH_{r}^o is the standard enthalpy of reaction and $(\Delta H_{\mathrm{T}})_P$ is the enthalpy of the products which leave the reaction at temperature T, relative to room temperature.

The values for ΔH_f^o, the standard enthalpy of formation, are commonly available [45], while the enthalpy ΔH_{T} is given by:

$$\Delta H_{\mathrm{T}} = \sum_i \int_{298}^{T} C_i dT, \tag{2.43}$$

where the sum is carried out over all the reactants or products and C_i is the specific heat of the element or compound i.

The heat energy contribution from the oxyfuel system can be derived from the reactions:

$$\begin{aligned} C_3H_8 + 5O_2 &\rightarrow 3CO_2 + 4H_2O \\ 2CO + O_2 &\rightarrow 2CO_2 \\ 2H_2 + O_2 &\rightarrow 2H_2O \\ CH_4 + 2O_2 &\rightarrow CO_2 + 2H_2O; \end{aligned}$$

N_2 is inert.

The resulting energy and mass balance for each reaction must take into account that the combustion is not complete. Factors such as temperature, nozzle design and combustion ratio dictate the mixing between the fuel gas and O_2 with the effect that η, the efficiency of mixing and combustion, is a strong function of the gas flow rates. Therefore η is an adjustable parameter that depends on the operating point of the oxyfuel burners. The resulting mass balances, in molar flow rate $\dot{N}_x$, are:

$$\dot{N}_{CO_2} = \eta(3\dot{N}_{C_3H_8} + \dot{N}_{CO} + \dot{N}_{CH_4})$$
$$\dot{N}_{H_2O} = \eta(4\dot{N}_{C_3H_8} + \dot{N}_{H_2} + 2\dot{N}_{CH_4})$$

The excess oxygen is given by

$$\dot{N}_{O_2} = \frac{d_{O_2}}{M_{O_2}} - \eta\big(5\dot{N}_{C_3H_8} + \frac{1}{2}\dot{N}_{CO} + \frac{1}{2}\dot{N}_{H_2} + 2\dot{N}_{CH_4}\big), \tag{2.44}$$

where d_{O_2} is the O_2 mass flow rate. Depending on the the burner mode of operation the excess oxygen will either report to the off-gas or the bath. In burner mode the low rate and pressure of injection mean that most of the oxygen is confined to the freeboard, while in lancing mode most of the high-speed oxygen stream will reach the bath. Integrating the above discussion into a format compatible with the original model derivation results in the following equations for the energy inputs from the oxyfuel system:

$$\begin{aligned}
p_{C_3H_8} &= -\frac{d_g X_{C_3H_8}}{M_{C_3H_8}}\{\eta(3\Delta H^o_{CO_2(T)} + 4\Delta H^o_{H_2O(T)}) + (1-\eta)(\Delta H^o_{C_3H_8(T)}) - \Delta H^o_{C_3H_8(298K)}\}\\
p_{CO} &= -\frac{d_g X_{CO}}{M_{CO}}\{\eta 2\Delta H^o_{CO_2(T)} + (1-\eta)(\Delta H^o_{CO(T)}) - 2\Delta H^o_{CO(298K)}\}\\
p_{H_2} &= -\frac{d_g X_{H_2}}{M_{H_2}}\{\eta(2\Delta H^o_{H_2O(T)}) + (1-\eta)(2\Delta H^o_{H_2(T)}) - 2\Delta H^o_{H_2(298K)}\}\\
p_{CH_4} &= -\frac{d_g X_{CH_4}}{M_{CH_4}}\{\eta(\Delta H^o_{CO_2(T)} + 2\Delta H^o_{H_2O(T)}) + (1-\eta)(\Delta H^o_{CH_4(T)}) - \Delta H^o_{CH_4(298K)}\}\\
p_{N_2} &= -\frac{d_g X_{N_2}}{M_{N_2}}\eta\Delta H^o_{N_2(T)}\\
p_{O_2} &= -\dot{N}_{O_2}\Delta H^o_{N_2(T)}
\end{aligned} \tag{2.45}$$

where X_i and M_i are the mass fraction and molar mass of gas i; d_g is the mass flow rate of the fuel gas and $H^o_{x(T)}$ is the enthalpy of compound (or element) x at temperature T - assumed equal to the bath temperature. p_x is the power (in [kW]) generated or consumed by x. Therefore, the net heat energy contribution from the oxyfuel system is $p_{12} = p_{C_3H_8} + p_{CO} + p_{H_2} + p_{CH_4} + p_{N_2} + p_{O_2}$.

2.2.3 Water cooling system

The water cooling has become a necessity in modern EAF design. This is mainly because of the high electrical power that is dissipated in the furnace. With this high power arc radiation it is important to cool the refractories that line the furnace walls and roof especially at flat bath conditions when the arc may be poorly insulated by foaming[10] [19]. It is possible that some contribution to the heating of the water cooling panels originates from the oxyfuel subsystem. However this is overshadowed by the excessive radiation from the arcs, and no literature has been found that studies the effect of oxyfuel radiation on the sidewalls.[11]

The energy lost to the cooling water system is given by

$$\Delta E = hv(T_{out} - T_{in}) \tag{2.46}$$

The temperature of the inlet and outlet flows are continuously measured. This makes the water cooling variables amenable for use as a feedback variable. While this may be so, the practical implementation of this variable set for feedback is not supported by the results that are presented in chapter 4.

2.2.4 Bath oxygen activity

The relationship between bath oxygen activity and carbon was described by Chou *et al.* [43]. The main formula is used here without the derivation (see the reference for details Chou *et al.* [43]):

$$\ln[\,\%\,\mathrm{O}][\,\%\,\mathrm{C}] \;=\; \ln P + \ln x_{\mathrm{CO}} - \ln K_{27} - \ln f_{\mathrm{C}} - \ln f_{\mathrm{O}}, \tag{2.47}$$

[10] When adequately foamed the arc is sufficiently shielded. Both foaming and water cooling have made possible the advent of ultra high power furnaces as they limit the erosion of the furnace refractories and sidewalls by arc radiation [46].

[11] A technique used to estimate the efficiency of the oxyfuel subsystem, is to monitor the temperature of the sidewalls adjacent to the burner lance. Increasing sidewall temperatures indicate a decrease in heat transfer to the scrap since the heat is now being transferred to the sidewalls instead of the scrap [40]. This indicates that the oxyfuel system will have an effect on the sidewall temperature, but it is expected to be relatively small under normal operation. A physical model for this behaviour is beyond the scope of this dissertation. However a state-space model based on the bulk furnace temperature and its effect on the water cooling temperature will be considered.

where

$$\begin{aligned}
\ln K_{27} &= 4.77 + \frac{2692.5}{T} \\
\ln f_{\mathrm{O}} &= 0.4606[\,\%\,\mathrm{O}] + 0.2994[\,\%\,\mathrm{C}] \\
\log f_{\mathrm{C}} &= 0.1666[\,\%\,\mathrm{C}] - 0.01585[\,\%\,\mathrm{C}]^2 + 9.9613 \cdot 10^{-7}[\,\%\,\mathrm{C}]^3(T-273) \\
&\quad +3.0246 \cdot 10^{-5}[\,\%\,\mathrm{C}](T-273) \\
\ln f_{\mathrm{C}} &= 2.303 \log f_{\mathrm{C}},
\end{aligned}$$

and f_x is the activity coefficient of component x, x_{CO} is the partial pressure of CO, K_{27} is the equilibrium constant for the reaction C+O=CO and $\ln P$ is the total pressure, assumed close to atmospheric, then $\ln P = 0$, since P is taken as the reference pressure. To obtain the dissolved bath oxygen, equation (2.47) must be solved (nonlinearly) for $[\,\%\,\mathrm{O}]$, at a given temperature and bath carbon - the latter are adequately modelled [5]. That (2.47) provides an adequate depiction of bath oxygen given bath carbon will be shown in the model fitting (chapter 5). The bath temperature lies within a confined range so that it has only a limited influence on $[\,\%\,\mathrm{O}]$; and, for bath carbon below $0.5\,\%\,\mathrm{C}$, the relationships are practically independent of temperature [36].

Alternatively, the bath oxygen can be determined from the prevailing slag FeO conditions [36]. The equilibrium constant of slag FeO is given by

$$K_{\mathrm{FeO}} = \frac{[a_{\mathrm{O}}]}{(a_{\mathrm{FeO}})} \approx \frac{[\,\%\,\mathrm{O}]}{\gamma_{\mathrm{FeO}} X_{\mathrm{FeO}}} \tag{2.48}$$

with

$$\log K_{\mathrm{FeO}} = -\frac{6320}{T} + 2.765, \tag{2.49}$$

where K_{FeO} can be obtained from standard thermodynamic tables, X_k is the mole fraction of component k and a_k is the corresponding activity. Therefore, given the slag FeO, the bath oxygen can be estimated or vice versa.

2.2.5 The reduced model

The simulation model as it stands has as its main drawback the long computational time. This becomes increasingly important when thousands of iterations of the model have to performed, especially during optimization. The object is then to obtain a reduced model that has fewer computations - by removing some unnecessary terms - while maintaining a reasonable level of accuracy compared with the original model. To establish notation, the reduced model will be referred to as $\mathcal{M}_{\mathcal{R}}$ and the original model as $\mathcal{M}$.

The system equations given in the previous section are valid for an entire tap. They describe the furnace conditions from the time that an initial basket charge is made through

refining until the final tap is made. An important assumption that stems from the model derivation is that the tap is a continuous uninterrupted process from start to end. Clearly this is rarely a case in practical furnace operation. Various changes can be made to the process at any stage during the tap; these include (among others): charging, levelling of input scrap, making additives, arcing, lancing, etc. In addition, there are also outright process interruptions due to delays, breakdowns, maintenance etc. These affect the validity of the assumption of process continuity to varying degrees. Some actions are directly accounted for in the model e.g. arcing, lancing, burner operation while others will simply invalidate the model.

The above discussion highlights the inherent unpredictability of the EAF operation. This leads to large variations in the various process variables between taps. A further complication is that very few of these variables are measured in the first place thus jeopardizing any efforts at increasing modelling accuracy.

One approach is to relax the assumption of process continuity, but this is accompanied by the burden of a more intensive modelling effort. This is better avoided. An alternative is to identify regions during a tap where the process is continuous and more consistent from one tap to the next. This is the approach followed by the current work. In particular, only the refining stage is isolated for study.

The choice of the refining stage leads to several advantages. Once an initial temperature measurement and sample have been taken at some initial time $t = t_1$, except for deslagging, the process is uninterrupted until a second measurement is made[12] (at $t = t_2$). These are the only times at which plant measurements are made in practice; these measurements can be used for model tuning. Furthermore, this is typically a flat bath stage when all melting has occurred; the modelling assumption of homogeneity is also valid. As far as bath conditions are concerned, consistency is assured from tap to tap.

Process variables that undergo significant change during refining are bath temperature, carbon and silicon concentrations (masses), masses of SiO_2 and FeO in slag and all the freeboard gases. Under the above assumption all masses of the bath and composite slag are at steady state - they can be treated as constants. The oxyfuel system injects large volumes of gases into the freeboard. Air entrainment is the only mechanism by which the furnace heat balance (and hence the bath temperature) can be affected by the freeboard gases; this happens only under negative pressure; otherwise for all practical purposes, the freeboard has no effect on the temperature and chemistry of the bath.

While air entrainment does represent a substantial energy loss, it is insignificant compared to contributions from arc input, bath oxidation and graphite injection. The relative

[12]The time at which the second measurement is taken in arbitrary: it depends on operator assessment of the progress of refining since the first measurement was taken.

contributions of these heat sources and sinks will be discussed in chapter 5. This motivates the omission of pressure from the reduced model.

With the above discussion and assumptions in mind, the model can be reduced since some of the states are unchanging or have little effect on the system dynamics under consideration: the time evolution of bath temperature and impurity concentrations. The modified system equations are given by

$$\begin{aligned}
\dot{x}_3 &= -k_{dC}(X_{\mathrm{C}} - X_{\mathrm{C}}^{eq}) \\
\dot{x}_4 &= -k_{dSi}(X_{\mathrm{Si}} - X_{\mathrm{Si}}^{eq}) \\
\dot{x}_7 &= \frac{2M_{\mathrm{FeO}}d_1}{M_{\mathrm{O_2}}} - \frac{x_7 k_{gr} M_{\mathrm{Fe}} d_5}{(m_{T(slag)} + x_7 + x_8)M_{\mathrm{C}}} + 0.13d_2 \\
\dot{x}_8 &= \frac{M_{\mathrm{SiO_2}}}{M_{\mathrm{Si}}} k_{dSi}(X_{\mathrm{Si}} - X_{\mathrm{Si}}^{eq}) + 0.045d_2 \\
\dot{x}_{12} &= (p_t + \eta_{ARC}d_4 - k_{VT}(x_{12} - T_{air}))/ \\
&\quad \left[\frac{m_{T(\mathrm{Fe})}C_{p(\mathrm{Fe}_L)}}{M_{\mathrm{Fe}}} + \frac{2m_{T(slag)} + 2x_7 + 3x_8}{M_{slag}} C_{p(slag_{(L)})}\right]
\end{aligned}$$

where the molar concentrations are given by

$$\begin{aligned}
X_{\mathrm{C}} &= \frac{x_3/M_{\mathrm{C}}}{m_{T(\mathrm{Fe})}/M_{\mathrm{Fe}} + x_3/M_{\mathrm{C}} + x_4/M_{\mathrm{Si}}} \\
X_{\mathrm{FeO}} &= \frac{x_7/M_{\mathrm{FeO}}}{m_{T(slag)}/M_{slag} + x_7/M_{\mathrm{FeO}} + x_8/M_{\mathrm{SiO_2}}} \\
X_{\mathrm{C}}^{eq} &= k_{XC}\left(\frac{m_{T(slag)}M_{\mathrm{FeO}}}{x_7 M_{slag}} + \frac{x_8 M_{\mathrm{FeO}}}{x_7 M_{\mathrm{SiO_2}}} + 1\right) \\
X_{\mathrm{Si}} &= \frac{x_4/M_{\mathrm{Si}}}{m_{T(\mathrm{Fe})}/M_{\mathrm{Fe}} + x_3/M_{\mathrm{Si}} + x_4/M_{\mathrm{Si}}} \\
X_{\mathrm{Si}}^{eq} &= k_{XSi}\left(\frac{m_{T(slag)}M_{\mathrm{FeO}}}{x_7 M_{slag}} + \frac{x_8 M_{\mathrm{FeO}}}{x_7 M_{\mathrm{SiO_2}}} + 1\right)^2
\end{aligned}$$

$m_{T(\mathrm{Fe})}$ and $m_{T(slag)}$ are the total masses of the slag formers and bath - both are assumed constant. At refining, the concentration of carbon and silicon in the bath is low (less that 0.1 % in weight); their effect on temperature is neglected. Furthermore, combined reduction of FeO in the slag by bath carbon and silicon is negligible when compared to that of graphite and oxygen injection, hence their contribution to x_7 (slag FeO) is omitted.

The heat balance changes accordingly. By the assumption of positive pressure, the heating losses due to air entrainment can be neglected: $p_6 = p_7 = 0$; the heat of combustion of CO can be eliminated since no oxygen is entrained: $p_3 = 0$. No continuous material feeds are made hence $p_8 = p_9 = 0$. A completely flat bath means $p_{10} = 0$ since these is no melting. The most significant components of chemical heat balance originate

from: bath oxidation p_2, graphite injection p_{11}; $p_1 + p_4$ has little effect on the heat balance since under refining conditions $\mathrm{Si\%} + \mathrm{C\%} < 0.25\,\mathrm{wt\,\%}$ and their overall contribution is negligible.

Over several taps, the average chemical energy contribution from each of the various sources will be discussed in chapter 5 - this also explains the choice of p_2, p_5 and p_{11} as the only chemical energy sources for $\mathcal{M}_{\mathcal{R}}$.

Thus, the equations for the heat balance are reduced to:

$$\begin{aligned} p_2 &= (-2H_{\mathrm{FeO}} d_1 / M_{\mathrm{O_2}})\eta_{\mathrm{FeO}} \\ p_5 &= \frac{d_1}{M_{\mathrm{O_2}}}(x_{12} - T_{\mathrm{O_2}})C_{p(\mathrm{O_2})} \\ p_{11} &= \frac{x_7 k_{gr} d_5 (\Delta H_{\mathrm{FeO}} - \Delta H_{\mathrm{CO}})}{(x_6 + x_7 + x_8) M_C} \\ p_t &= p_2 + p_5 + p_{11} \end{aligned}$$

The following map collects the parameters that are relevant to the reduced model:

$$\theta = \begin{bmatrix} k_{dC} \\ k_{dSi} \\ k_{gr} \\ k_{VT} \\ \eta_{ARC} \\ \eta_{\mathrm{FeO}} \end{bmatrix};$$

where k_{dC} and k_{dSi} are the rate constants for removal of carbon and silicon from the bath; k_{gr} is the graphite reactivity constant; η_{ARC} and η_{FeO} are the efficiencies of arc energy input and bath oxidation. The above equations also apply under negative pressure, particulary when the operating pressure is close to 0 Pa - this is assumed to be the prevailing condition, so that the $\mathcal{M}_{\mathcal{R}}$ is applicable under negative or positive pressure. This assumption is also supported by the relatively low contribution of the furnace pressure to the overall heat balance.

2.3 A typical tap

The following section essentially illustrates the previous discussions. The main aim is to demonstrate the dynamic behaviour of the various process variables under typical furnace conditions. These conditions are as close to the real operation as possible. Inputs and initial conditions are obtained from plant data as far as possible - these are discussed in detail in the chapters that follow. The refining stage of the simulation that follows is used throughout the dissertation to carry out the parameter estimation where the parameter

values will be chosen based on the difference between the simulation and the corresponding measured data.

2.3.1 Operating conditions

The furnace has a rated capacity of 80 ton[14], with a maximum power input of 40 MW. On average 86.3 ton of raw materials is charged onto a hot heel of approximately 5 to 10 ton, which is assumed to be at 1600 °C, slightly lower than the average 1650 °C specification on bath temperature at tap time. The freeboard volume is approximated as a cylindrical volume of 74 m^3 with a diameter of 5.6 m.

2.3.1.1 Inputs and initial conditions

The primary inputs to the furnace are the electrical arc input, the oxygen injection and fuel gas injection; another input is the graphite injection. Previous modelling [5] incorporated inputs such as DRI and slag, these do not exist as continuous inputs in the current process: they are part of the batch furnace charge instead. The choice of initial conditions will become clearer in later chapters.

2.3.2 The heat cycle

The heat cycle profile gives a graphic presentation of the power on (and off) time during meltdown and refining. Important events and delays are also marked by changes in the power profile. Also correlated to the power-on times are the oxygen and fuel gas inputs as the oxyfuel system cycles between burner and lancing (refining oxygen injection) modes. Figures 2.2 to 2.9 show the measured plant inputs and corresponding model outputs for one tap.

The off-times in the arc input (and oxygen) typically mark the time at which charges are made or when unscheduled delays occur. These off-times are accompanied by abrupt changes in pressure and the off-gas states.

Figure 2.3 shows a plot of the fuel gas and oxygen inputs. The variation in the levels of O_2 and fuel gas point to a change in the operating mode of the oxyfuel burners. The sharp rise in injected oxygen and slight decrease in fuel gas indicate the onset of oxygen lancing. At this stage the fuel gas serves only to cool the lance. After each basket charge, the oxyfuel system operates in burner mode, then switches to oxygen lancing when sufficient liquid metal is generated [15]. The operating mode after the third basket is strictly oxygen

[14] It is typical for the tap to operate with a total bath mass of up to 86 ton.

[15] This decision is typically based on the total electrical input consumed up to that time - the consumption of electrical input is a good indicator of the progress of melting in the bath.

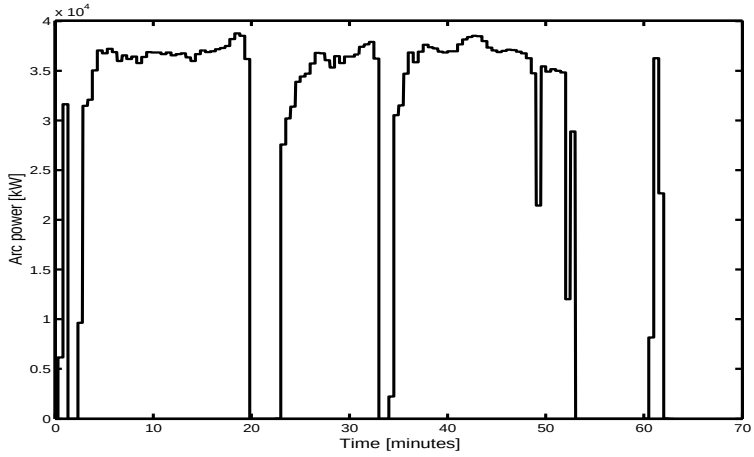

Figure 2.2: Arc input for an actual tap. The times at which power is off - $-1 < t < 1$, $17 < t < 19$ and $31 < t < 33$ minutes - are the charging times when raw material additions are made into the furnace. The refining stage begins near the end of tap. It is characterized by intermittent drops in power to enable temperature measurements. Temperature measurements were obtained at $t = [47, 49, 51]$ minute. The long dead time from 54 to 60 minutes marks the time at which oxygen injection was used to lower the high bath carbon of Tap 1 (see table A.1 of the appendix).

lancing since sufficient hot metal is available from melting of the previous two baskets.

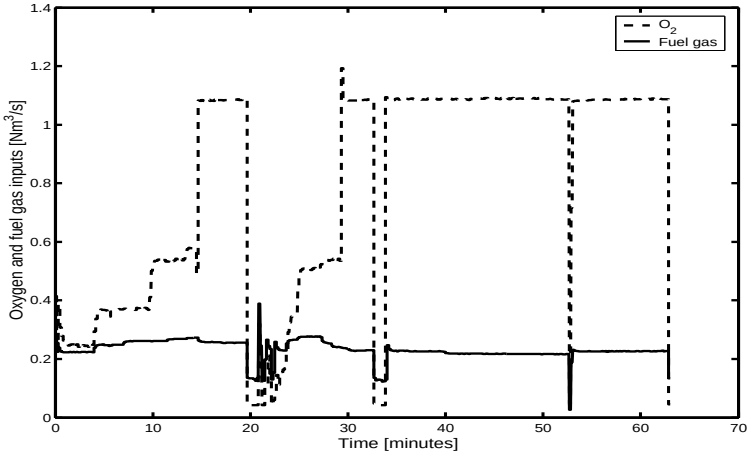

Figure 2.3: Oxygen and fuel gas input.

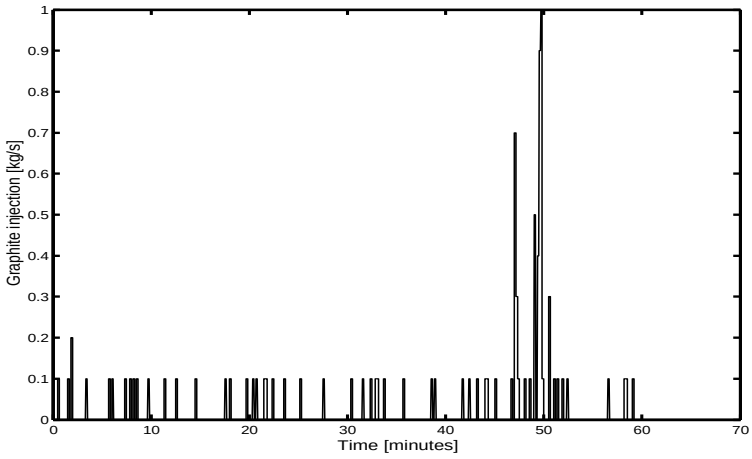

Figure 2.4: Graphite.

From the previous model derivation, it was assumed that the hot metal charge was the only source of carbon and silicon, and that comparatively low levels are to be found in the scrap and DRI charge [39]. The converse is true in the present case (and in most EAFs with little or no hot metal charge): the scrap is the main source of silicon and some carbon - while anthracite is the primary source of carbon. Therefore, in addition to decreasing in proportion to their distance from equilibrium, the bath carbon and silicon will also increase in proportion to the melting rate of scrap and dissolution of anthracite (assumed to be proportional to the scrap melting rate). Hence figure 2.6, depicting a gradual increase in carbon and silicon followed by an asymptotic decrease as the scrap melting and anthracite dissolution proceed. Figure 2.5 depicts the progress of melting as more scrap is added with every charge, first at $t = 0$, $t \approx 21$ and $t \approx 33$ minutes [16]. The corresponding change in temperature is shown in figure 2.9.

The melting of scrap can result in excessive heat loss during the initial stages of a tap when the liquid steel mass is significantly lower than the scrap mass T_l. This can result in a liquid temperature drop that is well below the melting point of steel. Physically, this means that some of the liquid steel solidifies. This effect is captured in the model by ensuring that all liquid steel below T_l is solidified. This is reflected in equations (2.10) and (2.11). Furthermore, the heat loss from liquid steel is made proportional to the fraction of liquid steel to total steel mass $x_2/(x_1 + x_2)$. This effectively prevents the instantaneous drop in liquid temperature (physically not possible) that would otherwise be reported by

[16]The rate of melting is governed by the coefficients k_{therea_1} and k_{therea_5}, their values will determine the extent of melting between charges. Melting may be complete between charges (especially when light scrap is used) or significant levels of solid scrap may be carried over to be melted with the additional charge. The values of the melting coefficients can only be estimated when an accurate measurement of the solid and liquid masses is available.

the model when scrap is added. This discussion also applies to liquid and solid slag.

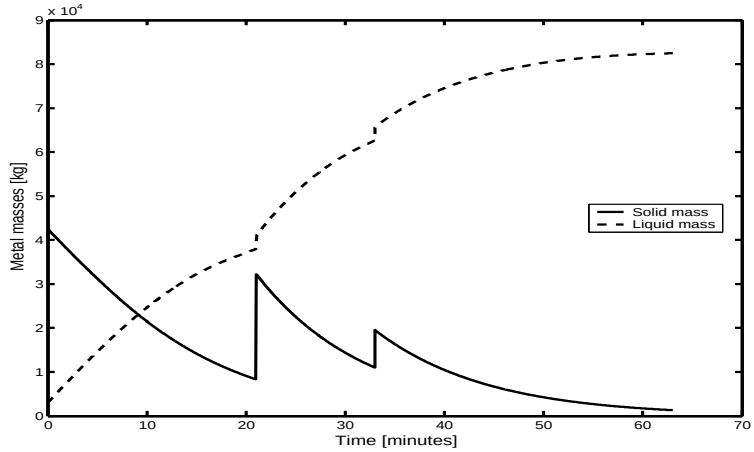

Figure 2.5: Solid and liquid metal masses.

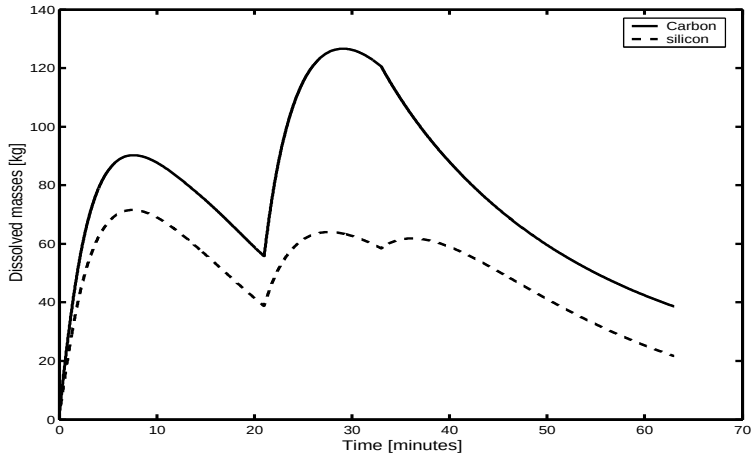

Figure 2.6: Masses of dissolved carbon and silicon.

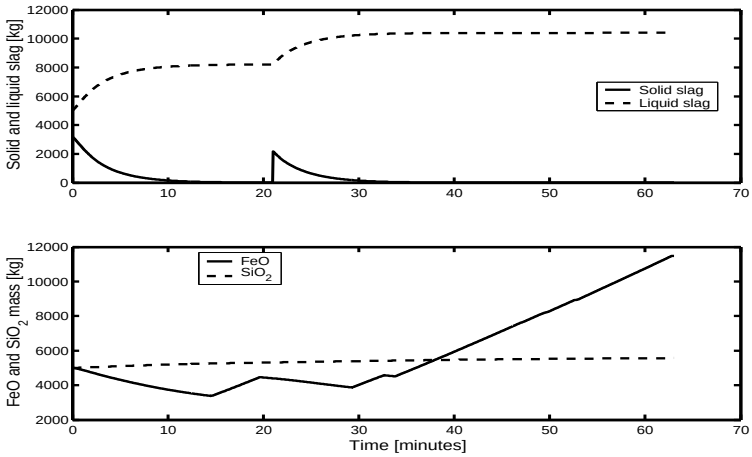

Figure 2.7: Mass of slag and associated oxides.

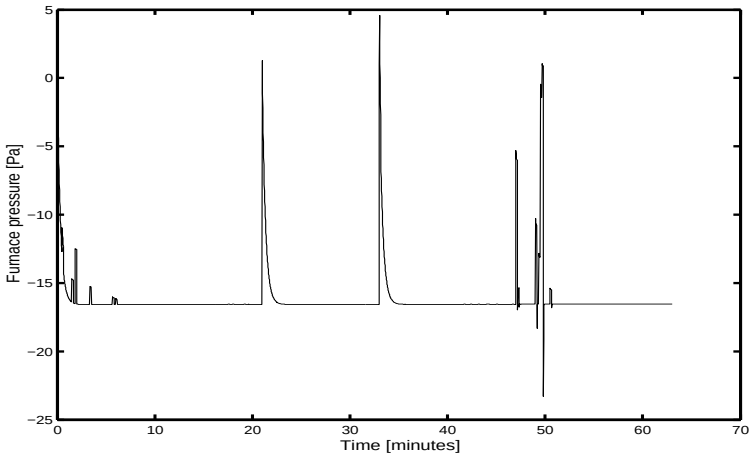

Figure 2.8: Furnace pressure.

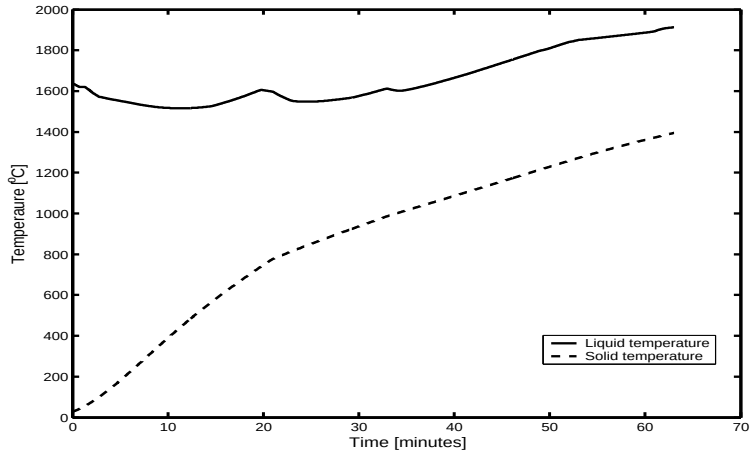

Figure 2.9: Metal temperature.

2.4 Conclusion

This chapter presented a description of a practical operation of an EAF process. The increase in bath mass, silicon and carbon were incorporated into the model to depict the progress of melting and the pickup of carbon and silicon.

Chapter 3

System identification

System identification (SID) is a broad field that deals with mathematical modelling of a process from experimental data. First a mathematical model of the system is formulated from observation of the process. The model is then adjusted to reduce its error relative to the process data. The final test of the model adequacy is how well it is able to represent the data. The purpose for this model design will determine how adequate the model is: feedback control might allow a less conservative model, while simulation and prediction may require better accuracy.

This chapter presents an overview of the methods and procedures commonly used for system identification. These will be used to obtain the results presented in the chapters that follow.

Any modelling exercise is frequently just an approximation of the real process. Many factors influence the process behaviour, some are too complex to model satisfactorily while others are simply not well understood. The object is then to model the process to capture important process interactions in order to fulfill the intended purpose of the model. All behaviour that is unaccounted for will constitute modelling errors. These generally result from errors in initial states, disturbances, model parameters and the model structure.

Section 3.1 presents an overview of the SID process. This is followed by a discussion of the parameter estimation problem in section 3.3. The specific problems of selection of appropriate error functions and regularization are discussed in sections 3.4 and 3.5. Model validation is discussed in section 3.6; this is followed by a brief chapter summary.

3.1 The SID loop

The system identification process follows four distinct steps [37]:

- *Experiment design and data collection*

  This stage of the process centres around the collection of process data that best

depicts the response of the process outputs to inputs. This data must be maximally informative, and therefore requires careful experiment design where decisions are made about the particular input-output set that must be measured and when to measure (including the frequency of measurement). At all times the various constraints will hold - such as practical limitations on inputs, and operational limitations dictated by production requirements in the case of industrial plants.

- *Model structure selection*
  Based on initial inspection of the data, a set of suitable candidate models is selected for evaluation. These models can be existing generic input-output mappings (such as ARX, NARX, etc); or a combination of physically based models that are derived from prior knowledge of process behaviour. The latter (called grey box models) reflect the basic physical laws governing the process and are predominantly characterized by adjustable parameters that have physical significance. Black box models however have parameters whose adjustment could lead to accurate depiction of the input-output relationship without regard to the internal physics of the process. This is said to be the most crucial yet difficult part of the SID procedure. For this dissertation, the model selection is not required since the model derived by Bekker [5] will be used as the basis for the SID; however, some modelling has been done (see chapter 2). Strictly, a grey box nonlinear model will be used. Possible model choices are the reduced or the linearized model.

- *Model selection/fitting*
  Once a candidate set of models is selected, the next step is to evaluate their performance/suitability against the collected data. A successful model must be able to reproduce the measured data as well as possible. In the case of this dissertation the model selection is essentially a selection of the parameter set (values) for which the model delivers acceptable results.

- *Model validation*
  Validation constitutes the final step where the successful model is tested for suitability for its intended purpose. This can be simulation or control design.

The above procedure is iterative. It may be necessary to iterate from step 1 to 4 as the model evolves until it is deemed suitable. An initial pass may fail because: the data were not informative enough to guide model selection, the model was not appropriate enough

or that it did not lend itself well to numerical procedures required to carry out the fit. Figure 3.1 illustrates the SID loop - it presents a combination of the procedures outlined in Ljung [37] and Norton [38].

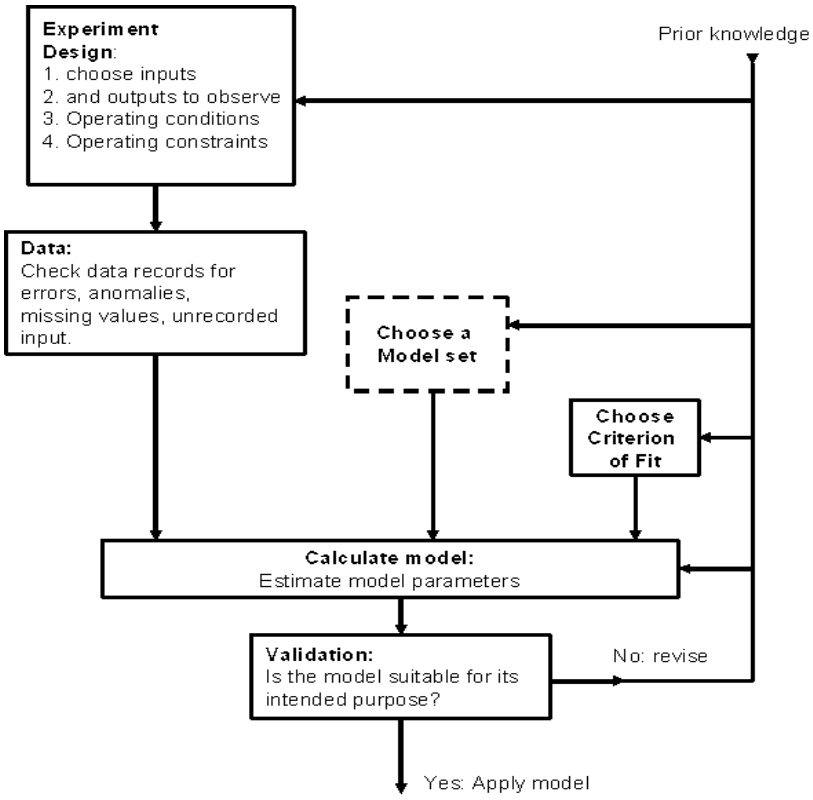

Figure 3.1: The SID loop [37, 38].

3.2 Prediction error methods

Prediction error (PE) methods deal with the ability of a model to predict new data given some sequence of previous data, $Z^{t-1} = [y(1), u(1), y(2), u(2), \ldots, y(t-1), u(t-1)]$. The PE is then given by

$$\varepsilon(t, \theta) = y(t) - \widehat{y}(t|\theta), \tag{3.1}$$

where $y(t)$ is the measured output and $\widehat{y}(t|\theta)$ is the model output at t, given some parameter vector θ. The error originates from unmodelled dynamics or measurement noise in its broadest sense. For successful prediction, the model output $\widehat{y}(t|\theta)$ must be forced to be as close to $y(t)$ as possible by appropriate choice of θ. That is, at $t = N$, select $\widehat{\theta}_N$ so that the PE's $\varepsilon(t, \widehat{\theta}_N)$, $t = 1, 2, \ldots, N$, become as small as possible [37].

The model output is given by

$$\mathcal{M}(\theta) : \widehat{y}(t|\theta) = g(t|Z^{t-1}, \theta) \tag{3.2}$$

Recast in state-space form, (3.2) becomes:

$$\mathcal{M}(\theta) : \begin{cases} \dot{x} = f(t, x, \theta, u) \\ \widehat{y} = h(t, x, \theta, u) \\ x(0, \theta) = x_0 \end{cases}$$

where $x \in R^n$, $u \in R^m$, $y \in R^p$ and $\theta \in R^q$ are the state, input, output and parameters of the system; x_0 is the initial condition vector. The input $u(t)$ is defined on $[0, T]$.

Using initial conditions x_0 and past data, from $t = 1$ to $t = N - 1$, determine θ that minimizes $\varepsilon(N-1, \theta)$. Then at $t = N$, select $\widehat{\theta}_N$ so that the prediction errors $\varepsilon(t, \widehat{\theta}_N)$, $t = 1, 2, \ldots, N$, become as small as possible.

3.3 Parameter estimation

The next step in SID is parameter estimation. At this stage, a suitable model set has been selected. The search for the best model within the set then becomes the problem of estimating θ [37]. The selection of parameters is based on how closely they allow the model to approximate the plant behaviour. That is, a set of parameter values for which the model output coincides (as well as possible) with the plant output under the same inputs and initial conditions. (The notation used in this section closely follows that of Ljung [37]).

The closeness between the model and the plant is easily determined by evaluating the error between the model output and the plant output. Assuming some parameter θ_* has been selected, the error of the corresponding model $\mathcal{M}(\theta_*)$ is defined as

$$\varepsilon(t, \theta_*) = y(t) - \widehat{y}(t|\theta_*), \tag{3.3}$$

that is, the difference between the plant output $y(t)$ and the model output $\widehat{y}(t|\theta_*)$ given the parameter θ_*. The error is evaluated at $t = 1, 2, \ldots, N$, from N input-output data points in the data record. The model output is given by the system

$$\mathcal{M}(\theta) : \begin{cases} \dot{x} = f(t, x, \theta, u) \\ \widehat{y} = h(t, x, \theta, u) \\ x(0, \theta) = x_0 \end{cases}$$

The parameter estimation problem can then be stated as

$$\widehat{\theta} = \underset{\theta \in D}{\arg\min} V_N(\theta) \tag{3.4}$$

where

$$\begin{aligned} V_N(\theta) &= \frac{1}{N} \sum_{t=1}^{N} l(\varepsilon(t, \theta)) \\ &= \frac{1}{N} \sum_{t=1}^{N} l(y(t) - \widehat{y}(t)), \end{aligned} \tag{3.5}$$

$y(t)$ and $\widehat{y}(t)$ are (respectively) the measured and model outputs at measurement time t; and $l(\cdot)$ is a scalar-valued function that is applied to the error $\varepsilon(t, \theta)$. A common choice is $l(\varepsilon) = \frac{1}{2}\varepsilon^2$, the least squares error. However, the least squares estimate suffers from the drawback that large errors are given more emphasis such that one large error could be allowed to dominate the resulting estimate. This is severely detrimental when outliers or bad data are present in the measurements - the results could become useless. An alternative is $l(\varepsilon) = \frac{1}{2}|\varepsilon|^R$, where R is chosen as $R = 1$ [47]. The resulting output will be the median of the data points instead of the mean which can be dominated by large-error data points.

Many approaches exist for solving (3.4) and some are built into software packages such as Matlab and Maple. For smooth error functions ($V_N(\theta)$) gradient-based methods can be successfully employed to determine θ. With this approach an iterative update of θ is carried out in the direction of steepest descent of the error function, i.e.

$$\theta^{\tau+1} = \theta^{\tau} - \eta \nabla V_N|_{\theta^{\tau}} \tag{3.6}$$

where $\nabla V_N|_{\theta^{\tau}}$ is the gradient of V_N evaluated at θ^{τ} in the iteration step τ; η is the learning rate. The iteration continues until $\nabla V_N = 0$ or some other stopping criterion is satisfied. A detailed discussion of steepest descent and other optimization methods is given in Bishop [47].

3.3.1 Handling constraints

Physically derived models often have parameters that have physical relevance. Their values will vary from process to process but will always lie within specific ranges that are practically feasible. Depending on the error criterion, the resulting parameters may be able to minimize the error but their values may not be justifiable in practice. This may lead to a problem of exaggerating certain process routes at the expense of others or allow behaviour that is totally erroneous: such as negative arc efficiencies and negative heat losses.

At a minimum, the parameter values must be confined within ranges that prevent behaviour that is completely erroneous. This applies to the sign and expected order of magnitude. On the other hand, sufficient freedom must be allowed so that reasonable variation can take place - this will account for the inherent variability in the process and errors that may be implicit in the modelling i.e. moderate model errors can offset by appropriate adjustment of the parameters.

Bounded constraints can be applied to the parameters so that the parameter estimation problem then becomes

$$\widehat{\theta} = \underset{\theta \in D}{\arg\min} V_N(\theta) \tag{3.7}$$

subject to

$$\theta_{min} < \theta < \theta_{max} \tag{3.8}$$

Several methods exist for augmenting the original penalty function in order to transform the constrained optimization problem to an unconstrained one [48, 49]. The main idea is to increase the penalty function value proportionally to the extent of constraint violation: the penalty function value increases as the parameters approach the constraints and is further inflated for as long as the constraint violation persists. These methods are, however, inefficient and have been replaced by methods that solve the Kuhn-Tucker (KT) equations[1] [50].

3.4 Norm selection

The original LSE penalty function may not be sufficient for some situations. One of the drawbacks of the standard LSE error function is that is responds significantly to data points that have the largest error. These outliers may well be valid data that represent extreme regions of plant operation; or they may result from incorrectly labelled data. These few outliers, (whatever their origin) will lead to values of the estimate that are

[1] The parameter estimation for the model fit will be carried out using the Matlab function **fmincon**(), this implements the Kuhn-Tucker equations to solve the constrained minimization problem.

strongly biased to the outliers while data that are representative of typical plant operation will be poorly fitted.

This situation can be remedied by using influence functions (subsection 3.6.1) for detecting outliers. In many cases, however, this may not be the most efficient procedure - in the current format the procedure relies on simulation results which are computationally expensive. Then the selection of an appropriate error function is a viable alternative.

The so-called robust norms have their origins in robust statistics [37, 47]; the idea is to use norms (error functions) that are robust to unknown variation in the *pdf* of the innovations (the past prediction errors i.e. that part of the output that is not predicted by the past errors). The Minkowski-R error function is given by Bishop [47] as

$$E = |\varepsilon|^R, \tag{3.9}$$

which reduces to the standard LSE when $R = 2$. When a large value of R is chosen, the error will tend to be dominated by a (generally) small number of outliers. However, for $R < 2$ the error will tend to give equal weight to all data points, reducing sensitivity to outliers [51]. When $R = 1$, a minimum error solution will result in a conditional *median* as opposed to the *mean* of the data.

To illustrate [47]: given the error function

$$E(y) = \sum_n |\widehat{y} - y^n|, \tag{3.10}$$

and minimizing with respect to $\widehat{y}$, leads to

$$\frac{\partial E}{\partial \widehat{y}} = \sum_n sign(\widehat{y} - y^n) = 0, \tag{3.11}$$

where

$$sign(x) = \begin{cases} -1 & x < 0 \\ 0 & x = 0 \\ 1 & x > 0 \end{cases} \tag{3.12}$$

To satisfy (3.11), $sign(\widehat{y} - y^n)$ must have an equal number of points greater than and less than zero - a condition that is satisfied when $\widehat{y}$ is the median of the data y^n. If data point y^n happens to be very large, it will not have undue influence on the solution for $\widehat{y}$.

While the absolute error is less sensitive to outliers, it does result in a biased estimate. That is, given some true value of the parameter vector θ^*, the estimate $\widehat{\theta}$ obtained using the absolute error with infinite data will result in a finite $\delta = E[\theta^* - \widehat{\theta}]$. Of primary concern in the estimation is to obtain a model that closely resembles the actual process, while maintaining the parameters within reasonable practical limits; the problem of finding the true parameter is secondary. In any event, it is not possible to determine the value of this bias since the real value of the parameter is unknown - nor can it be known perfectly, since the model is at best only an approximation of the process.

3.5 Regularization

In many applications the nonlinear least square (NLS) problem may be ill-conditioned, in the sense that the Hessian is ill-conditioned; or if the number of parameters is greater that the number of outputs, then the solution may not be unique, the parameters can take on any number of values. Regularization can be employed to impose constraints on the parameters, especially when they have practical significance. In particular, when θ has many parameters the new penalty function can have the form [37]:

$$\widetilde{V} = V + \delta\Omega \tag{3.13a}$$

$$\Omega = |\theta - \theta^{\#}|^2 \tag{3.13b}$$

where choosing $|\theta - \theta^{\#}|^2$ as the regularizing term penalizes the difference between θ and some fixed point $\theta^{\#}$. Some of the parameters will have a lesser influence on $\widetilde{V}$; these will tend the most to $\theta^{\#}$. A large value of δ will force more parameters to the vicinity of $\theta^{\#}$.

The choice of $\theta^{\#}$ will then dictate the default values of the parameters in θ that have the weakest influence on the system response. Regularization has the effect of pulling these parameters to known values. On the other hand, this may indicate that these parameters could have been disregarded from the estimation at the outset. Or, irrespective of the influence on system response, $\theta^{\#}$ can be chosen to contain default values for parameters whose values are well known. This choice will be informed by prior knowledge of the practical values of some parameters in θ. To reduce computational burden, it may be preferable to remove a well-known parameter from the estimation problem since the search space increases exponentially with the number of parameters.

An alternative interpretation is that when the matrix $\frac{\partial^2 V}{\partial\theta^2}$ is ill-conditioned, the term $\delta\Omega$ can be chosen to improve the conditioning, hence the name *regularisation*. The choice $\Omega = |\theta - \theta^{\#}|^2$ results in

$$\frac{\partial\widetilde{V}^2}{\partial\theta^2} = \frac{\partial^2 V}{\partial\theta^2} + \delta I, \tag{3.14}$$

thus making the Hessian better conditioned. This essentially translates to the previous interpretation where the conditioning of the Hessian matrix will determine the sensitivity of the error to the specific parameters - ill-conditioning points to an imbalance in influence of the parameters on the error function. The relative influence of a parameter on the error function is proportional to the inverse of the singular value of the Hessian corresponding to that parameter. That is, the smallest singular value corresponds to a parameter for which the error function has the largest curvature (in the direction of the corresponding eigenvector).

3.6 Model validation

Once a suitable model has been obtained - in this case, one whose parameters allow it to meet some performance criterion - the next step is to determine if it is adequate. That is, whether the model meets its intended purpose: to act as a predictor of process behaviour. One approach is to evaluate the variance in the parameters. Relative to the parameter value, a high variance in the estimate indicates an anomaly or a large uncertainty in the parameter values obtained [49].

An alternative method is to analyse the residuals [37]. The resulting sequence of the residuals should be small. A small cross-correlation (auto-correlation) in the residuals confirms the common assumption (and requirement) that the error sequence is white i.e.

$$R_N^{\varepsilon}(\tau) = \frac{1}{N}\sum_{t=1}^{N-1}\varepsilon(t,\widehat{\theta}_N)\varepsilon(t+\tau,\widehat{\theta}_N), \tag{3.15}$$

should be small for $\tau > 0$. In addition, the error sequence must be uncorrelated with the input i.e. $R_N^{\varepsilon,u}(\tau)$ must be small; where

$$R_N^{\varepsilon,u}(\tau) = \frac{1}{N}\sum_{t=max(1,1-\tau)}^{min(N,N-\tau)}\varepsilon(t,\widehat{\theta}_N)\varepsilon(t+\tau,\widehat{\theta}_N), \tag{3.16}$$

effectively computing the correlation between the input and error sequences shifted relative to each other via τ.

Another practical method of validation is simulation. Similar inputs are applied to the model and the true system. The difference between the two outputs should be small. The off-line equivalent of the procedure is to test that the model is able to produce the right input-output relationship for new data. This data not used for estimation is called *validation* data set. The set of data to which the model was fit, is called the *estimation* or *test* data set.

3.6.1 Influence function

The idea behind the influence function is to monitor the effect of outliers on the final parameter estimate [37]. It is prudent to remove (or reduce the influence of) any observation that has an overly predominant effect on the error function, since the data point (observation) may not be representative of the underlying process. This can happen due to drastic errors in measurement equipment or simple user-induced errors from inferior data collection methods (such as incorrectly matched or labelled input-output data pairs).

Practically, to determine the influence of a data point on the final estimate, compute

$$\mathscr{I} = \delta^T \delta \tag{3.17}$$

with

$$\delta = \widehat{\theta}_N - \widehat{\theta}_{N,k} \tag{3.18}$$

where $\widehat{\theta}_N$ is the estimate obtained for the entire data set and $\widehat{\theta}_{N,k}$ is obtained when data point k is excluded. Any data point that has a large influence on the estimate will lead to an equally large $\mathscr{I}$, which is essentially the euclidian distance between $\widehat{\theta}_N$ and $\widehat{\theta}_{N,k}$.

The practical application of the influence function is to identify data points that deviate significantly from the overall data set. A related approach is to monitor the error that is contributed by each data point. This is residual analysis.

3.6.2 Residual analysis

Residual analysis is another tool that can be employed to identify outliers. Once a reasonable model has been found - one that describes the majority of the underlying process data - residual analysis will reveal data points for which the error is significantly large. These data points the model was not able to reproduce are called the residuals, simply:

$$\varepsilon(t) = \varepsilon(t, \widehat{\theta}_N) = y(t) - \widehat{y}(t, \widehat{\theta}_N) \tag{3.19}$$

Any data point for which (3.19) is inordinately large may indicate that it is inadequately represented by the model. This may occur as a result of gross errors in data recording or collection (bad data) and when the system is operating in a region that is not adequately modelled (outlier).

In addition, the residuals have a lot to say about the quality of the model [37] - a good model will have small residuals. A further property of a good model is that the residuals must be uncorrelated with any past inputs; if they are, then some of the inputs were poorly modelled for in the first place. Furthermore, the auto-correlation of the residuals must be white i.e. they must not be correlated.

The relationship between the method of influence functions and residual analysis is that the method of influence functions shows the effect of the data on the estimate, while the residual analysis shows the effect of each data point on the model error.

3.7 Statistical properties of the estimates

Once a single-point estimate of the parameters is obtained, the question of the reliability of the estimate arises. That is, what is the level of confidence associated with the parameters?

This problem can be addressed by determining the variance of the estimate. A high confidence is assured for parameters with the smallest variance. This variance can be used to determine the confidence intervals that are commonly associated with any of the important variables in the parameter estimation: residuals and their correlations as well as the parameters themselves. The following equations for estimating the confidence bounds were derived in Ljung [37].

3.7.1 Confidence interval

Assuming that the kth component of the estimated parameter vector θ_N obeys

$$\sqrt{N}(\widehat{\theta}_N^{(k)} - \theta_0^{(k)}) \in As\, N(0, P_\theta^{(kk)}), \tag{3.20}$$

where $P_\theta^{(kk)}$ is the (k,k)th diagonal element of the matrix P_θ and θ_0 is the true parameter. That is, the variable $\sqrt{N}(\widehat{\theta}_N^{(k)} - \theta_0^{(k)})$ converges in distribution to a Gaussian distribution. Then, the probability that the estimate $\widehat{\theta}_N^{(k)}$ lies in the vicinity of the true parameter can be obtained from

$$P(|\widehat{\theta}_N^{(k)} - \theta_0^{(k)}| < \alpha) \approx \frac{\sqrt{N}}{\sqrt{2\pi P_\theta^{(kk)}}} \int_{|x|<\alpha} e^{-x^2 \cdot N/(2P_\theta^{(kk)})} dx, \tag{3.21}$$

the integral over a normal distribution with zero mean and variance $\sigma^2 = P_\theta^{(kk)}/N$.

A common requirement is to specify a 95 % (or other) confidence interval on the estimate. Then, using (3.21), a probability value P^* is specified for which α must be determined iteratively. At each iteration, the integral must be evaluated and α adjusted appropriately until $P(|\widehat{\theta}_N^{(k)} - \theta_0^{(k)}| < \alpha)$ is close to P^*. This procedure is commonly simplified by the use of statistical tables where probability values P^* are given along with the corresponding α [52] from which the bounds can be estimated. The bounds on the parameter will be $\theta_N^{(k)} - \alpha < \widehat{\theta}_N^{(k)} < \theta_N^{(k)} + \alpha$ with a confidence level of P^* (typically chosen as $P^* = 0.95$, the 95 % confidence level).

3.7.2 The covariance matrix

The covariance of the parameters can be determined from

$$\mathrm{Cov}\,\widehat{\theta}_N = \frac{1}{N} P_\theta, \tag{3.22}$$

where P_θ can be calculated from

$$P_\theta = \lambda_0 [E\psi(t, \widehat{\theta}_0)\psi^T(t, \widehat{\theta}_0)]^{-1} \tag{3.23}$$

where λ_0 is the variance of the zero mean error sequence and $\psi(t,\widehat{\theta}_0)$ is the derivative of the error with respect to θ - it is calculated as $\psi(t,\widehat{\theta}) = -\frac{d}{d\theta}\varepsilon(t,\theta)|_{\theta=\widehat{\theta}}$. These variables must be estimated at the true θ which is generally not known; therefore, they are approximated as [37]:

$$P_{_N} = \widehat{\lambda}_N \left[\frac{1}{N}\sum_{t=1}^{N}\psi(t,\widehat{\theta}_0)\psi^T(t,\widehat{\theta}_0)\right]^{-1} = \widehat{\lambda}_N \left[V''(\theta_N)\right]^{-1} \tag{3.24}$$

$$\lambda_N = \sum_{t=1}^{N}\varepsilon^2(t,\widehat{\theta}_N) \tag{3.25}$$

The above equations apply to the case of a continuous process. For the EAF, the refining stage is a batch process with only a few data points available per tap. To form the error function, the model error is evaluated for each tap at all the available data points and all the tap errors are summed to obtain an total error over all taps. This final error is deemed equivalent to $\varepsilon(t,\theta_0)$.

3.8 Conclusion

The method of influence functions helps to identify outliers so that they can be eliminated from the data set. Some of the data cannot be perfectly isolated. Robust norms ensure that the detrimental effect of these latter outliers is reduced. Regularization is a good mechanism to build prior knowledge into the error function and to deal with parameters that are insignificant. Finally, model validation can be used to assess the adequacy of a model for its intended purpose. The methods and tools discussed in this chapter will be used to obtain and analyse some of the results of the chapters that follow.

Chapter 4

Experiment design and data analysis

This chapter presents the first step in the system identification process: experiment design. It involves the progress from the information that is required in order to run a realistic simulation of the furnace to the procedures followed and the actual data collection process. It also gives a brief presentation and analysis of the data collected.

The first section (4.1) outlines the required information in order to run a realistic simulation of the process - this simulation is an essential building block for model fitting. Section 4.2 gives the process and detail on the specific requirements for measurement of plant input and output data in order to carry out successful parameter estimation - the discussion will centre around identifiability (and distinguishability). Some requirements on the necessary initial conditions will also be given. Section 4.3 details the data collection process; this includes a discussion on information available in practice and how far it fulfills the requirements. Finally, section 4.4 summarizes the data and draws comparisons with data presented in other literature; it will also include an analysis of the data and how they relate to furnace practice.

4.1 Model simulation requirements

In order to accurately depict the actual process, the conditions that prevail on the process must be known. For the model, it is important that information pertaining to all the model variables is available - this will be the initial conditions, the inputs, outputs and states. Many of the requirements are obvious and implicit from operation of the model however, they will be stated for completeness.

4.1.1 Model variables

A successful simulation will use information from several variables that are specific to every furnace practice. The obvious and main motivation for the need for such information is that if the simulator is to represent a particular furnace, it must be subject to the conditions that prevail on the real process. The objective in collecting the information is to obtain a picture of the process that is as realistic as possible.

4.1.1.1 Model inputs

The primary model inputs are: the average electrical power input, oxygen injection, fuel gas injection, graphite injection, DRI and slag input flow rates and the off-gas variables off-gas mass flow rate and the slip gap width. In the original model derivation slag and DRI were treated as continuous inputs, deposited through the furnace roof from conveyor belts. In this case however, all DRI and slag input is made as part of the furnace charge, and contributes instead to the initial conditions. All other inputs are continuous.

The fuel gas and oxygen inputs serve two roles. In burner mode, fuel gas is combusted to transfer heat energy to the bath. In lancing mode, the oxygen flow rate is significantly increased while that of fuel gas is reduced, serving only to cool the lance and shape the oxygen stream. The distinct changes in these flow rates are important to determine the prevailing mode of operation so that the appropriate effect can be produced from the model: heat transfer in burner mode and bath oxidation in lancing. The pressures of these material flows are directly correlated with the flow rates, providing alternative information to distinguish operating modes; these are, however, not used in this dissertation.

The width of the slip gap u_2 [m] determines the amount of air that is entrained into the duct at the exit of the fourth hole. This air reacts with and cools the furnace off-gas [19]. The product is extracted via the off-gas system at the flow rate given by u_1 [kg/s]. The variables are important to quantify the amount of gas that leaves the furnace and hence its contribution to the furnace mass balance. They are also important for the downstream properties of the off-gas such as temperature and composition. These have been dealt with in Bekker [5] where the main aim was a detailed study of the off-gas system; this is outside the scope of the current work, where the main focus is on the furnace itself.

4.1.1.2 Initial conditions

Unlike in linear systems (where superposition applies) the role of initial conditions cannot be ignored for this nonlinear system. The correct initial masses and temperatures must be available in order to obtain a true representation of the process.

A hot heel practice is adopted to prevent mixing between the steel and slag during tapping [7]. It is also used in modern furnaces where steel-slag mixing is not a problem since bottom tapping is used. However, this practice persists because of the added advantage of maintaining a high furnace temperature during the turnaround time before the next tap commences. This will decrease the overall losses since less energy will be expended on reheating the furnace up to the bath temperature. Therefore, the temperature and mass of the hot heel must be considered in the furnace heat and mass balances. This is particularly important when these variables change from one tap to the next as they will the affect the final steel temperature and mass.

The initial conditions relating to the gas phase have a limited effect on the process because of their short time constants, as opposed to the temperature and liquid/solid phases. That is, the residence time of any initial gas mass in the furnace is short due to the rapid decay in mass brought on by the off-gas system. A high initial gas mass will be accompanied by a corresponding high furnace pressure transient. All the same, there is no practical mechanism by which a high initial gas mass can exist. For the purposes of this dissertation, the initial mass of the gas phase is assumed to be zero [1]; the same is assumed for the initial relative furnace pressure.

Initial conditions on the furnace material states will be established by the mass and composition of the charge. The mass of each charge constituent is reliably measured. In addition, the approximate composition of the materials can be obtained from the product manufacturers, except scrap.

4.1.1.3 Initial temperatures

The temperature of both the initial solid and liquid states are required to simulate the process. Therefore, the mass and temperature of the liquid and solid steel must be available at the beginning of tap. These, together with other variables, will determine the melting rate and the bath temperature as a function of time.

The bath temperature at refining is crucial information that enables operators to make control decisions in order to meet the target steel properties. In practice, several of these measurements are obtained since manual control is an iterative trial and error process. The first temperature measurement will be used as the initial temperature for model simulation (and fitting) at refining. Under perfect mass and energy balances, this initial temperature is all that is required to accurately predict the temperature at any time. It is just as important for model fitting and subsequent simulation (or prediction) once an accurate model has been arrived at.

[1] For simulation purposes a minimum value of 10×10^{-6} kg is used.

The mass of the hot heel is typically less than 10 % of the total charge; furthermore, it can be relatively constant from one tap to the next. As a result, any error in the estimation of the hot heel temperature and mass will introduce only a fraction of error into the overall bath temperature and mass balance. The hot heel temperature can be reliably assumed to equal the temperature of the previous tap - this is accurately known. Any error in the hot heel mass estimate, should not introduce significant error in the estimate of the final temperature, provided the hot heel temperature remains close to the tapping temperature. Certainly, accurate estimates of the hot heel mass will improve the overall heat balance but in practice measurement of the initial refining temperature is more important than that of the hot heel.

The bath temperature is one of the two most important variables in the furnace operation; all efforts must be made to know it as much as possible.

4.1.1.4 Water cooling

In keeping with previous work [7], a strong motivation for the use information of the water cooling system is the favourable circumstance that the flow rate and temperature are continuously measured. This makes the water cooling system a good candidate for use as a feedback variable in process control since it could provide valuable information about the temperature variations in the furnace. It is expected that the difference between the inlet and outlet temperature is correlated with the furnace heat balance: water cooling was generally accepted as a common fixture in modern EAFs as it was able to cool the panels to prevent excessive wear of the refractories under increasing arc power [19]. Therefore, the flow rate and temperature of the cooling water must be obtained.

4.1.1.5 Material composition

Scrap is the most abundant raw material charged into the furnace yet it is also the one for which the least information is available. The composition of the final product will invariably depend on that of scrap. Scrap can be bought from suppliers where an accurate analysis of grade and composition is available but is often not cost-effective, a case that applies in this dissertation. Clean scrap will generally be low in impurities and can be assumed to be made up of pure iron. At the other extreme material such as concrete, hydrocarbons and high levels of residuals have been reported [22]. Hydrocarbons and other dirt will generally combust or be released for disposal in the slag but residuals are not easily removed - in fact this is the main drawback of the EAF practice: the inability to produce low residual steel [17, 19]. A charge high in residuals such as tin, copper, nickel, molybdenum and tungsten can render the final product unusable - it may have to

be retained in the EAF where it can be diluted by additions of DRI and cleaner scrap. Knowing the exact composition beforehand can allow selection of the right proportions of the scrap and DRI, which can successfully dilute these impurities to acceptable levels. For modelling purposes, only the mass is available, and it will be (weakly) assumed that the scrap is pure iron, with low levels of silicon and carbon.

The composition of injected graphite is important to determine the theoretical recovery rate and the composition of the slag into which it is injected. The carbon content will have direct implications for the extent of foaming in response to injected graphite. The graphite is made up mainly of carbon, with impurities such as ash and SiO_2, the latter being relevant for slag SiO_2 levels since the injected graphite will deposit some of its SiO_2 into the slag.

Bath oxygen activity is a good indicator of the slag FeO and the bath carbon. Bath carbon and FeO are inversely related [19, 18]: a high FeO is accompanied by low levels of bath carbon and vice versa. FeO is in turn directly related to bath oxygen activity: with high bath oxygen, the FeO will be high (and bath carbon low); the converse also applies.

4.1.2 Model parameters

With exception of inputs and initial conditions, the parameters are the most important variables required to carry out a realistic model simulation. Their values determine the effects of the various interactions in the model. The main heat and material balances are controlled by the various parameters: the extent of scrap melting, liquid steel heating, bath oxidation, decarburization and desiliconization is controlled by the various associated parameters. Accurate knowledge of the parameters that govern a given process is crucial for an accurate depiction of the process by the model, given the same inputs and initial conditions.

The input-output requirements to enable parameter estimation will be dealt with in detail in the next section. Other parameters, such as furnace characteristics of diameter and volume, material properties and relevant states are well known.

4.2 Identifiability

Parameter estimation presupposes the existence of a unique mapping from the parameters to the input-output set. To address the validity of this assumption the problem of identifiability must be considered. Identifiability fulfills the practical requirement that parameters can be expressed as a function of known system quantities, such as inputs and outputs [53]. It gives information about possibilities for estimation of parameters:

whether all system parameters can be estimated, and if not all, which can be estimated; suggestions are also made about the time interval during which measurements would produce the best results. Some of the results of this section were covered in Rathaba *et al.* [54].

4.2.1 Model parameters

Several parameters in the model are physico-chemical constants that are well known. Others depend on the specific furnace practice and must be deduced from prior knowledge about the specific operation. The parameters that will be considered for the identifiability study and the subsequent estimation are:

- k_{dC} - bath decarburization rate constant
- k_{dSi} - desiliconization rate constant
- k_{gr} - effect of graphite injection on reduction of FeO in slag
- k_{VT} - EAF heat loss coefficient
- k_{PR} - effect of EAF pressure on gas flow into and out of the furnace
- k_U - effect of off-gas slip-gap on air flow into the off-gas duct
- k_{therea_1} - scrap and solid steel melting rate constant
- k_{therea_5} - solid slag melting rate constant
- η_{ARC} - efficiency of transfer of arc energy to the bath
- η_{FeO} - heat transfer efficiency from bath oxidation

The parameters k_{therea_1} and k_{therea_5} replace the products $k_{area_1}k_{ther_1}$ and $k_{area_5}k_{ther_5}$ respectively. The latter were used in the original model derivation and are replaced here for convenience: the replacement reduces the number of parameters without affecting the model behaviour.

The above parameters are perfect candidates for model adjustment: they are highly process dependent and vary according to operating conditions. This section concentrates on identifiability of the model with respect to these parameters.

4.2.2 A brief outline of the theory

The work of Xia and Moog [53] presents the different concepts of identifiability from a differential algebraic perspective. In this section a brief outline of the results and their interpretation is presented.

The nonlinear model of subsection 2.2.1 has the form

$$\Sigma_\theta : \begin{cases} \dot{\mathbf{x}} = \mathbf{f}(\mathbf{x}, \theta, \mathbf{u}) \\ \mathbf{y} = \mathbf{h}(\mathbf{x}, \theta, \mathbf{u}) \\ \mathbf{x}(\mathbf{0}, \theta) = \mathbf{x}_0 \end{cases} \tag{4.1}$$

where $x \in \Re^n$, $u \in \Re^m$, $y \in \Re^p$ and $\theta \in \Re^q$ are the state, input, output and parameters of the system. Assume that

$$\text{rank}\frac{\partial h(x, \theta, u)}{\partial x} = p \, , \tag{4.2}$$

i.e. the measurements of the various outputs are linearly independent. θ is the parameter to be identified; and x_0 is independent of θ.

Definition 1 *The system Σ_θ is said to be algebraically identifiable if there exist a $T > 0$, a function $\Phi : R^q \times R^{(k+1)m} \times R^{(k+1)p} \rightarrow R^q$ such that*

$$det\frac{\partial \Phi}{\partial \theta} \neq 0 \tag{4.3}$$

and

$$\Phi(\theta, u, \dot{u}, \ldots, u^{(k)}, y, \dot{y}, \ldots, y^{(k)}) = 0 \tag{4.4}$$

hold on $[0, T]$, for all $(\theta, u, \dot{u}, \ldots, u^{(k)}, y, \dot{y}, \ldots, y^{(k)})$. $u, \dot{u}, \ldots, u^{(k)}$ and $y, \dot{y}, \ldots, y^{(k)}$ are the derivatives of the input $u(t)$ and output $y(t, \theta, x_0, u)$; $u(t) \in C^k\ [0, T]$, i.e. the input is continuous and k-times differentiable on $[0, T]$.

The above definition suggests a test for algebraic identifiability. Given the system Σ_θ, form an equation $\Phi^*(\theta, u, y) = 0$; in theory the assumption of observability (4.2) makes it possible to eliminate the state x completely. Differentiate, scale and multiply the left-hand side of $\Phi^*(\theta, u, y) = 0$ [55] to form (4.4) until (4.3) is satisfied; where (4.3) implies that a unique solution for θ can be determined from (4.4).

Note that for algebraic identifiability θ can (in theory) be expressed in terms of the input, output and their derivatives - no state information is required. If the system is not algebraically identifiable it may be geometrically identifiable.

Definition 2 *The system Σ_θ is said to be identifiable with known initial conditions if there exist a positive integer k and a function $\Phi : R^q \times R^n \times R^{(k+1)m} \times R^{(k+1)p} \rightarrow R^q$ such that $det(\partial\Phi/\partial\theta) \neq 0$, and*

$$\begin{aligned} \Phi(\theta, x_0, u(0^+), \dot{u}(0^+), \ldots, u^{(k)}(0^+), \\ y(0^+), \dot{y}(0^+), \ldots, y^{(k)}(0^+)) = 0 \end{aligned} \tag{4.5}$$

hold for all $(\theta, x_0, u(0^+), \dot{u}(0^+), \ldots, u^{(k)}(0^+), y(0^+), \dot{y}(0^+), \ldots, y^{(k)}(0^+))$; $u(t)$ and $y(t, \theta, x_0, u)$ are evaluated at $t = 0^+$.

Used as a test for identifiability, definition 2 follows a similar procedure as definition 1. The system Σ_θ is not algebraically identifiable since either (4.2) or (4.3) cannot be satisfied. If $\text{rank}\frac{\partial h(x,\theta,u)}{\partial x} < p$ some states cannot be estimated from input-output information alone. This is where initial conditions $x(0^+)$ can be used as additional information to complement the partially know $x(t)$; in this case, $x(t)$ (as well as u and y) will be evaluated at $t = 0^+$. As in definition 1, more equations are generated until (4.3) is satisfied. If this fails the system is also not identifiable with known initial condition. At the outset, this means the parameters cannot be estimated using available information; this generally leaves fewer options for any parameter estimation procedure and alternative models must be investigated.

For a given system algebraic identifiability implies that the parameters can be estimated using only input and output information. On the other hand, if a system is not algebraically identifiable or $\text{rank}\frac{\partial h(x,\theta,u)}{\partial x} < p$ it may still be possible to determine the parameters using some state information - in the form of initial conditions. Xia and Moog [53] have shown that identifiability with known initial condition is equivalent to geometric identifiability.

To summarize: form $n-1$ equations from the output equation $y = h(x,\theta,u)$. For algebraic identifiability, these n equations (including $y = h(x,\theta,u)$) will be used to solve for x in terms of y, u, and θ. Therefore, there are n equations with n unknowns $x = [x_1, \ldots, x_n]^T$. Taking more higher-order $(n+q)$ derivatives of the output, q more equations can be formed with q unknowns $\theta = [\theta_1, \ldots, \theta_q]^T$. θ can now be expressed in terms of the input and output, and their derivatives. A similar procedure is followed for geometric identifiability, with the exception that information about known initial conditions is used since some states are not observable.

The foregoing summary is valid for the single output case. An extension to the multi-output case follows a similar development [53], this will be used for the analyses that follow.

4.2.3 Identifiability analysis

Identifiability of nonlinear systems is studied using different approaches, and some characterization and algorithms are developed by [55, 56, 57, 58] - the approach is essentially differential algebraic. The complexity introduced by initial conditions on the identifiability results is touched on in Auduloy *et al.* [58]; Saccomani *et al.* [59] extends the results to characterize the identifiability when the system is not accessible from certain initial conditions, a situation that can lead to potentially erroneous conclusions.

The approach taken in this dissertation follows the procedures developed by Xia and

Moog [53] which go beyond a mere test for the identifiability of a system. It provides a suitable platform from which practical suggestions for the the actual parameter estimation can be explored. In essence, the result of the work is to determine if the system parameters can be expressed in terms of the input-output measurement set. It also goes further to determine the theoretical minimum number of these input-output measurements that must be made in order to estimate the parameters.

The first use of the identifiability analysis considers the simplified model of subsection 2.2.5. The following map collects the relevant parameters:

$$\theta = \begin{bmatrix} k_{dC} \\ k_{dSi} \\ k_{gr} \\ \eta_{ARC} \\ \eta_{\mathrm{FeO}} \end{bmatrix};$$

Let complete observability take on the form

$$h(t,x,\theta,u) = \begin{bmatrix} y_3 \\ y_4 \\ y_7 \\ y_8 \\ y_{12} \end{bmatrix} = \begin{bmatrix} x_3 \\ x_4 \\ x_7 \\ x_8 \\ x_{12} \end{bmatrix};$$

then (4.2) is satisfied. The above measurements are not uncommon in EAF practice: carbon and silicon can be obtained from bath analysis results and the bath temperature is also measured as standard practice. FeO and SiO_2 can be obtained from slag analysis; this is not standard practice but several samples have been collected for analysis (see table A.1 of the appendix).

Taking the first derivative $\partial h/\partial t$ $(= f(t,x,\theta,u))$ gives

$$\Phi = f(t,x,\theta,u) - [\dot{y}_3, \dot{y}_4, \dot{y}_7, \dot{y}_8, \dot{y}_{12}]^T. \tag{4.6}$$

Then, the Jacobian

$$\frac{\partial \Phi}{\partial \theta} = \begin{bmatrix} \Gamma & 0 & 0 & 0 & 0 \\ 0 & \Lambda & 0 & 0 & 0 \\ 0 & 0 & \Omega & 0 & 0 \\ 0 & -\frac{M_{\mathrm{SiO_2}}}{M_{\mathrm{Si}}}\Lambda & 0 & 0 & 0 \\ 0 & 0 & 0 & 0 & \Psi \end{bmatrix}, \tag{4.7}$$

and the corresponding rank

$$\mathrm{rank}\frac{\partial \Phi}{\partial \theta} = 4, \tag{4.8}$$

with

$$\begin{aligned}
\Gamma &= -X_{\mathrm{C}} + X_{\mathrm{C}}^{eq}\ , \\
\Lambda &= -X_{\mathrm{Si}} + X_{\mathrm{Si}}^{eq}\ , \\
\Omega &= -\frac{x_7 M_{\mathrm{Fe}} d_5}{(m_{T(slag)} + x_7 + x_8) M_{\mathrm{C}}}\ , \\
\Psi &= -\frac{2\Delta H_{\mathrm{FeO}} d_1 / M_{\mathrm{O_2}}}{\left[\frac{m_{T(\mathrm{Fe})} C_p(\mathrm{Fe}_L)}{M_{\mathrm{Fe}}} + \frac{2m_{T(slag)} + 2x_7 + 3x_8}{M_{slag}} C_{p(slag_{(L)})}\right]}.
\end{aligned}$$

That is, of the 5 parameters, only 4 can be uniquely determined from the measurements. Furthermore, the submatrix $\mathrm{diag}([\Gamma,\ \Lambda,\ \Omega,\ \Psi])$ must be invertible; this is satisfied when $(X_{\mathrm{C}} - X_{\mathrm{C}}^{eq}) \neq 0$ and $(X_{\mathrm{Si}} - X_{\mathrm{Si}}^{eq}) \neq 0$. Near equilibrium, $X_{\mathrm{C}} \approx X_{\mathrm{C}}^{eq}$ and $X_{\mathrm{Si}} \approx X_{\mathrm{Si}}^{eq}$. Therefore, measurement of carbon and silicon content must be made early in the tap, before the asymptotic stage is reached. This would be the early flat bath stage when all the scrap is fully melted and a homogeneous distribution is achieved.

It is clear that equations $\dot{x}_4$ and $\dot{x}_8$ are redundant in the parameter k_{dSi}; only one of them is necessary for estimation of k_{dSi}. In practice, a bath chemical analysis is taken for every tap while slag analysis may only be carried out during plant trials. Therefore, the bath silicon content ($x_4 = y_4$) is favoured as a measured output; the SiO_2 can effectively be discarded in subsequent identifiability analysis.

Computing the time derivative of $\dot{y}_{12}$ and rearranging leads to

$$\Phi = g(t, x, \theta, u) - [\dot{y}_3, \dot{y}_4, \dot{y}_7, \dot{y}_{12}, \ddot{y}_{12}]^T\ , \tag{4.9}$$

where

$$g(t, x, \theta, u) = \left[\dot{x}_3, \dot{x}_4, \dot{x}_7, \dot{x}_{12}, \ddot{x}_{12}\right]^T; \tag{4.10}$$

$\dot{x}_i$ are given in (2.50) and $\ddot{x}_{12} = \partial \dot{x}_{12} / \partial t$. The rank

$$\mathrm{rank} \frac{\partial \Phi}{\partial \theta} = 5. \tag{4.11}$$

That is, there are 5 equations in 5 unknown parameters: the system is algebraically identifiable. Under conditions of noise-free measurements and an error-free model, to determine the first time derivative of a measured variable would require two measurements, and three for the second derivative. Thus, from the vector $[\dot{y}_3, \dot{y}_4, \dot{y}_7, \dot{y}_{12}, \ddot{y}_{12}]^T$, only two measurements are required to evaluate $\dot{y}_3,\ \dot{y}_4,\ \dot{y}_7$; and three measurements for $\dot{y}_{12}$ and $\ddot{y}_{12}$. In both cases, finite difference methods can be employed to approximate the time derivatives [60].

In the next example, the model for the entire tap is used. This results in a 17th order non-linear model with 10 parameters:

$$\begin{bmatrix} \theta_1 \\ \theta_2 \\ \theta_3 \\ \theta_4 \\ \theta_5 \\ \theta_6 \\ \theta_7 \\ \theta_8 \\ \theta_9 \\ \theta_{10} \end{bmatrix} = \begin{bmatrix} k_{therea_1} \\ k_{therea_5} \\ k_{dC} \\ k_{dSi} \\ k_{gr} \\ k_{PR} \\ k_U \\ k_{VT} \\ \eta_{\text{FeO}} \\ \eta_{ARC} \end{bmatrix}, \tag{4.12}$$

Considering the ideal case when all states are measured as outputs, then $y = x$ and assumption (4.2) holds. Forming (4.4),

$$\Phi = g(t, x, \theta, u) - [\dot{y}^T, \ddot{y}_{12}]^T, \tag{4.13}$$

where

$$g(t, x, \theta, u) = [f(t, x, \theta, u)^T, \ddot{x}_{12}]^T, \tag{4.14}$$

results in

$$\text{rank}\frac{\partial \Phi}{\partial \theta} = 8; \tag{4.15}$$

i.e. 8 of the 10 parameters can be estimated, therefore, the system is not algebraically identifiable. On examining the rank loss in (4.15) when parameters are added or removed from (4.12) a tradeoff is noted among the energy-related parameters. Any two of the parameters in the triplet $[k_{VT}, \eta_{\text{FeO}}, \eta_{ARC}]$ can be estimated, provided one of them can be fixed. In practice, the heat loss coefficient, k_{VT} is well know from observation of bath temperature loss during operational delays. In fact, if k_{VT} can be fixed to a reasonable degree of accuracy, the system will then be algebraically identifiable since (4.13) would have 8 equations in 8 unknowns.

As an aid to experiment design, the above analysis also reveals that only 2 measurements are needed for each output; except for temperature (y_{12}) where 3 measurements are needed to evaluate the second-order time derivative. Also, to determine the effect of pressure (via k_{PR}) on air entrainment or expulsion of freeboard gases, it is necessary to sample only one of the freeboard gases. In the case of scrap melting, it is sufficient to measure either the mass of the bath or the scrap to estimate k_{therea_1}; the same applies to slag (for estimating k_{therea_5}). No sample of the SiO_2 content in the slag is required;

measurement of the actual silicon content in the bath will suffice for estimating k_{dSi}, the rate constant for removal of silicon from the bath. The conclusions made in example 1 about measurement of carbon and silicon content also apply in this case.

The above discussion applies for the entire tap. A more realistic scenario is the use of measurements that are part of standard EAF practice as well as the slag analysis that was obtained for the purposes of the model fitting - these apply to the refining period. The measurements are bath carbon, silicon, FeO, SiO_2, slag, temperature and pressure. This leads to $g(x,\theta,u) = [\dot{x}_3\,,\dot{x}_4\,,\dot{x}_6\,,\dot{x}_7\,,\dot{x}_8\,,\dot{x}_{12}\,,\dot{x}_{14}]^T$. At refining, all scrap and solid slag are fully melted so that the melting rate parameters k_{therea_1} and k_{therea_5} can be disregarded. Measurement for the compositions is always reported in terms of percentages. It is possible to use these percentage values to obtain the actual masses for each component since the bath and slag masses can be estimated from the charge additions and hot heel mass.

The identifiability results for the model given the above parameters and output measurements are as follows. Forming

$$\Phi = g(t,x,\theta,u) - [\dot{y}_3\,,\dot{y}_4\,,\dot{y}_6\,,\dot{y}_7\,,\dot{y}_8\,,\dot{y}_{12}\,,\dot{y}_{14}]^T\,, \tag{4.16}$$

and evaluating the jacobian results in

$$\text{rank}\frac{\partial\Phi}{\partial\theta} = 6. \tag{4.17}$$

That is, of the 10 parameters, 6 can be estimated - the system is not algebraically identifiable. Taking additional time derivatives on the pressure and temperature - so that $g(t,x,\theta,u) - [\dot{y}_3\,,\dot{y}_4\,,\dot{y}_6\,,\dot{y}_7\,,\dot{y}_8\,,\dot{y}_{12}\,,\dot{y}_{14}\,,\ddot{y}_{12}\,,\ddot{y}_{14}]^T$ increases the rank to 8 - any higher time derivatives cannot be practically obtained.[2] However, inspection of the bath temperature equation indicates that higher order derivatives are possible, so that the temperature-related parameters $[\eta_{\text{FeO}}\,,\eta_{ARC}\,,k_{VT}]$ can be estimated from $y_{12}^{(3)}$, the third order time derivative of temperature. As mentioned previously, k_{VT} can be estimated by other means; in that case, the model is algebraically identifiable.

When the test for algebraic identifiability fails, information about initial conditions can be used to test for geometric identifiability. This is a weaker system property but it removes the burden of having to measure outputs that are either too impractical or costly to obtain. Algebraic identifiability relies on eliminating all variables that relate to the state (the x's), and representing the system solely as a function of inputs, outputs and their derivatives. For geometric identifiability, however, some states cannot be eliminated (the system is not completely observable). For these states, information about initial

[2]The identifiability analysis was carried out using the Maple symbolic math engine called from within Matlab. Further time derivatives exceed the system resources available on an Intel Pentium 4, with 512 MB of RAM.

conditions can be used, so that as in the case of algebraically identifiability, the system can then be expressed as a function of inputs, outputs and their derivatives, where the unobservable states have been replaced by their initial conditions. The evaluation of the variables must be confined to the vicinity of the initial time $t = 0^+$.

Algebraic identifiability is a stronger system property; in fact, it implies geometric identifiability [53] - which generally requires more information to estimate the system parameters. In practice, this could mean implementing an additional sensor measurement - a generally expensive option.

4.2.4 Distinguishability

Parameter identifiability can also be defined in terms of output distinguishability [56]. Distinguishability answers the question of whether system outputs obtained with different parameter values can be distinguished from one another.[3]

Definition 3 *For the system (4.1) and the set of parameters* Ω *the pair of parameter values* $(\theta\,, \alpha)$, $\theta \in \Omega$, $\alpha \in \Omega$, *is said to be* indistinguishable *if*

$$h(x, \theta, u) \equiv h(x, \alpha, u)$$

for a given set of $[x_0, u(\cdot)]$ *and* $0 \leq t \leq T$. *Otherwise the pair is said to be* distinguishable.

Definition 3 provides an alternative method for analysing the identifiability properties of the system. It is a simple test that also formed the basis for derivation of identifiability results in Tunali and Tarn [57]. It is also not computationally expensive since the main computation involves a model simulation with varying parameter values. Since the method is simulation-based, both input information and initial conditions are necessary. In this sense, distinguishability is similar to geometric identifiability which uses partial or full information about the initial conditions. Distinguishability points to the uniqueness of model outputs under different parameters with similar initial conditions and inputs. Geometric identifiability shows the uniqueness of parameter values under similar inputs, outputs and partial or full information about the initial conditions. The distinguishability test will be shown to produce practically relevant results.

The distinguishability test is closely related to the question of model sensitivity to parameters. Here the sensitivity of each state (or output) is evaluated relative to parameter changes. A similar procedure was carried out in Vercruyssen *et al.* [11] to determine the influence of model parameters on a stainless steel converter model.

[3] With the same initial conditions and inputs.

The distinguishability test will be carried out by changing each parameter by 1%. For the parameter set $\theta = [\theta_1, \ldots, \theta_{10}]^T$ the output will be recorded at each turn when each parameter is perturbed by 1% while the rest are held at their nominal values. The nominal parameter values are : $\theta = [0.03,\ 0.005,\ 80,\ 10,\ 5.54,\ 0.1,\ 8.43,\ 5.9,\ 0.5, 0.5]^T$. The results are summarized in table 4.1 and figures 4.2 to 4.5 for some important outputs; the parameter numbers are assigned as in (4.12).

- The scrap (and other metallic charge) show little response to all the parameters since at refining all solids are fully melted. There is practically no change in bath mass (slag) for changes in the respective parameters k_{therea_1} and k_{therea_5}.

- At refining, the liquid metal mass is sensitive to several parameters: η_{FeO}, k_{gr}, $k_{d\text{C}}$ and k_{dSi}, in order of decreasing sensitivity.

- As can be inferred from the model derivation, the masses of carbon and silicon are most sensitive to their corresponding rate constants. Other parameters such as η_{FeO} will have an effect (albeit marginal) since they influence the equilibrium point and hence the removal of these impurities. The energy related constants such as η_{ARC}, k_{VT} have very limited influence.[4]

- The electrical arc makes the greatest contribution to the furnace heat balance - this explains the high sensitivity of liquid temperature to η_{ARC}. In order of decreasing sensitivity, other parameters with a marked influence on temperature are η_{FeO} and k_{VT}. Significant sensitivity to the efficiencies η_{FeO} (θ_9) and η_{ARC} (θ_{10}) is observed; these have a direct effect on the effective heat energy input and the resulting change in temperature.

- Air tightness has the greatest effect on the pressure via k_{PR}, this is followed by the off-gas flow constant k_U, graphite injection efficiency k_{gr} and decarburization rate constant $k_{d\text{C}}$. Figure 4.5 shows the results. It is understandable that k_U should produce a variation in the pressure since it controls the release of gases through the off-gas system. The parameter k_U controls the effect of the off-gas slip gap.

- Liquid metal mass and temperature exhibit little sensitivity to most parameters considering that the mean values are 1723.4 K and 1.3190×10^5 kg respectively. The liquid mass shows some response to changes in the parameter ($k_{ther1}k_{area1}$). This is to be expected since these parameters (heat transfer coefficient between

[4]The minute sensitivity to η_{ARC} and k_{VT} is mainly due to the effect of these constants on the bath mass.

liquid metal and solid scrap, and contact area between liquid metal and solid scrap) have a direct effect on the scrap melting rate - and the resulting liquid mass.

- As in the case with the carbon content, the silicon content of the bath is affected only by the scrap melting rate through the parameters k_{ther1} and k_{area1}. As expected it is predominantly affected by k_{dSi}.

The above discussion applies for a given set of nominal parameter values and operating point (input and state). Due to the nonlinearity of the system, different results will be obtained if the nominal parameter values are changed. In this case the nominal parameter vector was obtained from the estimation of chapter 5. It will be assumed these values are close to the operating point of the furnace [5]. Therefore, these results should apply over the typical operating region of the furnace. Very little deviation will occur in the case of parameters such as k_{dC}, k_{dSi} and the melting rates.

The above discussion is summarized in table 4.1.

Table 4.1: Response of model states to a 1% change in parameter values (the entries are multiplied by a factor of 100).

	k_{therea_1}	k_{therea_5}	k_{dC}	k_{dSi}	k_{gr}	k_{PR}	k_U	k_{VT}	η_{FeO}	η_{ARC}
x_1	0	0	0	0	0	0	0	0	0	0
x_2	0.019	0	1.4	0.019	0.35	0	0	0	0	0
x_3	0.00060	0	0	0.0060	0.071	0	0	0	0	0
x_4	0	0	0	0	0	0	0	0	0	0
x_5	0	0	0	0	0	0	0	0	0	0
x_6	0	0.054	0	0	0	0	0	0	0	0
x_7	0	0	0	0	0	0	0	0	59.0	0
x_8	0	0	0	0.55	0	0	0	0	0	0
x_9	0	0	0.83	0	0	0.21	0.067	0.00029	0.0026	0
x_{10}	0.0000032	0.0000027	0.80	0.00010	0.00017	14.0	0.029	0	0	0.00019
x_{11}	0.0000020	0.0000013	0.79	0.000055	0.000095	8.4	0.020	0	0	0.00014
x_{12}	0	0	0	0.083	0	0.44	0.0042	0	5.3	10.0
x_{13}	50.0	7.9	0	0.0027	0	0.019	0	0	0.18	0.34
x_{14}	0	0	1.2	0	0	0	0.30	0.0000039	0.0056	0

The response of the system to parameter changes has a strong time dependence. An obvious example is the case of the surface-to-area ratios and the heat transfer coefficients between phases, i.e. k_{theri} and k_{areai}: the system outputs (and states) only respond significantly to changes in these parameters at the early stages of melting. Their effect is negligible towards the flat bath stage. This can be clearly noted in the results of table 4.1. The liquid bath and slag masses are insensitive to the melting rate constants. The change in the solid mass is because only 1 kg solid scrap is allowed to remain at refining[6]; this small mass also has the effect of amplifying the sensitivity of the solids temperature

[5] An alternative method is to do a type of Monte Carlo analysis [7] but this will be computationally intensive in order to obtain a result that can be reasonably arrived at from inspection on a proper choice of operating point.

[6] This serves as a simulation convenience to prevent division by zero.

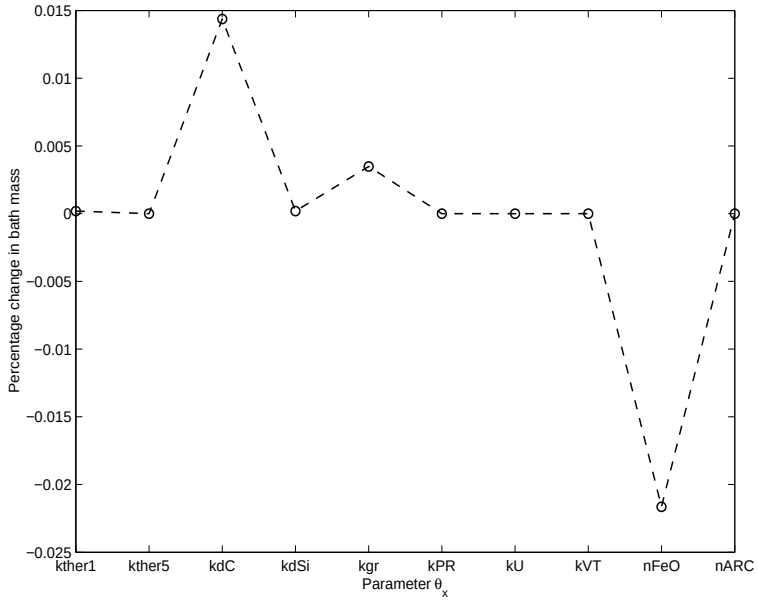

Figure 4.1: Change in bath mass for 1% excitation in the parameters.

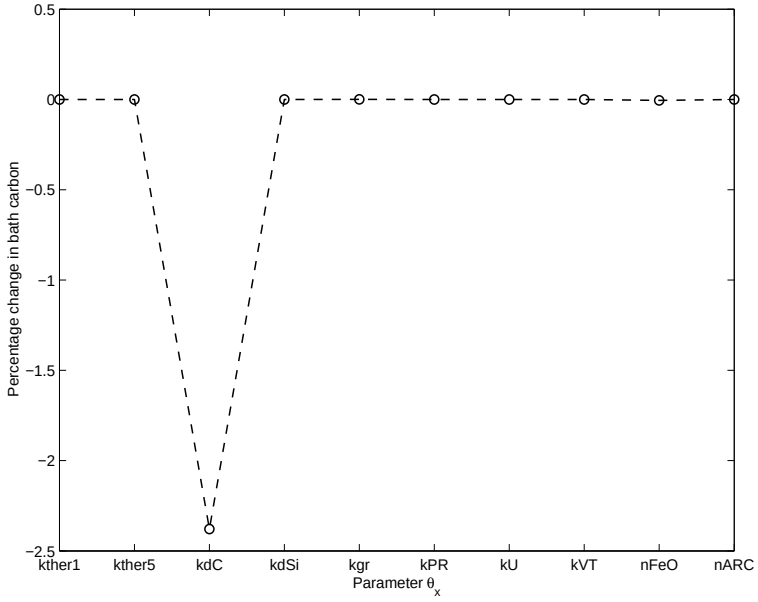

Figure 4.2: Change in carbon content for 1% excitation in the parameters.

(x_{13}) - in reality this temperature is undefined since there are (practically) no solids at refining.

A valuable result of the current study is that while not all the parameters can be identified, suggestions are made about which parameters can be identified. This reduces the uncertainty in the model since there are fewer parameters that are estimated without taking into account the system behaviour - the other parameters are obtained using input-output data, and initial conditions.

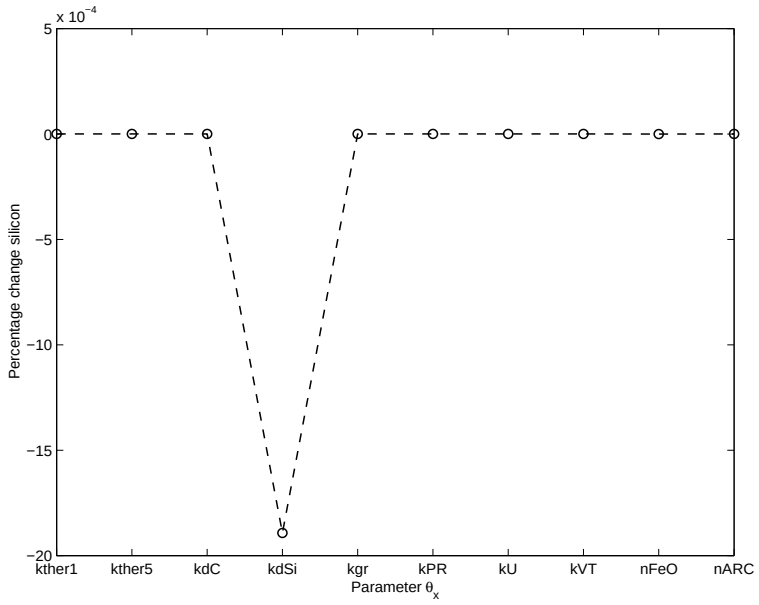

Figure 4.3: Change in silicon content for 1% excitation in the parameters.

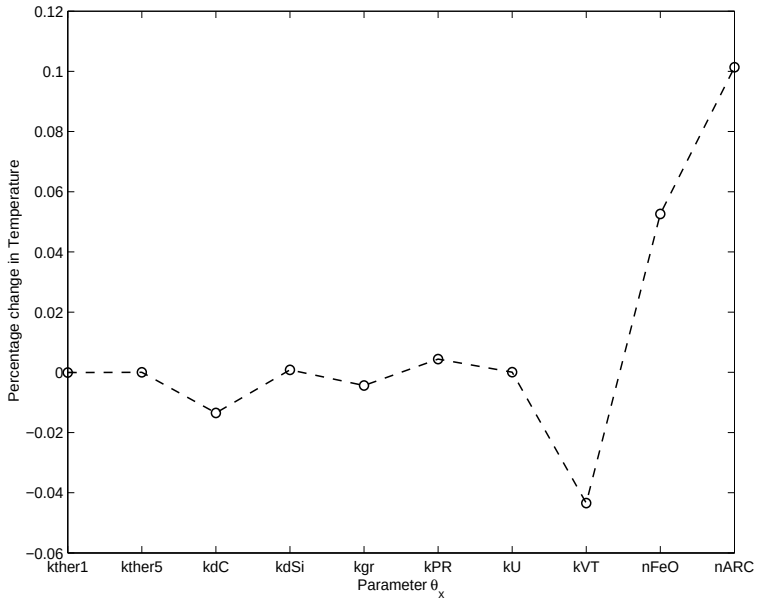

Figure 4.4: Change in bath temperature for 1% excitation in the parameters. The small values are because the change (and the temperature range during refining) is taken with respect to the relatively large temperature value of approximately 1500 °C.

An extension of the above result was provided by the distinguishability test. It was possible to decide which parameters have the greatest influence on which outputs. This enables the choice of parameter-output pairings that can result in more accurate parameter estimates. The time dependent nature of the system sensitivity to parameter changes gives an indication of the time during a tap when measurements should be taken.

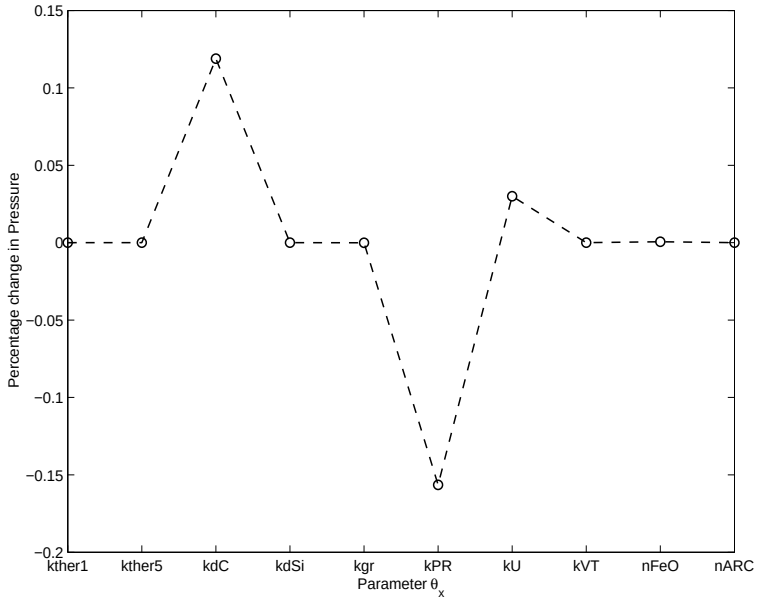

Figure 4.5: Change in relative pressure for 1% excitation in the parameters.

Designing for a small variance in a certain component of θ means the predictor has to be sensitive to that component. It is important to choose measurement outputs $y(t)$ and inputs $u(t)$ so that the predicted output becomes sensitive with respect to parameters that are important for the application in question [37]. This justifies the distinguishability analysis.

The results provide an analysis of which parameters can be estimated using input-output data. Once this requirement on the plant information is known any method can be used to carry out the actual parameter estimation. That is, the identifiability establishes the requirements on plant information for parameter estimation; they provide confirmation about the parameters that can be estimated from measured data - some of results are intuitive and can be traced back to the original model derivation. Refining is of relatively limited duration, and thus presents little flexibility in the choice of intervals over which best estimation results can be obtained.

4.2.5 The time interval for estimation

The identifiability results suggest that measurement of carbon should only be carried out at the early melting stage but before the asymptotic stage is reached. For practical reasons, the measurement at early melting will not produce reliable results. At this stage, large blocks of scrap, particularly cast iron, can still be found in the molten pool. Any sampling for composition will not take into account the significant change that may occur as this scrap melts. On the other hand, bath carbon displays small variations towards the

late asymptotic stage as a result, it will also be least sensitive k_{dC}. Because of the low magnitudes of the carbon, the effect of measurement errors will increase. Therefore, the time between the late melting and the late asymptotic stage is most practically feasible. This also applies to measurement of bath silicon although it will be shown in chapter 5 that its levels are too low to observe any systematic behaviour.

4.2.6 Model sensitivity

The question of model sensitivity is a generalization of the test for distinguishability.

The sensitivity of the model states and outputs to parameters can be analysed by considering the response of these variables to changes in the parameter values. A simple technique to achieve this is to temporarily set the model parameter to zero and monitor the response [47]. A more rigourous approach is to consider the Hessian of some scalar function of the state or output [47, 61]. The Hessian can be used to identify the least significant parameters in the model.

Consider some scalar function $g(t, \theta)$, where θ is a parameter vector of m components. The Hessian is defined as

$$H = \begin{bmatrix} \frac{\partial^2 g}{\partial \theta_1^2} & \cdots & \frac{\partial^2 g}{\partial \theta_1 \partial \theta_m} \\ \frac{\partial^2 g}{\partial \theta_2 \partial \theta_1} & \ddots & \vdots \\ \frac{\partial^2 g}{\partial \theta_m \partial \theta_1} & \cdots & \frac{\partial^2 g}{\partial \theta_m \partial \theta_m} \end{bmatrix} \tag{4.18}$$

It is evaluated at relevant values of state, output and parameter. For the purposes of the current model, the choice of $g(t, \theta)$ can be the point value (in time) of the state or output itself or their mean time integral. The latter will be chosen as it takes into account the cumulative effect of the variation in parameter. This results in $g_i(\theta) = \frac{1}{t_2 - t_1} \int_{t_1}^{t_2} x_i dt$ for state x_i and similarly for outputs.

Due to the complexity of the model, symbolic computation of the Hessian is involved[7], if not impossible. Numerical computation is preferred as it fits seamlessly into the original simulation framework - the main difference is the use of perturbations on the parameter values. The finite difference method of central differences results in the following components of the Hessian [47]:

$$\frac{\partial^2 g}{\partial \theta_i \partial \theta_j} = \frac{1}{4\epsilon^2}\{g(\theta_i + \epsilon, \theta_j + \epsilon) - g(\theta_i + \epsilon, \theta_j - \epsilon) - g(\theta_i - \epsilon, \theta_j + \epsilon) + g(\theta_i + \epsilon, \theta_j + \epsilon) + \mathcal{O}(\epsilon^2)\} \tag{4.19}$$

where ϵ is the perturbation on each possible pair of parameters θ_i and θ_j; the second-order terms can be neglected.

[7] Symbolic computation using a computer package such as Maple was carried out with poor results. Evaluation of the large resulting matrix proved to be unwieldy.

The operating region at which the Hessian is evaluated will have an effect on the results. To circumvent this problem, process data from several taps will be used and the resulting components of the Hessian will be the average obtained per parameter per data set. The expectation is that any parameter with no effect on the state (or output) will have lead to a zero or small value of the corresponding Hessian component. From this it can be reasonably assumed that the results apply to all taps.

The relative magnitudes of the Hessian elements also point to the relative importance (the so-called saliency [47]) of the parameter to a particular variable. The saliency of parameter i is calculated as

$$S_i = H_{ii}\theta_i^2/2 \tag{4.20}$$

where H_{ii} is the $(i,i)th$ diagonal element of the Hessian.

4.3 Data collection

4.3.1 Furnace inputs

Most furnace inputs are part of the overall automation system. The average power input, the oxygen, fuel gas and graphite injection rates are measured online. These inputs were sampled at intervals of 10 seconds. The choice of this sampling time was a practical convenience as it short enough to capture the essential input variations - particularly of the gases - while still allowing time and space for storage in the appropriate databases[8]. A shorter time is preferable at refining since some consecutive temperature (at times simultaneously with carbon and oxygen activity) can be separated by just one minute, making a shorted time interval all the more important. In the end 10 s proved adequate.

The only available information on the off-gas system inputs is the size of the slip gap and the overall mass flow rate. Unlike the original derivation [39, 5], the off-gas fan power (and resulting mass flow) is constant and cannot be manipulated. The reported off-gas volume flow rate is given as 66000 Nm^3/h [22]. This corresponds to a molar flow rate of 808 mol/s. Off-gas systems are designed to exhaust a mass flow that is four times that which actually exists the furnace at the fourth hole [19]. Therefore, of the 808 mol/s, a fifth (161.6 mol/s) will be the moles of gas that leave the furnace. The off-gas composition will vary depending on the mode of operation: early meltdown will have high levels of CO_2 and water vapour from combustion of fuel gas while higher volumes of CO will be generated from decarburization at refining. Adopting these values leads to a mass flow rate of approximately $u_1 = 4.5\,\mathrm{kg/s}$, made up of CO.

[8] A shorter time interval would place a high burden on the database for the online processing and storage of the data.

4.3.2 Slag data

In total, 48 slag samples were collected from 18 taps. The first 30 samples were collected from 10 successive taps, with 3 samples per tap. One sample was extracted at first deslagging before the bath sample and temperature are obtained. The second sample was extracted at some time during refining[9]; and the last sample was obtained at tap time. The 8 remaining samples were collected from another set of 8 successive taps at turndown.

In practice, the slag contains FeO and ferric iron [17]. The analysis results report FeO and Fe_2O_3 so the final FeO used is the total iron oxide content of the slag, obtained as

$$(\,\%\,\mathrm{FeO})_t = \,\%\,\mathrm{FeO} + \frac{2M_{\mathrm{FeO}}}{M_{\mathrm{Fe_2O_3}}}\,\%\,\mathrm{Fe_2O_3} = \,\%\,\mathrm{FeO} + 0.9\,\%\,\mathrm{Fe_2O_3} \tag{4.21}$$

Due to mixing between the slag and bath, some pure iron was found in the slag - this iron was not taken into account as it relates to the bath and not the slag.

4.3.3 Initial conditions

The following is a list of initial conditions on the various model states and how they were obtained. A distinction is made between initial conditions at the beginning of tap and at the beginning of refining. Few numerical values will be given, these vary from tap to tap and will be presented along with the main results of the model fitting (see chapter 5).

- **Solid steel mass**
  It is assumed there is no solid mass at refining. For the entire tap the mass of steel is determined by the metallic charge inputs such as scrap, DRI, cast iron, etc.

- **Liquid steel mass**
  The hot heel mass will fix the initial conditions for the liquid steel mass at the beginning of tap. The estimated bath mass at refining is based on the metallic charge inputs less the estimated FeO (discussed below) and impurities.

- **Bath carbon**
  Bath carbon at the beginning of a tap is fixed by the mass of the anthracite input, the estimated carbon composition of cast iron and pool iron. It is assumed there is no carbon originating from either scrap or the hot heel; if there is, it would be negligible compared to anthracite.

- **Bath silicon**
  Bath silicon originates from the DRI, pool iron and scrap. The initial silicon in the

[9]Preference would be for the middle of the refining stage but this cannot be known a priori, since the length of the refining period varies from tap to tap.

steel is determined from the slag chemistry at refining and the estimated mass of SiO_2 - a product of the oxidation of the corresponding bath silicon (the values are given in chapter 5, subsection 5.5.1).

- **Solid slag**
  At the beginning of tap, the solid slag is fixed by the slag additives in the charge. Most slag will be fully melted at refining therefore it is assumed there is no solid slag at refining.

- **Liquid slag**
  Some liquid slag may be retained with the hot heel, this will be small, so, for all practical purposes, no liquid slag exists at the beginning of tap. Refining slag is established mainly by slag additives in the charge, with low levels of MnO, MgO, P_2O_5, TiO_2 and chromium oxidized from the bath - these are neglected.

- **FeO in slag**
  As in the case of liquid slag, there is no FeO in the slag at the beginning of tap. Refining slag FeO is based on the slag analysis: given the slag FeO and CaO percentages, the mass of CaO is known reliably from the lime and doloma inputs for the charge. Then the approximate mass of FeO can be determined.

- **SiO_2 in slag**
  The initial SiO_2 at the beginning of tap is obtained by the same procedure used for FeO; this value is added to the bath silicon content at refining.

- **Furnace gas phase**
  All gas masses, either at the beginning of tap or at refining are zero since the beginning of refining or a new tap follows the opening of furnace which will remove all the gases.

- **Bath temperature**
  The initial bath temperature at the beginning of tap is the temperature of the hot heel, taken as the temperature of the previous tap. Taking an average over all taps results in $x_{12}(0) = 1647\,^{\circ}\mathrm{C}$. At refining, a temperature measurement is taken before operator control can take place - this temperature will be used as the initial temperature.

- **Scrap and solid slag temperature**
  Room temperature is assumed for the charge inputs at the beginning of tap. There are no solids at refining, so that the corresponding temperature is immaterial; a value of $1400\,^{\circ}\mathrm{C}$ will be used.

4.3.4 Model outputs and states

Special trials were carried out to obtain measurements from the furnace that are otherwise not carried out as part of normal furnace operation. These are additional temperature measurement, bath and slag chemistry analysis. The timing for extraction of these samples was dictated mainly by operational constraints so that it was not possible to obtain samples at regular time intervals[10]. However, all times for extraction of samples or measurement of temperature, carbon and oxygen activity were recorded.

The following is a list of states and outputs and discussion how each variable was measured.

- **Solid and liquid steel mass**

  The mass of scrap and other raw materials is measured as it is charged into the furnace. However, the changes in these masses as melting progresses cannot be practically measured. The flat bath (the time at which bath sample is extracted) provides a crude estimate for the time at which all the scrap has melted: this interval from charging to flat bath establishes the maximum time for a complete melt - it is possible for the flat bath stage to be reached earlier so that the melting rate obtained from the model will be lower than in practice. On the other hand, late melt-ins and scrap cave-ins mean that melting proceeds beyond the supposed flat bath stage, but the masses involved are relatively small so that it can be assumed that only a small error will be introduced by these effects.

- **Bath carbon**

  Dissolved carbon is measured as a percentage of the total elements dissolved in the steel. At the flat bath stage, a sample of the bath is extracted for laboratory analysis. It takes 4 to 9 minutes from the time a sample is extracted to the time the analysis results are made available to the operator [11]. In practice, subsequent measurements for dissolved carbon are obtained using a composite probe that reports the oxygen and carbon content instantaneously. This is essentially an oxygen probe that samples the bath oxygen content and estimates the carbon based on a predetermined empirical relationship. For the experiment runs, in addition to the standard initial bath sample, two bath samples were extracted (for analysis) at various times during refining - all times for the actual extraction of the sample were recorded. Therefore,

[10] Foaming and deslagging are integral operations in refining - no temperature sample can be taken until the slag layer covering the bath is sufficiently reduced, the same applies for extraction of the bath sample. The slag sample can only be extracted once the foamy slag has stopped flowing through the slag door; this is important for safety reasons.

[11] Based on the times recorded for the actual extraction of the sample and when the analysis data is reported.

the bath carbon measurements were obtained either by laboratory analysis or the composite lance readings. Some discrepancy in these measurements was observed and is discussed in the appendix (subsection A.5.1).

- **Silicon**

  The report on dissolved silicon is obtained from the analysis of the bath sample (the same samples used for carbon). The silicon composition was obtained from three samples at various times during refining.

- **Solid and liquid slag**

  As in the case of solid metal, only the initial mass of the solid slag additives is available. The melting rate can only be inferred from the assumption that all slag is fully melted by the flat bath stage. Some of the slag additives are lost as part of EAF dust through the off-gas system - a mechanism called carryover [19]. Clearly this will reduce the effective mass of the slag - but this loss is assumed negligible as it represents just a part of an overall EAF dust at 9-18 kg/ton of melted steel. This EAF dust will be made up of slag additives, dirt, rust and anthracite. The composition of the slag was obtained from analysis results of 10 taps. 3 slag samples were extracted for at refining for each tap: one at the first deslagging, the second at an intermediate time and the last at tapping. The analysis results are given in the appendix in tables A.1 and A.2. The slag is predominantly made up of CaO and MgO, with traces of MnO and Al_2O_3 - other components such as chromium, phosphorus and TiO_2 constitute an average of 1.18 %. The mass of slag at the time of analysis can be calculated based on the composition and known mass of the slag additives - the results are given in section A.3 of the appendix.

- **FeO and SiO_2**

  The analysis of the slag also reports the percentages of FeO and SiO_2. The corresponding masses can be calculated based on the known mass and composition of the slag (in the previous paragraph).

- **Gas phase**

  The gas phase masses are not measured. Analysis of the off-gas has been carried out by other authors to study the effects of the oxyfuel subsystem [26, 62].

- **Solid temperature**

  No practical method exists for measuring the temperature of the solid steel as melting proceeds. The evaluation of this model output will be based on what can be reasonably expected based on process understanding.

- **Liquid temperature**
  The minimum liquid temperature is the melting temperature of 1500 °C - a check on the value of the temperature is that it must not drop below this value. The refining temperature is measured at several times after the first deslagging up to tap time.

- **Furnace pressure**
  The furnace pressure is measured continuously as part of the overall furnace automation system. As in the case of inputs it is sampled at 10 s intervals.

- **Oxygen activity**
  Due to the relationships among bath oxygen activity, carbon and FeO an empirical equation can be used to describe the effect of oxygen on the bath carbon and FeO. Stated differently, the carbon content and FeO can be used to estimate oxygen activity. This is the preferred approach since it uses information about carbon and FeO which are adequately modelled.

Bath carbon and FeO are inversely related [18,19]: a high FeO indicates very low levels of bath carbon and vice versa. FeO is in turn directly related to bath oxygen activity: with high bath oxygen, the FeO will be high (and bath carbon low) and vice versa.

4.3.4.1 Cooling water measurements

Implementing water cooled panels has become a necessity in furnace design due to the high temperatures the side walls become exposed to. The cooling water absorbs some heat energy from the excessive arc radiation. As with other online measurements the temperatures of the inlet T_i and outlet water T_o streams are measured continuously. The flow rates are constant at $f_r = 230\,\mathrm{m^3/h}$ for roof panels and $f_w = 135\,\mathrm{m^3/h}$ for the side wall panels. Figure 4.6 shows a representative tap run along with the measured inflow and outflow water temperatures. A definite response to energy inputs can be observed, however it lies within a small range of temperature values: an average of $\mu_{T_r} = 42.5\,^\circ\mathrm{C}$ and a standard deviation of $\sigma_{T_r} = 3.06\,^\circ\mathrm{C}$ for the roof and for the wall, $\mu_{T_w} = 40.51\,^\circ\mathrm{C}$ and $\sigma_{T_w} = 3.68\,^\circ\mathrm{C}$. Over all taps (tap 1 to 10 of table A.1) these values become

$$\begin{aligned} \mu_{T_r} &= 45.64\,^\circ\mathrm{C} \\ \sigma_{T_r} &= 4.36\,^\circ\mathrm{C} \\ \mu_{T_w} &= 42.50\,^\circ\mathrm{C} \\ \sigma_{T_w} &= 1.92\,^\circ\mathrm{C}. \end{aligned}$$

A maximum temperature difference between the input and output water flows of 10 °C,

and a flow rate of $365\,\mathrm{m^3/h}$ means that the cooling water absorbs

$$\frac{365\,\mathrm{m^3/h}}{3600\mathrm{s/h}}(4.2\mathrm{kJ/kg\,^\circ C})(10\,^\circ\mathrm{C}) = 4.3\ \mathrm{MW}, \tag{4.22}$$

where $4.2\mathrm{kJ/kg\,^\circ C}$ is the heat capacity of water. Given that the arc is 50% efficient, this represents approximately 22% (4.3MW/(40MW*50%)) of the total arc loss. A much larger value would be expected since the water cooled panels are expressly designed to absorb a large part of the radiated arc heat losses. The difference $T_o - T_i$ should also be much larger than the maximum $10\,^\circ\mathrm{C}$. This points to a possible fault in the temperature measurements or a poor water cooling system.

The use of the water cooling temperature as a feedback variable (as suggested by Oosthuizen [7]) will be hampered by the limited range over which this temperature varies. These measurements can provide indirect information about the temperature of the bath. With a range of approximately $10\,^\circ\mathrm{C}$, the resolution on the actual bath temperature will be (assuming a range from 1500 to $1700\,^\circ\mathrm{C}$) approximately $10\,^\circ\mathrm{C}$. This will still be subject to measurement errors on the temperature of the water itself. It is also heavily dependent on the assumption that the temperature of the water cooling system is a reflection of the bath temperature - and not the temperature of the freeboard. It also depends on the contribution of each of these sources to the water temperature. These issues are beyond the scope of the current dissertation; therefore, the cooling water temperature will not be considered for the remainder of this dissertation.

4.3.4.2 Freeboard temperature measurements

During the plant trials where slag samples were collected, the freeboard temperature was measured for two taps (tap 5 and 6 in table A.1 of the appendix). A thermocouple was inserted in an opening near the centre of the furnace roof. In both cases, the thermocouple results were recorded. The results are shown in figures 4.7 and 4.8; each figure plots the measured temperatures and the corresponding inputs: arc, oxygen and fuel gas. There is a clear correlation between the measured temperature and the furnace inputs - mainly arc energy input. However, it is not possible to conclude from the plots if the temperature response is a result of arc energy input, burner energy input or oxygen lancing.

The original model derivation assumed a freeboard temperature equal to the bath temperature. For modelling convenience, a temperature of $1400\,^\circ\mathrm{C}$ was assumed for all reactions. This is also the temperature at which the gases leave the furnace - it is higher than the average measured freeboard temperature. Therefore, the modelled heat loss to the off-gas will be higher than in practice.

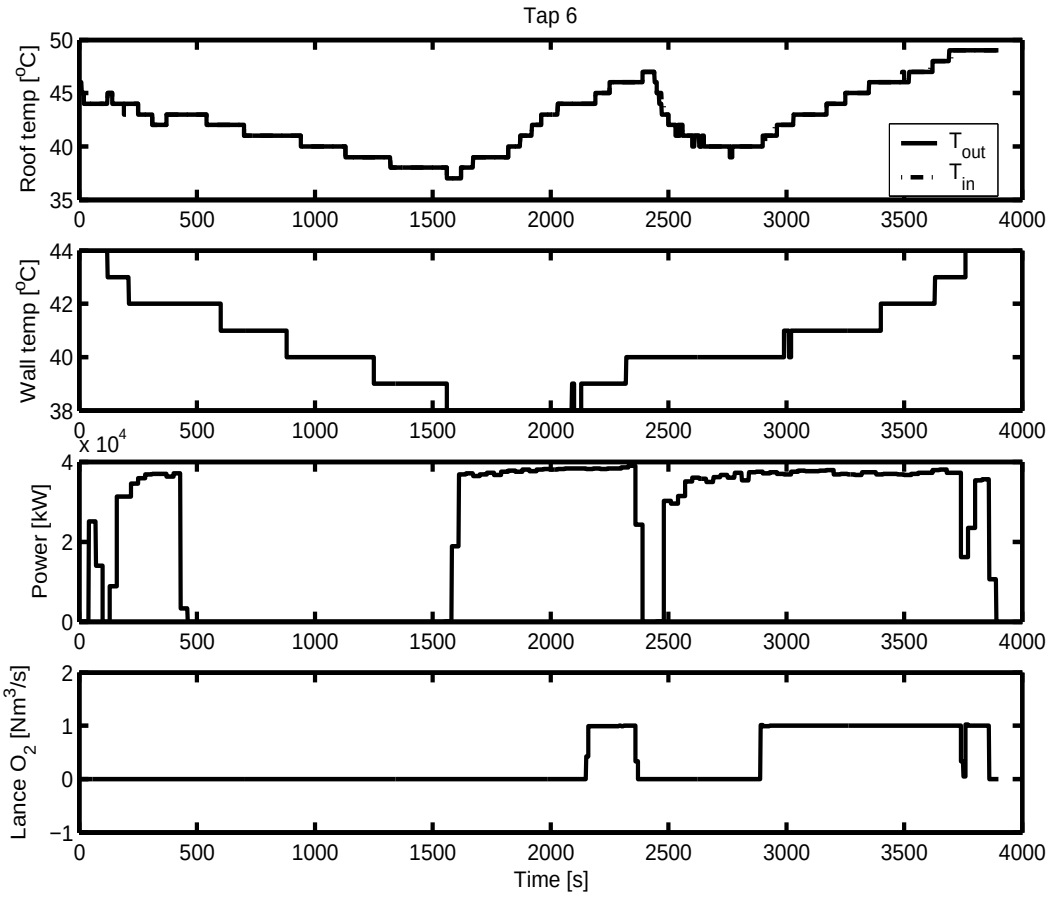

Figure 4.6: Change in the cooling water temperature over a single tap. The wall inlet water temperature is not measured directly. For the roof temperature, very little difference is observed between the inflow and outflow temperatures - the values are nearly coincident. The average change in temperature is approximately $-0.0077\,^{\circ}\mathrm{C}$ with a standard deviation of $0.168\,^{\circ}\mathrm{C}$. These values point to a very small change in temperature - only the absolute changes in the outlet temperatures depict any meaningful trends.

4.3.4.3 Furnace hot heel

Reliable information about the hot heel enables accurate estimates of the total steel mass (since the metallic charge mass is well known). This in turn will enable accurate temperature prediction. Under the assumption of consistent practice, the average mass and temperature of all hot heels will be the same (while the impurities will be negligible). This assumption is consistent with that made in Bekker [5]. This means the hot heel will not have a significant effect on the whole tap. To estimate the size of the hot heel the furnace was initially emptied then normal operation resumed for 21 taps after which the furnace was emptied again. During this period the mass of all metal tapped was measured. With this setup it was possible to arrive at a value for the average hot heel mass, given by the difference between total steel tapped and the estimated metal at tap time. This results in $\mu = 2.43$ ton and a high standard deviation $\sigma = 7.81$. This points

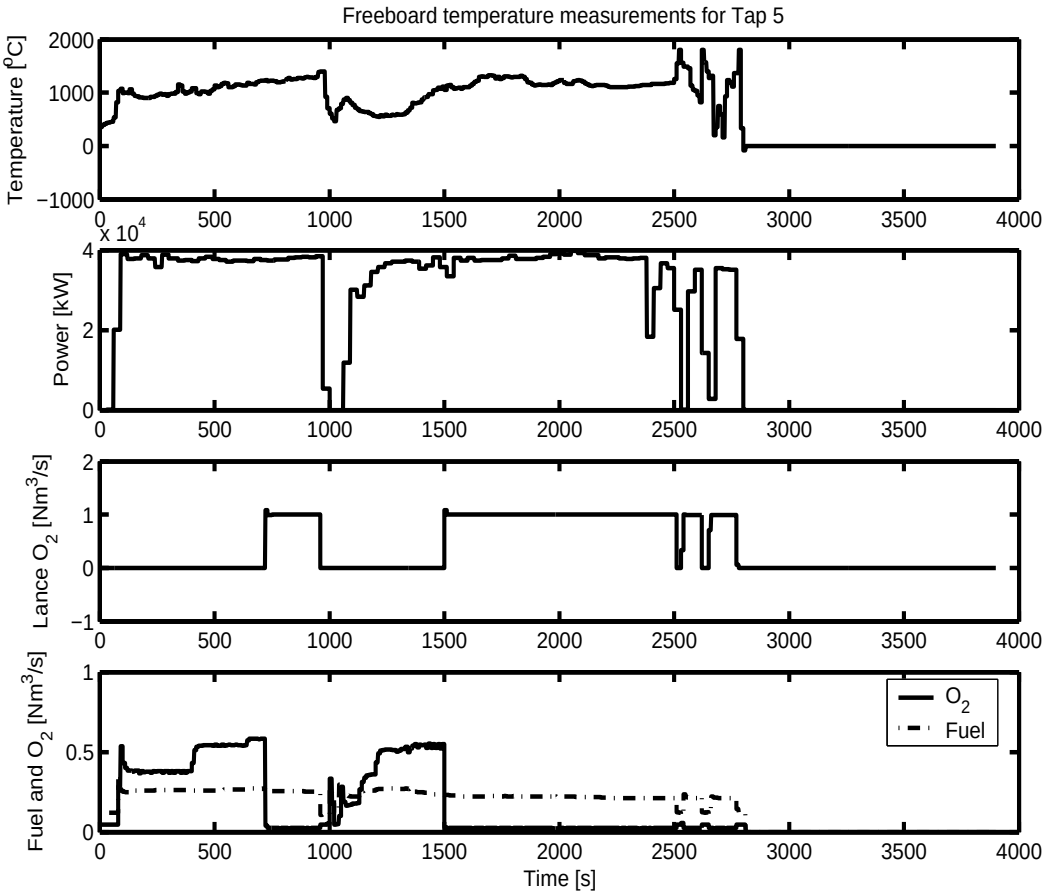

Figure 4.7: Measured freeboard temperature. The inputs are shown to explain the change in the temperature values over time. Oxygen lancing takes place in the intervals $700 < t < 950\,\text{s}$ and $1500 < t < 2750\,\text{s}$, coinciding with a rise in lancing O_2 and a drop in burner O_2 and fuel gas inputs. Although the fuel decrease is only slight, the burning effect is nullified by the choice of flow rates and the shaping of the oxygen stream - during lancing the fuel gas only serves to cool the lance.

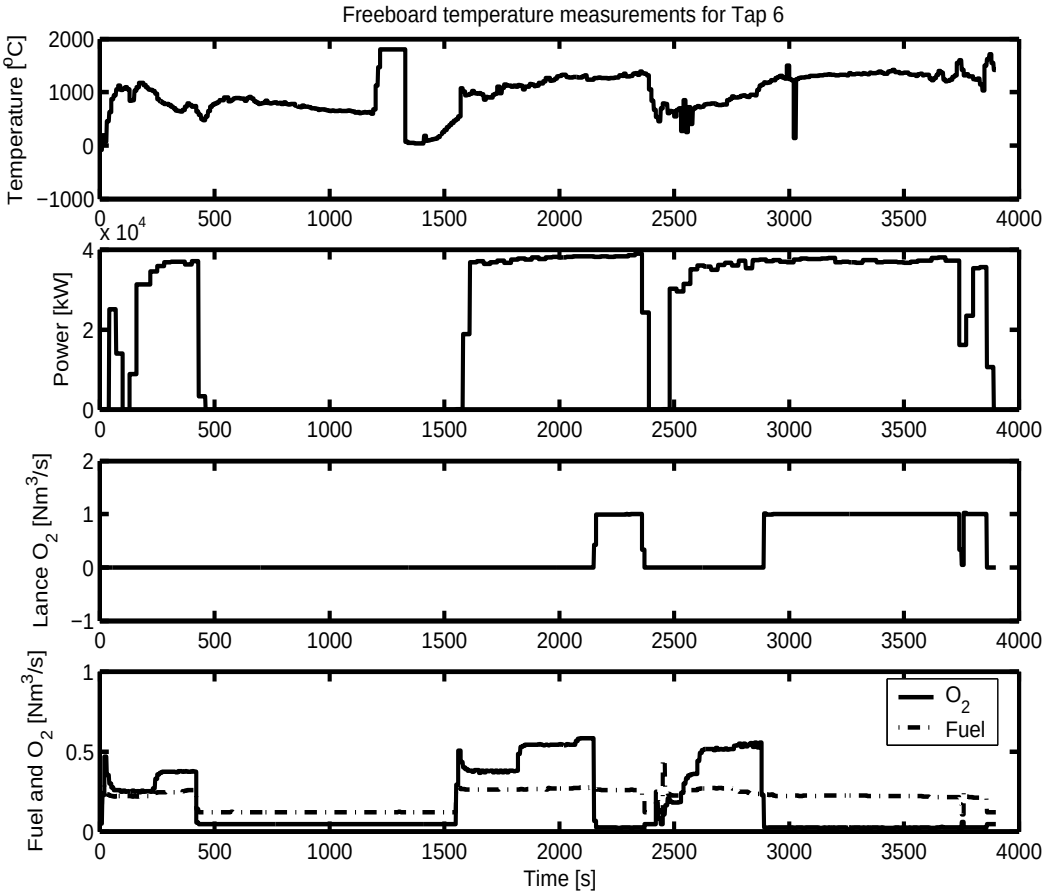

Figure 4.8: Measured freeboard temperature. The inputs are shown to explain the change in the temperature values over time. The delay from 450 s to 1550 s is due to installation of a second thermocouple - the measurements during this interval may be erroneous. Oxygen lancing takes place in the intervals $2150 < t < 2350$s and $2900 < t < 3850$s.

to potentially large variations in the hot heel mass; these variations are also evident in the mass of tapped steel shown in table 4.2 - for tap 1, the difference between the tapped steel and the total charge (11.42 = 86.97 - 75.55 ton) originates from the hot heel of the tap.

Table 4.2: Mass of steel tapped per charge.

Tap	Tapped [ton]	Charge [ton]	Calculated hot heel
1	86.97	75.55	0
2	60.39	76.13	15.74
3	73.51	78.03	20.27
4	62.67	76.99	34.59
5	73.98	76.26	36.86
6	74.54	76.09	38.41
7	74.54	75.19	39.05
8	73.44	74.17	39.78
9	64.67	75.61	50.73
10	78.68	75.10	47.14
11	74.54	76.59	49.19
12	82.82	77.10	43.46
13	53.84	75.79	65.41
14	66.32	75.56	74.65
15	77.65	75.70	72.71
16	69.37	75.78	79.12
17	71.05	72.31	80.37
18	76.58	75.92	79.71
19	69.02	76.18	86.87
20	77.22	75.89	85.54
21	69.45	75.80	91.89
22	86.28	74.80	0

The hot heel listed is the calculated hot heel mass. The hot heel mass in each tap is based on the difference between the total metallic charge and the mass of steel tapped. From an empty furnace, for example at tap 2, the hot heel mass is the difference between total metal input and the mass tapped. Not all the metal charged is tapped or is retained as hot heel. Some metal is lost to the slag, impurities are oxidized out of the bath, and dirt (which is included in the mass measurement) is transported to the slag. These cannot be practically accounted for, and introduce error into the estimated total furnace mass. This error accumulates, leading to the increase in the calculated hot heel mass from one tap to the next.

Based solely on the difference between the net metallic charge (with iron losses through slag taken into account) and the mass of steel tapped, the hot heel mass from one tap to the next escalates. This indicates that other metallic losses are not taken into account. This error will be a result of any of several sources:

- the uncertainties in the slag mass (and the corresponding metal loss);
- the metal loss through the off-gas (by vaporization);
- dust, dirt, oils and other contaminants that are included in the measurement of the metal charge mass;
- the composition of the metallic charge (which may be high in impurities that subsequently report to the slag);
- the latter could mean the slag mass and the corresponding iron losses were underestimated.

No accurate measurement of the slag mass is available; however, an estimate of the average slag mass per tap can be obtained. This is estimated based on the total amount of slag transported from the furnace over a given period. The total slag removed from the furnace over a period of 12 hours is 240 ton. During this period, 12 taps were recorded, leading to an average slag mass per tap of 20 ton [22]. This is nearly twice the estimated (average 12.9 ton) total slag mass. From this result, the total iron loss will be higher, and so will the contribution to the slag from the metallic charge - in the form of oxides and dirt. Nonetheless the initial mass of slag, FeO and SiO_2 was calculated based on the measured slag composition and the recorded mass of slag additives (see section A.2.2)

Taps 1 and 22, are the taps for which the furnace was fully emptied into the ladle. This mass will include some slag carried over from the furnace since deslagging cannot remove the slag completely. One of the advantages of a hot heel practice is to prevent slag carry-over; therefore, it will be assumed that this slag is insignificant.

On the other hand no other method exists to obtain the exact mass of the hot heel. It cannot be determined merely based on the mass balance from tap to tap since the amount of steel tapped is highly variable and there is a high uncertainty in the mass of the slag [12]. The best accuracy that can be obtained with respect to the mass balance is an average over several taps instead of at an individual tap basis.

In any event, with the assumption of constant hot heel mass holding, the hot heel should have little effect on the average heat and mass balance (and hence the temperature). It will be clear from the model fitting results that this assumption may be valid since a reasonable temperature fit is obtained.

[12] Deslagging invariably removes high volumes of iron, but the mass of slag removed is not measured - only an average over several taps is available. A lower limit on this iron loss can be estimated from information about of slag additive - under the assumption that all slag is removed at the end of tap. Then, based on the known slag analysis, the bath steel loss can be determined.

4.4 Analysis of collected slag data

The main aim of this section is to provide a summarized presentation of the slag data and relate it to similar data collected in other furnace literature, particularly Fruehan [19]. Three slag samples per tap were collected at various stages of refining for 10 taps; a further 8 samples were collected from 8 taps at tap time. This section presents the analysis results of the EAF slag; similar data was presented in Fruehan [19] for the BOF and Q-BOP. The experimental conditions such as basicity however, may not be the same.

Bath carbon is a strong function of the slag FeO. Low bath carbon will generally be accompanied by high levels of FeO. This is a direct consequence of decarburization by FeO: high carbon in the bath will reduce the slag FeO, otherwise the FeO will remain in the slag, and even increase due to higher levels of O_2 injection. This relationship is shown in figure 4.9.

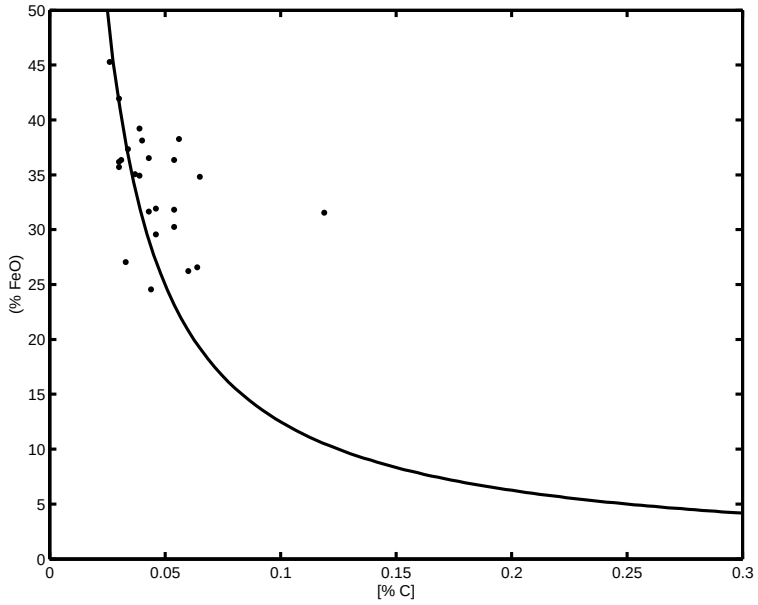

Figure 4.9: Relationship between slag FeO and bath carbon. The bath carbon values are the combined results of direct bath sample analyses and estimates based on the measured steel oxygen activity (reported by the composite lance).

This is in effect the relationship captured by the bath decarburization equation of (2.12). The equilibrium equation for the decarburization is given by Bekker *et al.* [39] as

$$(\,\%\,\mathrm{FeO})[\,\%\,\mathrm{C}] = 1.25, \tag{4.23}$$

this is also plotted in figure 4.9. Figure 4.10 presents an alternative plot, where the slope of the straight line is calculated as

$$(\,\%\,\mathrm{FeO})\sqrt{\%\,\mathrm{C}} = 7.5, \tag{4.24}$$

for $C < 0.1\,\%$; similar results were presented in Fruehan [19] in the case of the basic oxygen furnace where the slope was calculated to be $(\,\%\,\mathrm{FeO})\sqrt{\%\,C} = 4.2 \pm 0.3$ for $C < 0.1\,\%$, with a temperature range of $1610 \pm 20\,^{\circ}\mathrm{C}$. The temperature range of the collected data is larger at $1617 \pm 31\,^{\circ}\mathrm{C}$; this narrow temperature range will have a negligible effect on the FeO-carbon equilibrium.

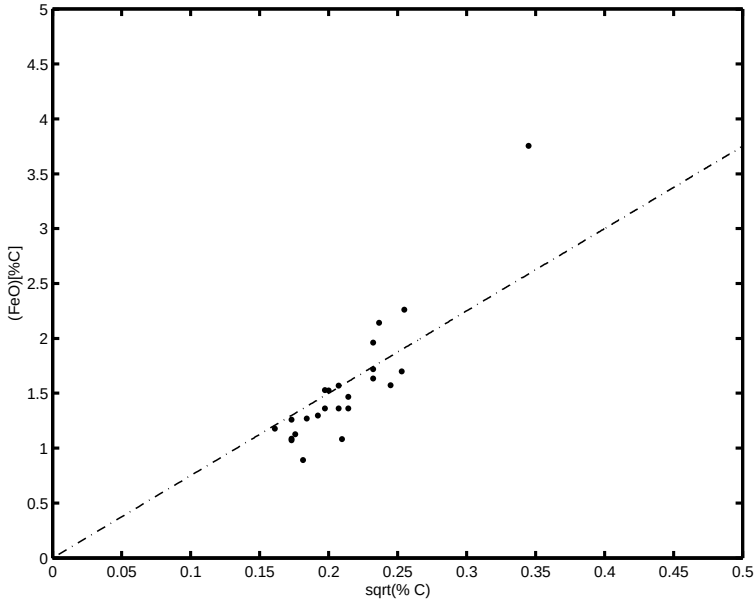

Figure 4.10: Relationship between slag FeO and bath carbon.

Figure 4.11 shows the plot of the relationship between the bath oxygen and the slag FeO. This relationship was discussed in subsection 2.2.4. Some of the scatter in the data can be explained in terms of the bath carbon content and other dissolved elements such as manganese and silicon. These will influence the concentration ratio

$$\frac{[\,\mathrm{ppmO}]}{(\,\%\,\mathrm{FeO})} = K, \tag{4.25}$$

where, for equilibrium, $K = 26 \pm 9$ with basicity $B = 3.2 \pm 0.6$ [19] and $K = 20.86$ for the corresponding concentration ratio line. For instance, a high bath carbon will lower the bath oxygen, hence the tendency of the data to scatter above the concentration ratio line for $C > 0.05\,\%$.

As an alternative to the oxygen-carbon relation of subsection 2.2.4, the following empirical relation can be obtained from the data:

$$K_{\mathrm{O-C}} = \frac{[\,\%\,\mathrm{O}][\,\%\,\mathrm{C}]}{p_{\mathrm{CO}}} = \frac{[\,\%\,\mathrm{O}][\,\%\,\mathrm{C}]}{P x_{\mathrm{CO}}}, \tag{4.26}$$

where $K_{\mathrm{O-C}} = 2.4 \cdot 10^{-3}$ (at $1600\,^{\circ}\mathrm{C}$) for equilibrium concentrations [36] and p_{CO} is the partial pressure of CO, here determined as being proportional to the mole fraction x_{CO};

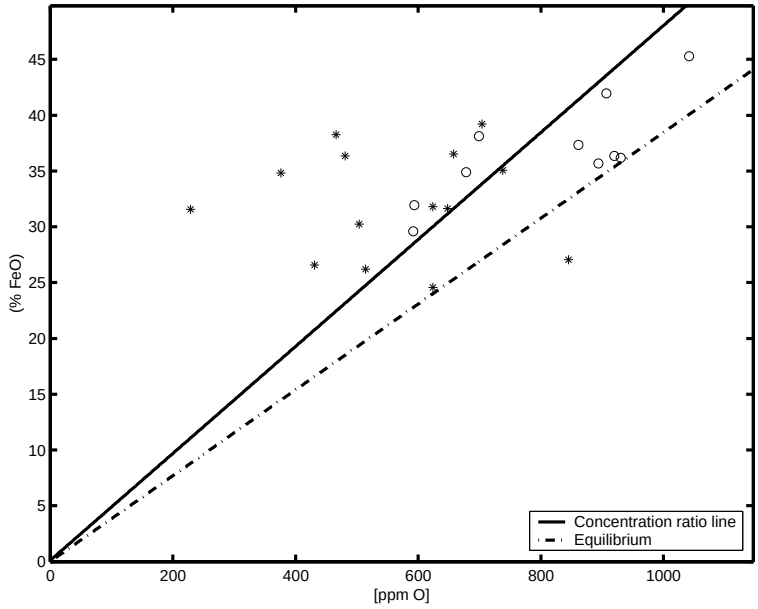

Figure 4.11: Relationship between slag FeO and bath oxygen. The concentration ratio line is a fit to the data resulting in $K = 20.86$ and $\circ$ - $\%\,\mathrm{C} < 0.05$; $*$ - $\%\,\mathrm{C} > 0.05$.

P is the total pressure, assumed to be atmospheric[13]. Figure 4.12 plots the bath oxygen-carbon relationship from collected data (see table A.1 in the appendix). One set of data is obtained from the composite oxygen lance. This lance analyses the bath for oxygen activity and estimates the bath carbon based on a predetermined empirical oxygen-carbon relationship. The second set of data (also on figure 4.12) is the bath oxygen content vs the analysis carbon. In this case the carbon content is from the analysis of samples obtained closest to the time when the bath was analysed for oxygen content. The carbon samples chosen were extracted within 2 minutes from the oxygen analysis - no other taps have carbon analysis results that lie within this period, hence the low number of data points.

Fitting the data to (4.26) results in $K_{\mathrm{O-C}}p_{\mathrm{CO}} = 2.749 \cdot 10^{-3}$. Assuming a partial pressure of $0.9P$ - since the gas generated in the slag-metal interface is predominantly CO - results in $K_{\mathrm{O-C}} = 3.1 \cdot 10^{-3}$. From the scatter of the analysis carbon and oxygen data (denoted by *) it is clear that the constant $K_{\mathrm{O-C}}$ will be higher than $3.1 \cdot 10^{-3}$. However due to the lack of sufficient data, the value of $K_{\mathrm{O-C}} = 3.1 \cdot 10^{-3}$ will be assumed accurate enough for all practical purposes since the estimated carbon (reported by the composite probe) is used in practice as a reliable measure of the actual bath carbon.

[13]This is a valid assumption since the furnace pressure deviates only slightly around the pressure $P = 100$ kPa.

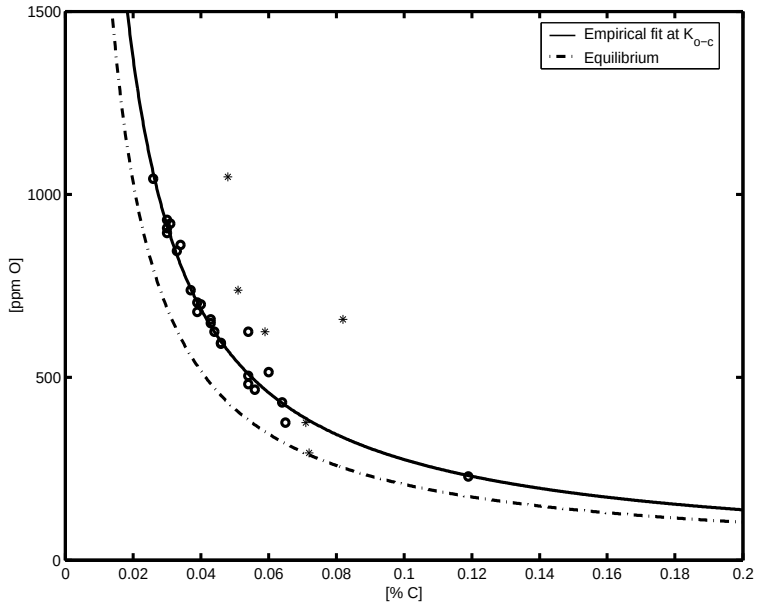

Figure 4.12: Relationship between bath carbon and oxygen. Concentrations for equilibrium conditions and the fit to the data are shown. o - composite oxygen probe: oxygen analysis and estimated carbon composition; * - oxygen analysis vs actual carbon analysis.

4.5 Conclusion

Experiment design is essential to any model fitting exercise. The requirements on the plant data must be met in order to carry out a realistic simulation of the actual process. This in turn forms an integral part of the parameter estimation process. The relationship between the model outputs, inputs and the parameters was studied - this is essential to establish whether available plant information can be used to estimate the model parameters. The collected data was analysed and compared with data obtained in other plant trials. This data is used for the model fitting of chapter 5.

Chapter 5

Identification of furnace data

The focus will mostly be on the bath carbon and temperature. These are the more commonly available data that are measured as part of standard furnace practice. Refining is also the most practical stage for which the model can be fit to a reasonable extent. The flat bath and stirring typical at refining mean that the modelling assumption of homogeneity (in the material and temperature) holds [39].

The problem addressed by this chapter is to fit the model to plant data. This mainly involves the selection of appropriate parameter values so that the model response matches the plant response to similar input. This also extends to other variables of interest such as initial conditions, heat losses and inputs that are not precisely known but are important in solving the problem. As far as possible the estimation of parameters will be carried by breaking down the model into its component parts. This will avoid the curse of dimensionality where the computational burden involved in the parameter estimation will increase exponentially with the number of parameters [47].

This chapter applies the results of the previous chapters to fit the model to data collected from an EAF installation. Comments and discussions regarding other variables will be made as appropriate.

This chapter is organized as follows. An overview of the estimation process as implemented in this dissertation is presented in section 5.1. Practical considerations that are possible threats to model validity are discussed in the next section (5.2). Brief model fitting for the meltdown temperature and slag phase elements is carried out in sections 5.3 and 5.4, respectively. The main results of the fit for refining temperature, carbon, oxygen activity and pressure are presented in section 5.5. Properties of the resulting parameters such as bias and variance are discussed in section 5.6. Section 5.7 summarizes the parameter estimate results and relates them to the furnace mass and energy balances.

5.1 The parameter estimation process

The estimation of the parameters will be carried out using the tools outlined in chapter 3. Each tap is treated as a separate batch with associated initial conditions, input and output measurements. These variables were discussed in chapter 4. In this section an overview of the parameter estimation process is given.

Two approaches can be followed: batch or online estimation. In batch estimation, the model is presented with the relevant plant data and the sum of the error over all taps is evaluated. The parameter estimate is computed by minimizing this total error. The estimate is computed over an entire set of taps. In sequential or online estimation, an estimate is obtained for data from each tap[1] and updated for each new set of tap data. In the current problem the data set is not large enough to take advantage of online estimation. The sequential estimation is suitable for online parameter estimation where the parameters can be updated as the conditions of the furnace change. For the dissertation, only batch estimation will be used.

The general process is to select a parameter vector, present the model with initial conditions of the specific tap, apply the measured inputs from the tap and then obtain a record of the corresponding model output. The error between the model output and the plant output is evaluated at some t_i where the plant output was measured. The measurement of output data (bath chemistry and temperature) was not obtained at regular intervals so that $t_{i+1} - t_i \neq t_{i+2} - t_{i+1}$ [2] and the model error is evaluated at arbitrary intervals during the refining period. The overall mean error is evaluated for each tap up to the last tap; the average is taken over the number of measurement points per tap. The overall mean error is then calculated as the sum of the average tap errors which in turn is averaged over the total number of taps. The parameter estimation problem is then to minimize this total average error by appropriate selection of the parameters. That is:

1. select an initial parameter vector θ_0,
2. simulate each tap using the corresponding measured data and evaluate the average error over the data points;
3. then compute the total average error V over the total number of data points

[1] In the case of the EAF data collected, a set of tap data will be a collection of data containing the inputs and outputs sequence and initial conditions for the particular tap. Therefore, in the sequential case each set of tap data can be treated as a single data "point" that is used to estimate the parameters. This modification is necessary since the furnace is a batch process with only a few data points per batch (tap). Each tap has only a few output data points with associated initial conditions. There is no continuity in time from one tap to the next.

[2] In the case of measured temperature, interpolation was used between actual measurements - this increases the number of samples and improves the model temperature fit.

4. if V is a minimum, stop else continue
5. update parameter vector θ_j
6. if V is a minimum, stop else go to step 2

The process is illustrated in figure 5.1

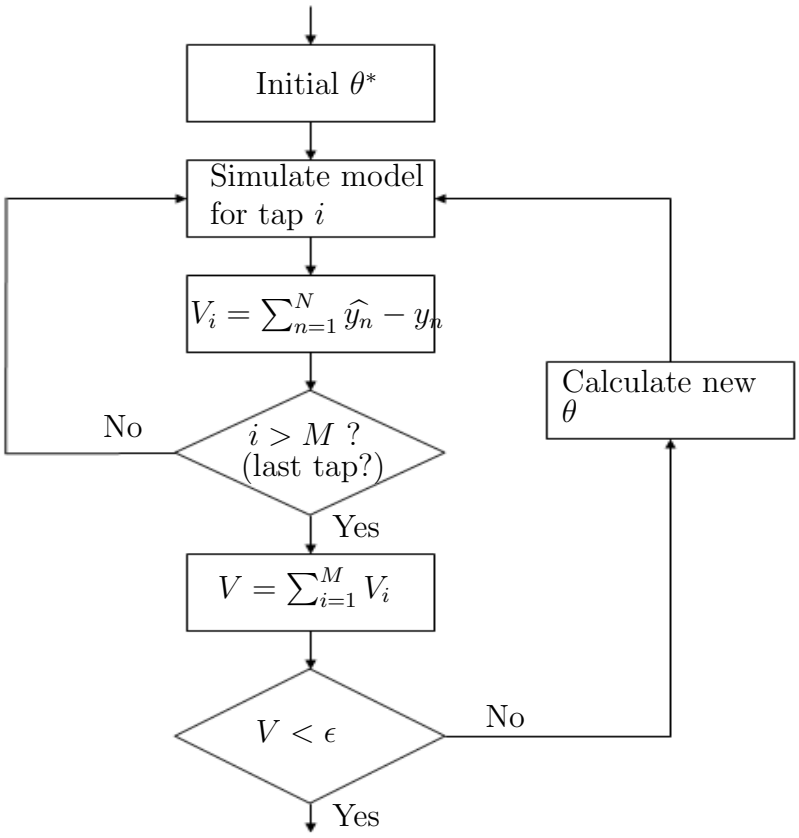

Figure 5.1: The parameter estimation loop for N data points per tap and a total of M taps.

5.2 Threats to model validity

The EAF is a highly stochastic process. While a majority of the behaviours in the furnace are deterministic, practical and operational considerations will have a marked effect on the states in the furnace.

The model was derived under the assumption that all the states in the furnace evolve deterministically. This assumption is valid most of the time but unmeasured disturbances will have an effect on the process such that the assumption will cease to hold. For instance,

under applied energy input, the bath temperature does not always increase nor does the bath carbon content always decrease in the presence of sufficient slag FeO or oxygen injection. These problems arise mainly from the distributed nature of the temperature and composition in the bath; a discussion of an approach that takes this distributed nature into account is given by [63] and [64]. The results were obtained for the submerged arc furnace but it is expected that they will apply in the case of the EAF. However, it must be borne in mind that an extensive sampling campaign was carried out to obtain the data that was used to arrive at reliable statistical results - much less data was used in the current dissertation.

This section will investigate the regions of operation of the furnace under which the state behaviours will proceed as expected based on theory, and conditions under which these expectations are not met. Possible explanations for the anomalous behaviour will be given based on observed furnace practice.

5.2.1 Effect of scrap cave-in

Scrap cave-in occurs when pieces of scrap fall into the molten bath. Depending on the size and shape of the scrap, some of the scrap will remain attached to the furnace side walls. As the charge melts, most of this scrap will fall into the bath. This generally occurs early during meltdown but has also been observed in the late stages of refining. A typical example of the latter case normally occurs after temperature and carbon measurements are being taken for adjustment. In this case all measurements of temperature and carbon up to the time of cave-in will be invalid. This is the case that has direct implication in this dissertation.

The effect of the cave-in on the temperature and composition of the bath will depend on the properties of the falling scrap. Qualitatively, a cave-in will always result in a decrease in the bath temperature and, depending on composition of the scrap, a decrease, increase or no change in the bath composition. In all instances, to quantify the resulting changes to the bath the mass and composition of the scrap must be known. This information is generally not available.

Plant data where cave-in has been observed resulted in an average change in bath temperature of $-15\,^{\circ}\mathrm{C}$; the increase in carbon composition can be negligible or as high as $0.023\,\%$. On average, a larger change in bath temperature was observed as opposed to carbon composition. Since the oxygen content is closely related to the carbon, it also undergoes comparatively little change.

5.2.2 Effect of unmelted scrap

During refining some solid scrap in the bath can go undetected. The effect of this scrap on the validity of bath temperature and analysis is similar to that of cave-in, but may be less detrimental. A cave-in is suspected when a sudden excessive splashing of the slag occurs. Then the operator is able to take additional measurement once the scrap is fully melted. On the other hand, unmelted scrap can hardly be detected under a foamy slag and measurement readings will be used under these (unfavourable) conditions. As in the case of cave-in a temperature decrease will occur with the effect that larger energy inputs are required to increase the temperature to the desired level. Late melt-in is proposed as a possible explanation for the disproportionately slow increase in temperature that is observed for some taps.

Cave-ins and late melt-ins are a common occurrence in the EAF practice. However they are an undesirable occurrence as they upset the normal running of the furnace, this in the form of delays. They are variable, and due to the lack of data relating to the masses and compositions involved, they cannot be reliably quantified. Therefore, these anomalous occurrences will not be included in the model fitting. That is, all data for which a cave-in was observed or a late melt-in is suspected will be rejected. This approach is similar to that adopted by operators in practice: reject all measurements up to the time of cave-in or suspected melt-in and take new measurements on which new control decisions will be based.

On the other hand, these abnormal occurrences could be avoided by judicious choice and treatment of the scrap charge: large pieces of heavy scrap must be cut before charging, or a regime for charging could be adopted where most of the large scrap is introduced in the first charge, affording longer time for melting the high density scrap. The positioning of the oxyfuel lances can be optimized to better cope with cold spots. In fact some melt shops employ manipulatable lances that are able to follow the scrap as it melts (or to be targeted to specific cold spots for accelerated melting) [19].

5.2.3 Unscheduled delays

Some unscheduled delays during refining will have a marked effect on the consistency of refining operation. While heat and energy balances will be maintained, the source and extent of inputs and disturbances will vary depending on the delay. Several cases are worth a mention, viz. slipping and joining of electrodes, maximum demand power off and delays in obtaining bath samples.

In the absence of any foaming events (and arc input), prolonged delays will decrease the foam height since the gases trapped in the foam will only last a finite time - the gas

residence time is finite. This will in turn increase the coefficient k_{VT} by increased heat loss from the bath surface. The heat loss from the furnace will therefore be higher. However little or no measurement takes place during these delays, so the loss will be impractical to quantify.

Maximum demand power-off occurred in approximately 28 of all 78 taps collected[3]. These occur when the power consumption of the EAF exceeds the hourly limits that are set based on the maximum power that may be drawn from the electrical supply utility [22]. They will typically influence the refining stage, since they occur towards the end of tap when high levels of electrical energy have been consumed. On average, the delay lasts for 3.7 min with a standard deviation of 2.0 min. With no graphite injection (and negligible bath carbon), there is little gas generation to sustain a stable foam even under suitable slag conditions. The interfacial area between the slag and bath is small since no oxygen injection takes place; therefore the effect of decarburization will be too insignificant to sustain a steady foam. Therefore, the foam will gradually decay, leading to increased heat losses.

5.2.4 The effect of deslagging

In practice, deslagging presents several complications that cannot be reasonably or practically quantified. Several cycles of deslagging take place during refining. The first is the main deslagging that removes a large volume of slag[4] before a bath sample is extracted and temperature measurements are taken. The mass of this eliminated slag will vary depending on the prevailing slag volume and the time for which the deslagging takes place. The difficulty posed by the deslagging is that the eliminated slag is not measured.

For convenience, it will be assumed that this deslagging does not have high associated temperature losses since the slag and bath are at the same temperature - the only loss will result from a reduced foam. Then the overall heat loss coefficient k_{VT} will account for the heat loss that may occur from this deslagging (along with other heat loss routes such as radiation).

5.3 Model fit for meltdown temperature

Very little measurement of process output takes place during meltdown. One piece of output information relating to this stage is the temperature at flat bath. The time at which this temperature measurement is taken is regarded in this dissertation as the practical onset of the flat bath stage: it is loosely assumed that when a first temperature

[3]Of the 78 taps only 18 were monitored and for 10 taps out of the 18 more extensive data was collected.
[4]This has the added advantage of removing sulphur and phosphorus before they revert into the steel.

measurement is taken the bath has fully melted - this may not be true at all times. The decision that a flat bath stage has been reached - and therefore that the bath is ready for temperature measurement - is usually based on operator intervention or can be an estimate from the computer control system based on the EAF static model [22]. This decision is based on several factors:

- visual inspection of the furnace slag or bath - the colour and viscosity of slag changes as a function of temperature;
- interpreting the audible noise patterns emanating from the furnace - the level and frequency of the noise is a strong function of the current state of the furnace,
- monitoring the activity of the arc voltage and current levels - large current and voltage fluctuations take place at early meltdown then decrease near flat bath (along with the audible noise levels), and
- the total electrical energy consumed is often a good indicator of when melting has occurred; however, its accuracy will depend on the quality of scrap and the size of the charge.

These indirect methods are used successfully by operators to make decisions about when a flat bath stage has been reached.

A study of a related problem of estimating the furnace conditions based on arc current and voltage signal variations has revealed a close correlation between the various signal patterns and the state of the furnace [33]. An analogue to this is the interpretation of audible noise patterns (by operators) as indicators of the furnace state.

Once a flat bath is detected (according to the opinion of the operator), a bath temperature is taken and a sample extracted for laboratory analysis. The temperature will be a function of all the prevailing furnace conditions from beginning of tap up to $t = t_1$. It will depend on all material additions, inputs and initial conditions - information in respect of these has a varying degree of availability. The temperature will also be strongly influenced by the energy losses during the tap, which are largely affected by unmeasured disturbances. In the ideal case, a successful fit for temperature will indicate that the model was able to depict/represent the main behaviour of the plant and that unmodelled disturbances were insignificant after all or that their effect was successfully smoothed out of the model by using a number of taps for the parameter estimation.

Significantly, a successful fit means that the energy balance of the furnace is maintained by appropriately taking into account the energy inputs, sinks and losses. The losses will be the balance of all input energy not accounted for in the sinks. That is, all energy not

used to melt and then provide the superheat to raise the temperature of the raw materials above melting point.

The chemical energy defined by P_T is the net energy. This energy results from the reactions that take place in the bath, the slag, the freeboard and the interface between these phases. It also takes into account the significant loss of calorific and sensible energy of the product gases to the off-gas.

The parameters that influence the final temperature of the bath are

- η_{ARC}
- η_{OXF}
- η_{FeO}
- k_{VT}

As mentioned, only one measurement of temperature is available per tap. For any one tap, the system is underdetermined: there are 4 unknowns in only one equation $\Phi(\eta_{ARC}, \eta_{OXF}, \eta_{\mathrm{FeO}}, k_{VT}) = 0$.

The melting rate constants k_{therea_1} and k_{therea_5} determine the rate at which melting will proceed. When a solid is introduced into the furnace, the temperature of the liquid group will drop to a level dictated by the existing energy balance - the solids will effectively cool the furnace. Based on the model, a situation will occur where the bath temperature drops well below the melting point of 1538 °C [17] and thus solidify - this does not occur in practice. The main reason is the assumption of homogeneity that was made in the original model derivation: in practice, only liquids in the vicinity of the solids will solidify, on the other hand the model will predict low levels of liquid temperatures since the energy balance applies over the entire charge and not at the solid-liquid interface, as happens in reality where there is a finite interface for heat transfer. Therefore care must be taken not to have melting rates that force the liquid temperatures too low - to preserve as close a depiction to reality as possible, otherwise it must always be borne in mind that this deviation from reality is a modelling convenience. The melting rate is inherently distributed in nature - treating it as a constant is a simplification. However, only an average representation is important for the application of the model. A lumped parameter model will be adequate for control purposes where feedback is used to compensate for modelling errors.

An analysis of the off-as composition will reveal valuable information on the value of η_{ARC} and possibly η_{FeO}. Products of the combustion of the oxyfuel system are exhausted with the off-gas. The extent of this combustion is controlled by η_{OXF}. In the presence of sufficient O_2, a $\eta_{OXF} = 1$ means that all fuel inputs to combustion are consumed, leaving only H_2O, CO_2 and excess O_2 as products to be removed through the off-gas. On the other hand, low efficiency will present the entire fuel gas to the off-gas analysis, together

with the unused O_2. Some contribution to the off-gas composition will come from the slag-metal reactions and graphite injection into the slag. Nonetheless, an analysis of the off-gas is the most practical and direct method to obtain information pertaining to the oxyfuel system and the parameters that govern it.

During lancing, O_2 is injected as a high energy stream directly into the bath. Some fuel gas is also injected; in this case its main role is to shroud the O_2 stream. It also serves to cool the lance nozzles under the extreme heat of the furnace environment. Very little combustion takes place. Lancing will be accompanied by generation of large volumes of FeO. A measurement of the changes in slag FeO and the injection of O_2 will indicate just how much FeO is generated for a given volume of O_2, whence the value of η_{FeO} can be estimated. Indeed the FeO being generated will depend on the bath decarburization and any foaming that may be taking place - these factors must be taken into account in estimating η_{FeO}. The rate of FeO generation disregarding decarburization and foaming will provide an upper limit on the value of η_{FeO}.

The effect of $k_{_{VT}}$ is attributed to the inherent losses that result by virtue of the furnace being at a higher temperature than its immediate environment. When a fully charged furnace is put into an idle state - with no arc or burner heat input - the heat losses will be governed largely by $k_{_{VT}}$ (and to a lesser extent by cooling water losses). Such an idle state under a complete foam, closed roof and slag door, result in a reported temperature loss of 2 to 3 °C/minute [22]. A minimum value of $k_{_{VT}}$ can then be estimated from

$$\dot{x}_{12} = -\frac{k_{_{VT}}(x_{12} - T_{_{AIR}})}{\left[\frac{x_2 C_p(Fe_L)}{M_{Fe}} + \frac{x_3 C_p(C)}{M_C} + \frac{x_4 C_p(Si)}{M_{Si}} + \frac{2x_6+2x_7+3x_8}{M_{slag}} C_p(Slag_{(L)})\right]}, \tag{5.1}$$

giving $k_{_{VT}min} = 0.837$ kW/K. This value will be higher when there is no adequate foaming, and when the slag door or furnace roof are open. This will happen at various stages during meltdown: when the roof and slag door are opened for charging, furnace inspection or relining (fettling) of the furnace walls and when conditions are not conducive to proper foaming. Generally, a higher value for $k_{_{VT}}$ should be expected.

Water cooling is another distinct mechanism by which the heat energy of the furnace is lost. The detrimental effect of excessive arc radiation on the refractories is alleviated by the cooling of the panels onto which the refractries are attached. The water loss will be a function of all the heat inputs to the furnace, with the overriding contribution coming from the arc radiation (and to a limited extent from the oxyfuel system). When the furnace is idle for charging the cooling loss is at its minimum, while a peak in this value is reached during arcing (and oxyfuelburner mode). The heat energy removed with the water will be given by

$$\Delta E = (T_{out} - T_{in})\dot{N}_{\mathrm{H_2O}}, \tag{5.2}$$

where T_{in} and T_{out} are the temperatures of the inlet and outlet flows; $\dot{N}_{\mathrm{H_2O}}$ is the molar flow rate of the cooling water, generally flowing at a maximum of 23 mol/s. For this dissertation the average ΔE per tap will be taken as the constant loss over the tap, except at off-times when no power is applied and little change in the water temperature takes place.

η_{ARC} can be defined as the ability of the arc to transfer its heat energy to the bath. Under ideal conditions all the arc energy will be transferred to the bath, in which case $\eta_{ARC} = 1$. However significant losses occur when large regions of the arc are not covered either by the scrap or foam. Scrap bore-in keeps large regions of the arc covered - this only happens at early meltdown. Under flat bath conditions foaming can be used to shield the arc. At all other times the arc is exposed and significant losses occur by arc radiation to the furnace walls and roof.

The efficiency of the arc at meltdown is reported as $\eta_{ARC} = 0.6$ [19]; this will serve as the starting value for all parameter estimation that will follow. Arc energy contributes at least 75 % of all energy inputs to the furnace [19] - it will have the largest effect on the bath temperature, therefore η_{ARC} will be the main parameter used for fitting bath temperature. For an equivalent-sized furnace the oxyfuel subsystem contributes 5-10 % to the energy input, and chemical reactions 30-40%, of which a large part originates from bath oxidation. In order of fitting authority the efficiency parameters are: η_{ARC}, η_{FeO} and η_{OXF}. Assuming that a similar practice is followed for the current plant, the initial values arrived at are

$$\begin{aligned} \eta_{ARC} &= 0.506 \\ \eta_{\mathrm{FeO}} &= 0.748 \\ \eta_{OXF} &= 0.7 \\ k_{VT} &= 0.420 \end{aligned}$$

These are used as starting values in the penalty function minimization procedure that follows. Collecting the parameters into a single vector gives:

$$\theta = [\eta_{ARC}, \eta_{\mathrm{FeO}}, \eta_{OXF}, k_{VT}]^T, \tag{5.3}$$

arranged in order of decreasing output sensitivity. The parameters: k_{dSi}, k_{dC} and k_{gr}, will have a marked effect on the chemical energy of the furnace, but their primary effect is on the mass balance, from which they will be estimated. It is assumed that no foaming occurs during meltdown. This may not be completely valid since an automatic foaming system is in place [5]. This will control the injection of graphite but, when it occurs, it will

[5]The decarburization reaction will generate high levels of CO which will foam any slag that has melted at that time.

generally be confined to the late melting stage, no more than 5 minutes before meltdown ends. The average effect of this foaming on η_{ARC} will generally be negligible since the foaming only occurs for a short period during the entire meltdown stage. Therefore the assumption is valid for all practical purposes.

An improved accounting for the energy losses in the furnace will help the determination of the true values of temperature parameters. Underestimating the losses will lead to higher energies being made available to use in the furnace, thus leading to an overestimate of the temperature values. To remedy this, the values arrived at for the efficiency parameters will be lower than in practice, or as obtained in other work (where efficiency is reported [19]). The converse is also true. Therefore an incorrect estimate of the losses will lead to impractical values for efficiency, even if a good fit for temperature is obtained.

5.4 Model fit for the slag phase

The original model derivation treats the slag as one composite state made up mainly of CaO and MgO; these are lumped together into one state with equivalent heat of fusion, heat of solution, molar mass and specific heat [39]. FeO and SiO_2 are modelled separately as materials dissolved in the slag. Other components such as Al_2O_3 , MnO, phosphorus and chromium are assumed negligible. This assumption is verified by the results of table 5.1, which shows the average slag compositions. CaO, MgO, FeO and SiO_2 make up, on average, more than 90 % of the slag. The values in table 5.1 are averages over the total collected slag data - the actual values will vary depending on the properties of the scrap and the slag additives.

Table 5.1: Average slag composition.

Component	Composition [%]
CaO	38.85
MgO	5.73
FeO	33.27
SiO_2	11.17
Al_2O_3	3.90
MnO	3.83

5.4.1 Model fit for refining slag

Based on the reported slag analysis and charge composition the average slag mass can be computed. The important constituents in the slag are FeO, CaO, SiO_2 and MgO, with trace contributions from Al_2O_3 and MnO. CaO results from slag additions of lime and doloma; the masses of these additives are known - part of the charge practice is to measure

all the additives to achieve accurate proportions. All the lime and doloma charged are melted to form CaO and MgO in the slag. The composition of CaO in lime is 90 % and 63 % in doloma. Using the composition of CaO and the mass of slag additives, the slag mass can be calculated for each tap. In summary, the average percentage FeO in slag per tap is $\mu = 33.3\,\%$ with a standard deviation of $\sigma = 6.1\,\%$.

5.4.2 Model fit for refining FeO

The charge DRI makes a small direct contribution to the slag FeO (FeO$\approx 10\,\%$ DRI [6]), with the main component originating from bath oxidation. On the other hand, the FeO mass is decreased through reduction by decarburization and graphite injection. Therefore, variables with the most direct influence on the change in FeO are: the parameters ($\theta_{slag} = [\eta_{\text{FeO}}\,, k_{gr}\,, k_{d\text{C}}]$) and inputs: oxygen injection, graphite injection, bath carbon. No DRI injection takes place, therefore it does not contribute to changes in the FeO (since all the charge DRI is fully melted before refining).

Slag FeO levels have direct implications for the decarburization and desiliconization. It, together with slag and SiO_2, establishes the equilibrium conditions which drive the rate of these reactions. The slag is fixed by material additions and most bath silicon is oxidized to SiO_2 early at refining - very little changes occur in the mass of slag and SiO_2 at refining except by deslagging. Therefore FeO is the only slag constituent that fluctuates during refining: by decarburization, graphite injection and bath oxidation.

Figure 5.2 depicts the model output relative to the measured slag output where the adjustable parameters are $[\eta_{\text{FeO}}\,, k_{gr}]$; $k_{d\text{C}}$ is only used for the adjustment for decarburization as it is the primary parameter that governs this behaviour. The 95 % confidence interval is used to depict the variation in the model output when the parameters are varied from their nominal values. From section 3.7.2, the variation in parameters is of the form $\theta_N^{(k)} - \alpha < \widehat{\theta}_N^{(k)} < \theta_N^{(k)} + \alpha$, where α is the parameter variation that corresponds to the 95 % confidence level. This confidence interval depends on the properties of the model after it has been fitted to the data. It will therefore not hold if the operating point of the furnace or the statistical properties of the data change significantly.

The time axis of the plots in figure 5.2 and all other plots in subsequent sections is taken as the time in minutes from midnight; i.e. the time of day converted to minutes. The refining period of tap 1 begins at approximately 424 minutes, equivalent to 7:04 AM. The model FeO output has a consistent offset above the measured FeO. This is due mainly to the effect of a high η_{FeO} - it was adjusted to accurately model the bath carbon and temperature at the expense of the slag FeO.

[6] Based on the difference between the total and metallic Fe content of DRI (88 − 78 %) [22].

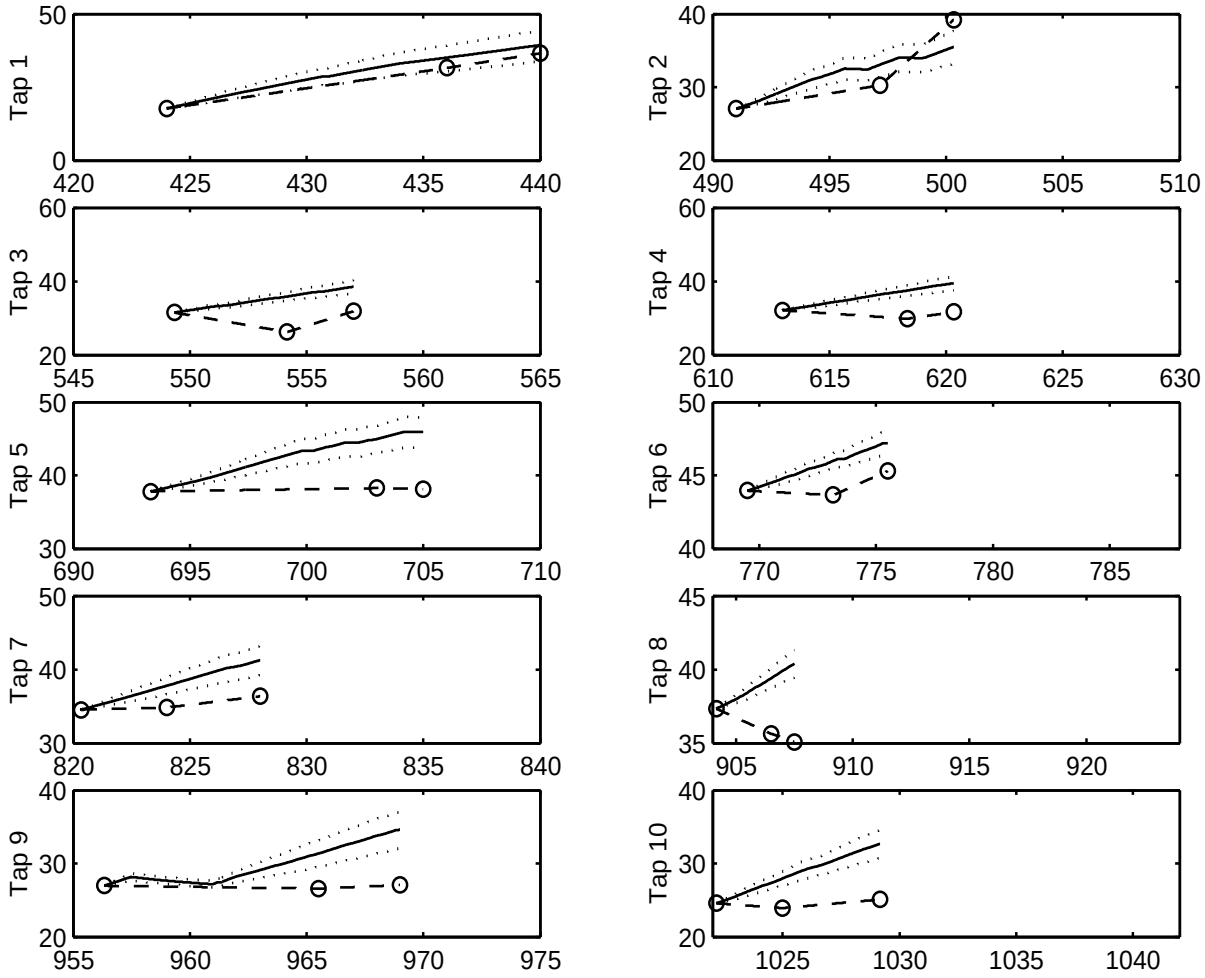

Figure 5.2: Model slag % FeO (solid) compared to the measured % FeO [wt %]. The line − − − depicts the interpolation between the measured FeO values; the solid line —— depicts the model FeO output. The model 95 % confidence interval is shown as the dotted line (· · ·). Each plot is generated over a time window of 20 minutes from the first minute of simulation - this enables comparison among the taps.

5.4.2.1 The relationship between bath carbon and slag FeO

Measurement of slag FeO is not standard practice. The average slag FeO calculated in table 5.1 can be used as an estimate for all unmeasured slag FeO. Another approach is to take advantage of the relationship between the bath carbon and slag FeO. High levels of bath carbon are accompanied by low levels of FeO and vice versa. This relationship was discussed in section 4.4. Using the measured carbon and corresponding slag data, an empirical relationship can be determined; this can be used to estimate the FeO based on the measured bath carbon[7].

[7]The model decarburization is derived from a similar relationship: the difference between the bath carbon at a given time and the equilibrium carbon. Near equilibrium, the relationship between the model carbon and FeO approaches that of the measured values.

5.4.3 Model fit for refining SiO_2

Direct contributions to the slag SiO_2 originate from lime and DRI additions. Each contains approximately 3 % SiO_2. Over the 18 taps, these sources translate to an average of 3.1 % SiO_2 and not the measured 11.17 % - the deficit must originate from the bath. This means 0.73 % Si was oxidized from the bath - this value fixes the initial bath Si, in addition to the negligible 0.028 % Si that remains as the minimum bath Si (see subsection 5.5.1).

5.5 Model fit for refining

Refining is the final stage in EAF operation where the properties of the steel can be adjusted to meet specifications as required by downstream processes. A meltdown temperature of the bath is taken and a steel sample is extracted for laboratory analysis. The analysis will report the compositions of the various alloying elements and impurities in the bath; carbon is the most important alloying element. Based on this information about bath temperature and chemistry, controlled adjustment of these variables commences.

It is common to have more than one temperature measurement during refining. Many reasons exist for this. The main one being that obtaining the required bath temperature is a continuous adjustment process: a measurement is taken followed by operator control; this process continues until the aim temperature is reached. Other reasons are the error in instrumentation, improper placement of sampling probe during measurement or sampling before all scrap is fully melted (including cave-in) - each of these is remedied by taking additional measurements.

This section presents the results of the model fit for the bath carbon, silicon, temperature, and other furnace states. Input data and initial conditions obtained in the previous chapter will be applied to the model derived in Bekker [5] - with some modifications from chapter 2 and Oosthuizen [7]. A comparison of the model and plant response to the same inputs is presented and evaluated. A final set of parameter values is obtained.

5.5.1 Model fit for refining silicon

The sources of SiO_2 in the slag are the bath and direct SiO_2 contribution from DRI and lime. The latter can be assumed to have been fully melted at refining and will contribute no additional SiO_2 to the slag. Due to its large quantity, the bath contributes significant levels of silicon, despite a small percentage of 0.73 %. Regardless of the source, bath silicon reaches its asymptotic stage well before refining since it is oxidized early in the process [19]. A strong confirmation of this is the composition of bath silicon at refining, measured simultaneously with carbon. The average composition (over the entire refining period) is $\mu = 0.028\,\%$ with standard deviation $\sigma = 0.0046\,\%$, a constant composition

for all practical purposes - this also establishes the minimum bath silicon. In comparison, carbon decreases significantly from the beginning to the end of refining: from an average initial $\mu = 0.096\,\%$ and standard deviation $\sigma = 0.041\,\%$, it drops to a final average of $\mu = 0.040\,\%$ (with standard deviation $\sigma = 0.0093\,\%$). In fact the actual composition of silicon is always much lower than the minimum specification of $0.1\,\%$ - adjustment to meet this specification is relegated to the ladle furnace.

For all practical purposes the bath silicon is assumed to be at its minimum at refining, with very little desiliconization taking place. Therefore, the corresponding rate constant will be chosen at $k_{dSi} = 0$ i.e. no desiliconization takes place at refining.

5.5.2 Model fit for refining carbon

Previous work in model adjustment of carbon to plant data was to fit the model output for an entire tap simulation to a constant carbon measurement at tap time [5]. The fact that the measured carbon is constant does not show the ability of the model to depict decarburization sufficiently. Because data from only one tap was used, the extension of the model to variations such as bath mass, carbon content, slag chemistry etc. were not take into account. On the other hand, an exhaustive simulation was carried out where natural variations were allowed in material feed rates and compositions, and power transfer efficiencies [7]. The resulting effect on output was considered but not the accuracy of the output itself, as it would respond in an actual furnace to the same variations. In all cases, however, the response to input was the same as expected from an actual process, but could not be verified sufficiently due to lack of plant data.

The dynamics of bath carbon and temperature are one-way decoupled. As the model stands, temperature has a limited effect on decarburization. This was shown in the identifiability study in chapter 4. In practice, the removal of carbon from the bath is independent of temperature. On the other hand, decarburization will have an effect on temperature by the reduction of FeO which is endothermic. A similar argument can be made for desiliconization. For this reason the fit for carbon and silicon will be carried out first, and then the parameters fixed to be used in the next section for the model fit for temperature.

With the slag conditions established as in the above section, the fit for carbon essentially reduces to that of estimating the decarburization rate constant. Several measurements for bath carbon were obtained along the refining stage. The model fit was carried out by minimizing the error between the model output and the measured bath carbon content. The output is the percentage composition of bath carbon, given by Oosthuizen [7]:

$$y = \frac{x_3/M_{\mathrm{C}}}{x_2/M_{\mathrm{Fe}} + x_3/M_{\mathrm{C}} + x_4/M_{\mathrm{Si}}}. \tag{5.4}$$

An alterative is to use the actual mass of bath carbon, but this may be prone to errors in the modelling for the bath mass.

The results for the carbon fit over the test taps are shown in figure 5.3. The model output is shown relative to the measured values. The corresponding decarburization rate constant is $k_{d\mathrm{C}} = 53.341\,\mathrm{kg/s}$, with a mean error of $\sqrt{V_N} = 0.012\,\%$.

In each of the plots shown, the model bath carbon is initialized to an arbitrary value until a valid measurement is available. It is then re-initialized to the first valid measured carbon as soon as it is available at some t_1 - hence the instantaneous rise or drop in bath carbon at the first valid measured carbon. The model fit for the carbon is then carried out between t_1 and t_{end} i.e. the error is evaluated only at points subsequent to the first measured data point. This is necessary since the measured results for each of the variables are obtained at different times. A similar procedure is followed for the temperature fit; this is not necessary for fitting to the slag data since the slag was always the first measurement to be obtained during the plant trials.

The one measurement at Tap 1 was deemed unreliable as it deviates significantly from the carbon trajectory. Furthermore, for this tap, no cave-in was detected or late melt-in suspected; a consistent temperature increase was also observed (see subsection 5.5.4), therefore, accepting this measured carbon would introduce a significant deviation from the general trend of the other data points of the same tap. A similar argument can be made for Tap 9 and Tap 10 where an increase in the measured carbon is observed. In most cases, a cave-in or late melt-in seldom has a significant effect on the carbon content although exceptions are possible in the cases of the high carbon cast iron or pool iron being involved in the cave-in or late melt-in. The possible explanations for the deviations are: improper sampling conditions, improper placement of sampling probes, or inherent error in the measuring instrument.

In practice, the last measurement is used as a conclusive record of the bath carbon. For all practical purposes, the bath temperature and composition can be assumed to be fully homogeneous near tapping. Therefore, this last measurement can be treated with the highest confidence and used as a benchmark for assessing the plausibility of other measurements during refining. The first measurement will not be as reliable since the bath may not be fully melted or the temperature not appropriate for extraction of a sample.[8]

[8] In practice, samples may be rejected because the temperature is too low or the sample was extracted close to a piece of solid scrap. This is rare (one sample was rejected from the 10 monitored taps), but it may occur unnoticed during a tap in which case, the analysis results may be inaccurate.

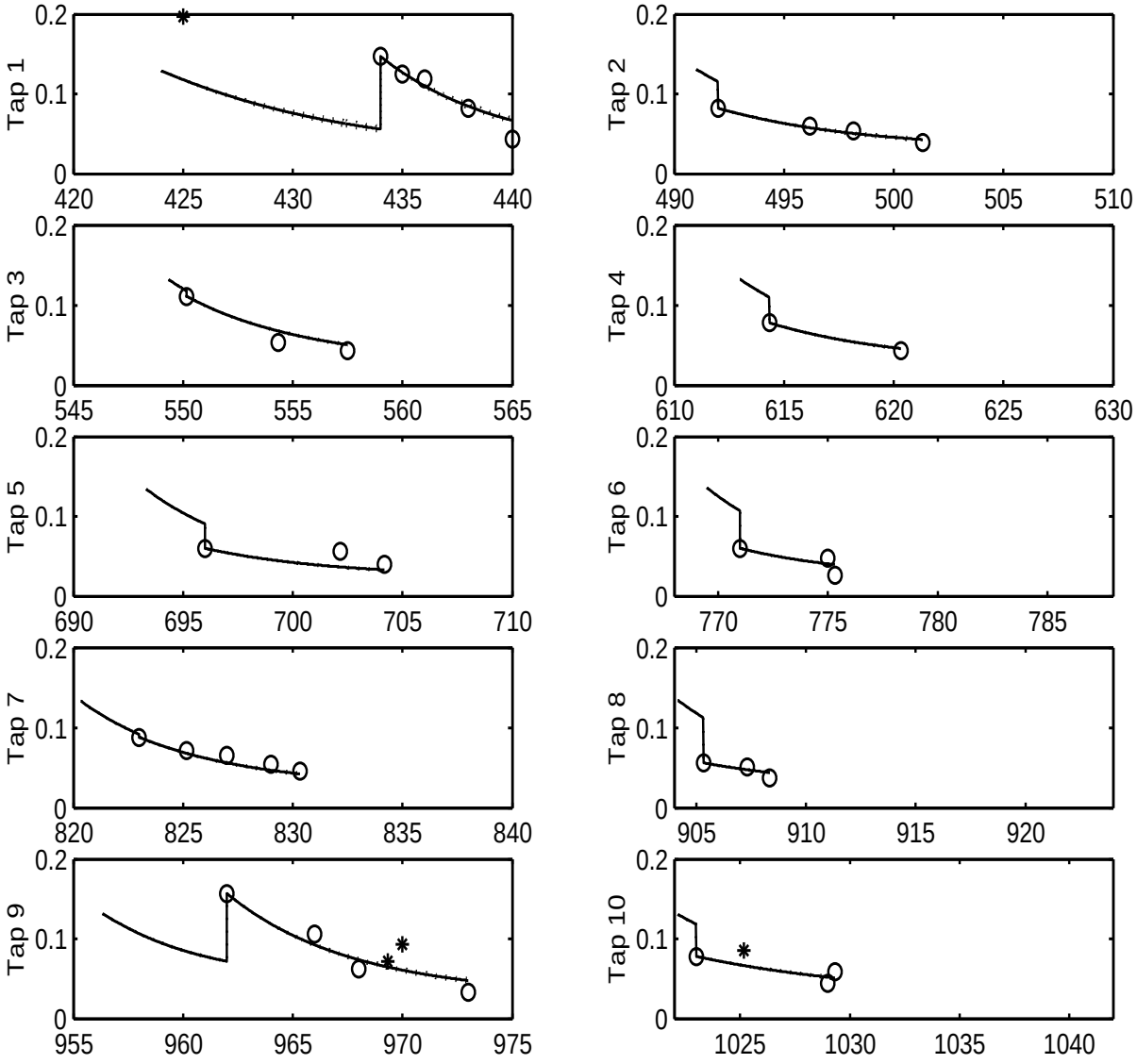

Figure 5.3: The model fitting to measured carbon data [wt %]. o - measured carbon; * - rejected carbon measurement and the solid line —— is the model carbon output. The model is initialized to an arbitrary bath carbon level (0.1 %) - the carbon level is updated as soon as a valid measurement is made available, hence the instantaneous rise or drop in carbon near the first valid measured carbon. The model 95 % confidence interval is also shown as the dotted line (· · ·). It is only slightly visible in tap 1 - it is too narrow to be visible on the other taps. Each plot is generated over a time window of 20 minutes from the first minute of simulation and over a carbon range from 0 to 0.2 wt % - this enables comparison among the taps.

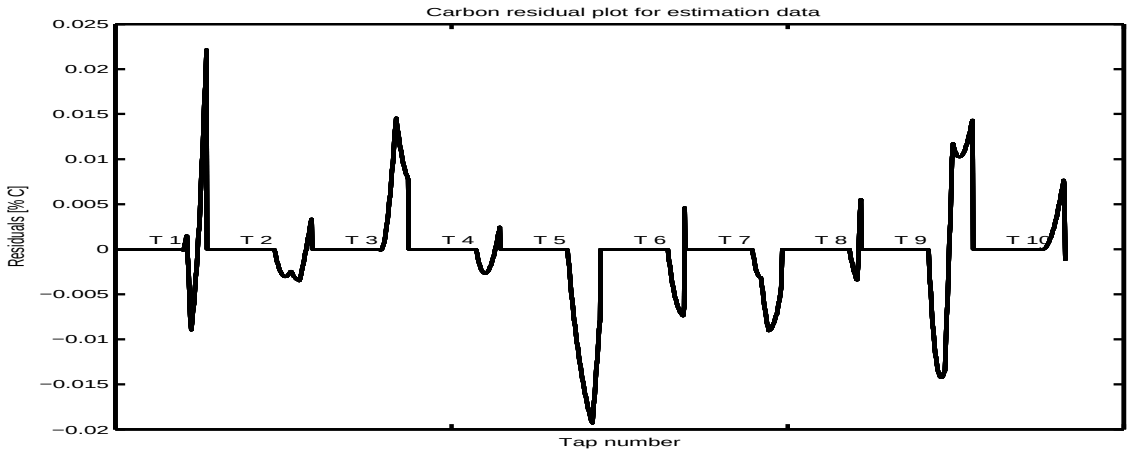

Figure 5.4: Residuals of the carbon output for all test taps. The tap number T_i, $i = 1, \ldots, 10$, is followed by the error at the single-point carbon measurements for the refining period shown in figure 5.3. Tap 4 has no error.

5.5.3 Bath oxygen activity

As mentioned, oxygen injection provides a valuable source of chemical energy. Depending on the bath conditions, some of the oxygen injected will oxidize the bath while some of it will remain dissolved in the bath. It is the limits on this dissolved oxygen that restrict the degree to which oxygen can be injected into the bath. High oxygen has detrimental effects on the quality of the final product. This is in the form of metallic oxide inclusions that result from oxidation of iron, manganese, silicon, aluminium, etc - they affect the cleanliness of the steel [36]. The oxygen also has the effect of reducing the alloying efficiencies (recovery rate) and leads to generation of gas (CO) as the steel solidifies [17]. Although deoxidizers can be used to lower the oxygen content, they introduce additional raw material costs and compromise the cleanliness of the steel by introducing oxides that may have to be removed by downstream processes. A low oxygen content is also important for the removal of sulphur from the steel.

Two important factors determine the solubility of oxygen in the steel. These are temperature and the presence of deoxidizers such as silicon, manganese and carbon; the latter being the more prevalent at refining. Solubility is directly proportional to temperature; at typical refining temperatures (from 1500 to 1700 °C), it ranges from 0.15 to 0.3 % [O] [20]. This is based on the calculation

$$\begin{aligned} -\log(\%\,\mathrm{O}) &= 0.8 \\ \%\,\mathrm{O} &= 0.15\,\% \end{aligned}$$

and

$$\begin{aligned} -\log(\%\,\mathrm{O}) &= 0.5 \\ \%\,\mathrm{O} &= 0.3\,\% \end{aligned}$$

In practice, the measured oxygen content lies in the range 0.02 % (200 ppm) to approximately 0.12 % (1200 ppm), so that it is always within the solubility limits.

At high levels of bath carbon, decarburization is able to lower the oxygen to a content approaching equilibrium conditions [17]. The slag FeO and bath oxygen are also well correlated: high levels of FeO are accompanied by high levels of bath oxygen and vice versa. Therefore, oxygen activity will be a function of the bath carbon content (and the injected oxygen).

The oxygen activity output was derived in chapter 2. Figure 5.5 presents the model bath oxygen activity output compared to the measured oxygen activity. The model output uses the bath carbon to calculate the oxygen activity and any error in the oxygen activity is a direct consequence of the error in bath carbon[9]. Therefore, the model fit for carbon will dictate the final oxygen activity. An alternative is to use the bath FeO content to calculate the oxygen activity, but the model carbon fit is considered more reliable and is the preferred choice; and, a reasonably accurate oxygen-carbon relationship was determined in section 4.4 by fitting equilibrium concentration to measured data therefore, no further fitting for the oxygen-carbon relation is necessary.

[9] Assuming the oxygen-carbon relation of subsection 2.2.4 is sufficiently accurate.

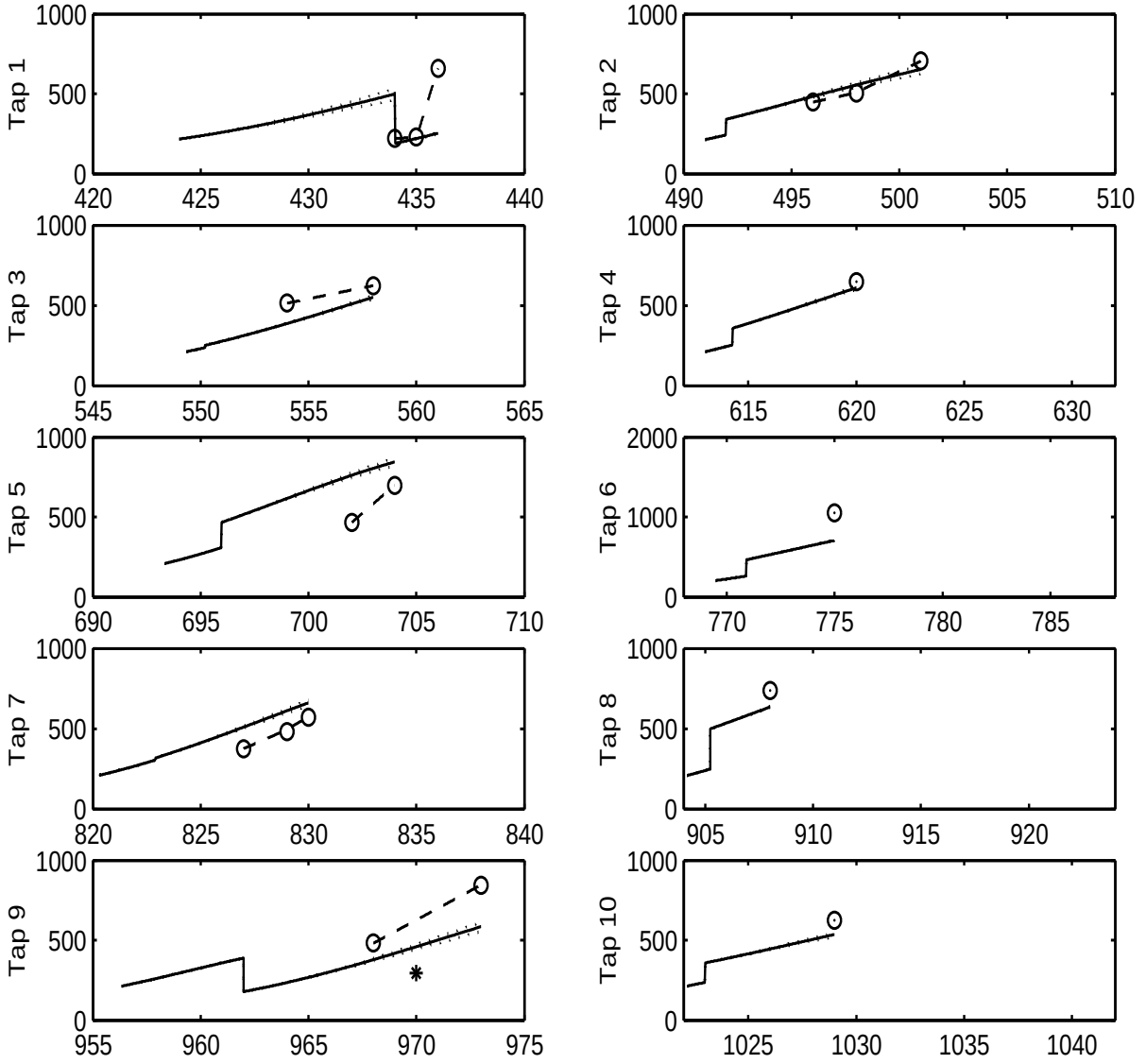

Figure 5.5: The model fitting to measured bath oxygen [ppm]. o - measured oxygen; * - rejected measurement. The line – – – depicts the interpolation between the measured oxygen values; the solid line —— depicts the model oxygen output. Not every measurement of oxygen activity has a corresponding bath carbon measurement - some carbon measurements were reported from the bath sample analysis for which O_2 activity measurements are not available, hence the fewer data points for oxygen activity compared to the carbon.

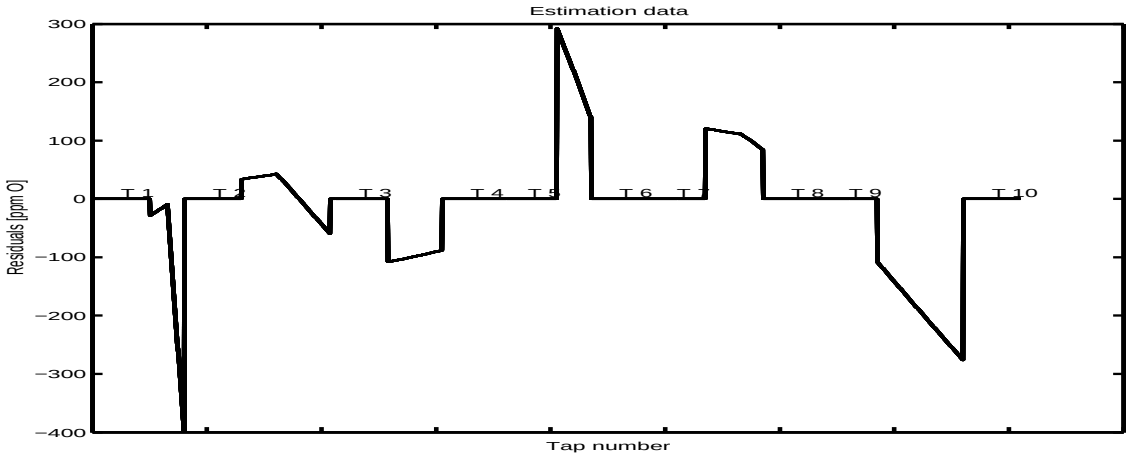

Figure 5.6: Residuals of the oxygen activity for test taps.

5.5.4 Model fit for refining temperature

Under flat bath conditions, all solids are fully melted therefore, it can be assumed that the net heat input is superheat used for increasing the temperature of the bath and slag. Arc power, O_2 and fuel gas inputs are maintained at constant levels[10], where the fuel gas serves only to cool the lances during oxygen blowing. The constant oxyfuel inputs mean the efficiencies η_{FeO} and η_{OXF} - which is very low at refining - are also constant throughout refining. The O_2 stream is highly energetic, flowing as a supersonic jet - it is assumed a change in slag depth has little effect on the ability of the stream to reach the bath.

The slag depth will have a marked effect on η_{ARC}. A thick slag layer will improve the efficiency of heat transfer from the arc to the bath. By shielding the arc, the slag will receive a significant amount of heat by radiation directly from the arc. Some of this heat will be transferred directly to the bath from the slag. Secondly, most radiant energy from the arc is maintained in the vicinity the slag-metal region as a result, a great portion of it will be absorbed by the bath. Whatever the mechanism, a thick foam is known to increase the efficiency of the arc.

The foam has the effect of stabilizing the arc - one of the necessary conditions for maximum power transfer to the bath [35]. A sufficient foam will thus allow for higher voltages to be applied to the bath.

The opening and closing of the slag door has a marked effect on the furnace temperature. When open, the slag door acts as a radiator, becoming a conduit for heat to leave the furnace by radiation to the outside environment. Under refining operation, a low pressure exists, carrying with it large volumes of entrained air. This air is entrained only to be heated then removed with the off-gas - it can represent a significant heat loss.

[10]Power and O_2 are at maximum levels, except when measurements are taken, in which case the power input may be lowered or switched off; the same can be said for oxygen injection.

After the first deslagging, the furnace slag door remains open until tapping. The open door allows measurement of bath properties and enables slag outflow that results from intermittent foaming and deslagging. The heat losses via the slag door will be relatively constant and accounted for by k_{VT}, the heat loss coefficient.

Strictly, the ability of foaming to prevent heat loss from the bath surface will also have a direct effect on k_{VT}. The foamy slag - made in large part of gas bubbles - is a poor heat conductor. By covering all areas of the bath surface, it presents better heat insulation to the bath. In addition, less heat energy is lost to the water cooling system. Thus, foaming tends to decrease the furnace heat losses (k_{VT}) and increase the overall furnace thermal efficiency.

Arc efficiency has a much higher influence on temperature and furnace heat balance than the heat loss resulting from k_{VT}. Therefore, to simplify derivation, it will be assumed that foaming will have a direct influence only on arc efficiency. Omitting this effect on k_{VT} will have a negligible effect on the overall energy balance. It could, however, overestimate furnace losses at the expense of higher arc efficiency. When no deslagging occurs, the increase in arc efficiency (above its level with no foaming) will be proportional to the foam depth, which in turn is proportional to the mass of graphite injected [6]. Successful foaming will also rely on a steady supply of FeO in the slag, generated by injection of O_2.

Steelmaking slags are maintained at conditions that are conducive to foaming [18,19], i.e. high viscosity and surface tension, FeO in slag at 15 to 20 %, and basicity $B > 2.5$, estimated as

$$B = \frac{\%\,\mathrm{CaO} + 1.4\,\%\,\mathrm{MgO}}{\%\,\mathrm{SiO_2} + 0.84\,\%\,\mathrm{P_2O_5}} \approx 1.17\frac{\%\,\mathrm{CaO}}{\%\,\mathrm{SiO_2}}, \tag{5.5}$$

where the approximation applies when $\mathrm{MgO} < 8\,\%$ and $\mathrm{P_2O_5} < 5\,\%$ [18]. The average basicity obtained from plant data (see table A.1) is $\mu = 4.151$ with a standard deviation of $\sigma = 0.624$. It is controlled as part of standard charge practice by using appropriate quantities of lime (a source of CaO and SiO_2) and sources of SiO_2 such as DRI with 1.0 to 5.0 % SiO_2, [17] and scrap (though to a limited extent). Therefore, high slag basicity is guaranteed for all practical purposes.

The average FeO content of the slag is $\mu = 33.27$ with standard deviation $\sigma = 6.089$. This is higher than the average 15 to 20 % stated above but successful foaming has been observed at these higher slag FeO levels [22]. Furthermore, successful foaming studies have been carried out at higher slag FeO contents [29,30,31]. In each one of the taps (recorded in table A.1) successful foaming was observed. With this in mind it can therefore be assumed that the plant slag conditions were conducive to foaming. However, no comment can be made about the optimality of these foaming conditions since only visual inspection was used.

5.5.4.1 The effect of foaming on arc efficiency

As discussed previously, slag foaming has a direct effect on arc efficiency and bath temperature. Under the assumption of adequate foamy slag conditions, the arc efficiency at refining is given by:

$$\eta_{ARC} = \eta_{ARC\,0} + \alpha d_{gr} \tag{5.6}$$

where α is an adjustable constant; $\eta_{ARC\,0}$ is the nominal arc efficiency without foaming and d_{gr} is the graphite injection rate. Recast, the above equation can be written as

$$\begin{aligned} \dot{\eta}_{ARC} &= \alpha \dot{d_{gr}} \\ \eta_{ARC}(0) &= \eta_{ARC\,0}, \end{aligned}$$

allowing straightforward incorporation into the original state-space model. The above expression (5.6) simply evaluates the increase in arc efficiency as a function of the total graphite injected during refining.

An alternative method for incorporating the effect of foaming on arc efficiency is based on the results obtained in Oosthuizen *et al.* [6], presented here with limited detail. The slag depth (in centimetres) is given as

$$H_f = V_g \Sigma$$

with the foam index

$$\Sigma = 20172.58(\%\mathrm{FeO})^{-2.07},$$

obtained empirically for slag FeO concentrations of 20% to 40%. (The foam index can be interpreted as the gas retention time [30].) V_g is the superficial gas velocity [cm/s], obtained from the total volume of gas generated in or flowing through the slag. Then, the arc efficiency is assumed to increase as a linear function of slag depth as:

$$\eta_{ARC} = \eta_{ARC\,0} + \beta H_f, \tag{5.7}$$

subject to a reported practical upper limit $\eta_{ARC} < 0.9$, with the nominal efficiency chosen as $\eta_{ARC\,0} = 0.4$ [19], applicable when no foaming takes place. The above limits also apply to (5.6).

Consistent with the reasons of Oosthuizen [7], above a thickness of 30 cm the slag has no effect on arc efficiency increases. Below 30 cm, there will be a linear change in efficiency (as a function of slag depth), governed by the adjustable parameter β. The use of both $\eta_{ARC\,0}$ and β in (5.7) means that η_{ARC} is effectively a sum of two unknown parameters. To simplify parameter estimation, β will be determined as the gradient of the straight line that relates the arc efficiency to slag depth, where $\eta_{ARC\,0}$ is the y-intercept. Then

$$\beta = \frac{0.9 - \eta_{ARC\,0}}{30 - 0}, \tag{5.8}$$

resulting in only one adjustable parameter, η_{ARC0}.

The results of the model fit for refining temperature are shown in figure 5.7 for fitting to the recorded tap data. Inspection of the plots indicates an overall good fit. However, Tap 1 and Tap 5 have the large offset errors; with Tap 1 having a generally poor fit. The latter was a high carbon tap - to reduce this carbon level, only oxygen injection was used, with the arc power switched off for most of the refining stage. A better fit for this tap can be achieved by increasing η_{FeO} but this will occur at the expense of a temperature overshoot for other taps since these low carbon taps have lower energy generation by oxygen injection. A better presentation of the fitting accuracy and the comparison of the error from tap to tap is shown in residuals plot of figure 5.8.

A linear interpolation is used between two adjacent measured temperatures to approximate the furnace temperature. This is considered adequate since most adjacent measurement points are separated by only a few minutes and, under flat bath, the predominant relationship between temperature and arc input is linear. This interpolation provides flexibility in evaluation of the error function and prevents the need to solve the problem as merely a two-point boundary problem: in this case any trajectory for temperature is possible as long as target temperature is reached - this could introduce temperature changes that are not physically possible. In effect the interpolation is a method of introducing prior knowledge about bath temperature into the error function.

The parameters adjusted for the model fit are η_{ARC} , k_{VT} and, to a lesser extent, η_{FeO} whose value was adjusted in the fit for FeO, although it does have a substantial effect on the bath temperature due to its effect on bath oxidation.

The initial single-point values arrived at for the parameters are:

$$\begin{array}{llll} k_{VT} & = 2.08 & 0.40 < k_{VT} & < 8.00 \\ \eta_{ARC} & = 0.51 & 0.40 < \eta_{ARC} & < 0.80 \\ \eta_{\text{FeO}} & = 0.75 & 0.50 < \eta_{\text{FeO}} & < 0.80 \\ \beta & = 0.00 & 0.00 < \beta & < 0.02 \\ k_{d\text{C}} & = 54.90 & 5.00 < k_{d\text{C}} & < 100.00 \\ k_{gr} & = 0.42 & 0.30 < \eta_{ARC} & < 10.00 \end{array} \tag{5.9}$$

with a corresponding mean squared penalty of $V_N = 215$. The results of the model temperature response compared to the measured temperature are shown in figures 5.7 and 5.8.

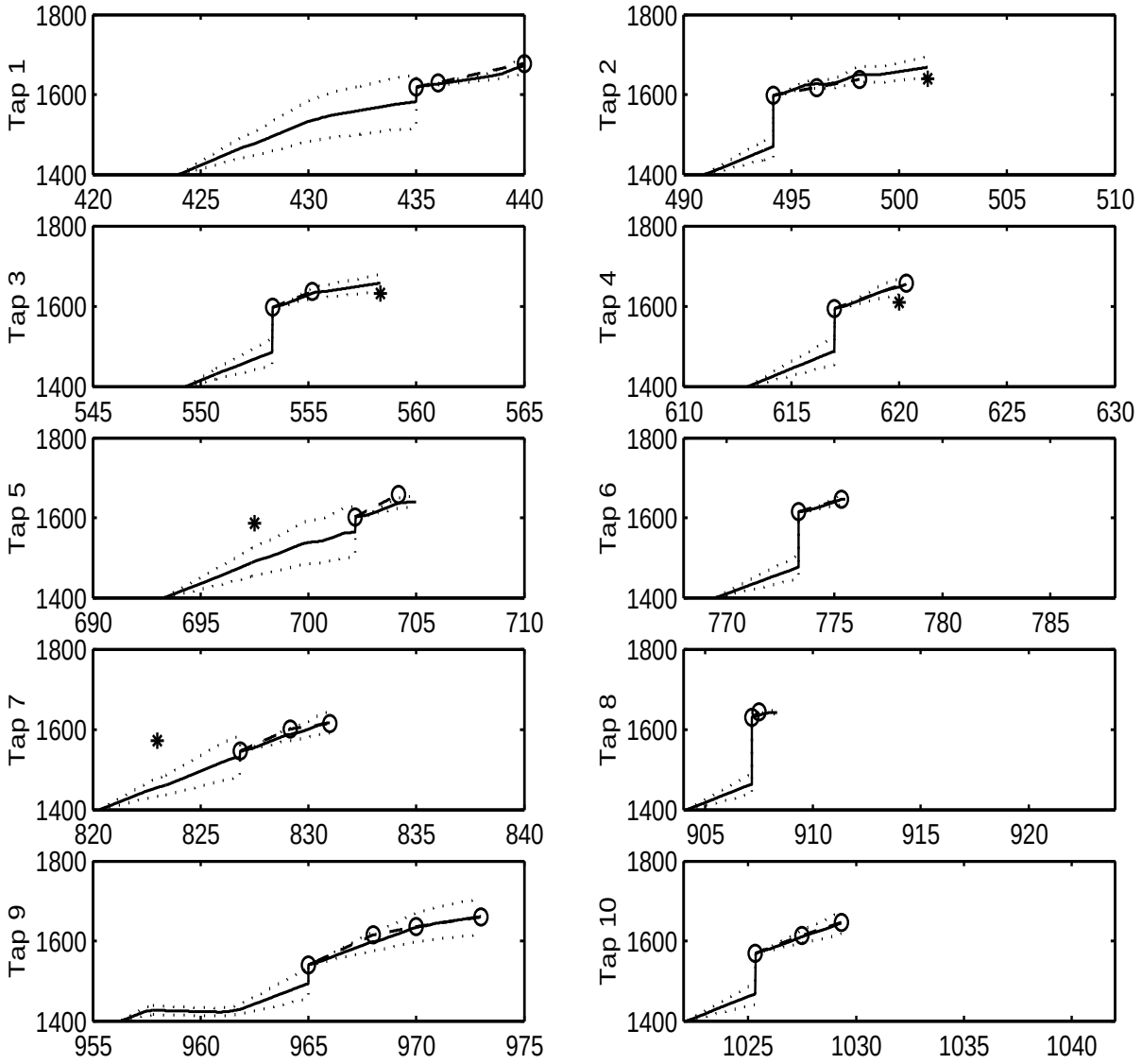

Figure 5.7: Model temperature output compared to the measured values [°C]. o - measured temperature; * - rejected temperature measurement. The model is initialized to an arbitrary bath temperature (1400 °C) - the temperature is updated as soon as a valid measurement is made available, hence the instantaneous rise or drop in temperature near the first valid measured temperature. The model 95 % confidence interval is also shown (· · ·). Tap 8 was rejected altogether since only 2 temperature measurements were available, separated by approximately 40 seconds with an increase from 1630 to 1643 °C - this range is too short to allow any meaningful conclusions to be made about the data. Each plot is generated over a time window of 20 minutes from the first minute of simulation and over a temperature range from 1400 to 1800 °C - this enables comparison among the taps.

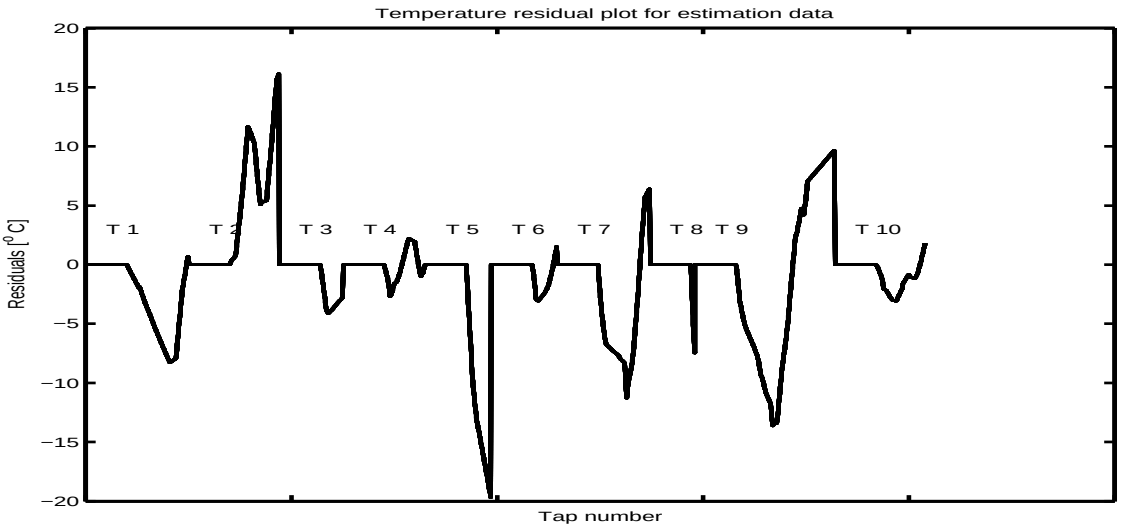

Figure 5.8: Residuals of the temperature fit for all test taps. The tap number is followed by the corresponding residual plot over the relevant period of the tap as shown in figure 5.7. For each tap, the residual is evaluated from the first to the last valid measured temperature.

5.5.5 Model fit for refining pressure

The furnace pressure has important implications for the gas mass balance and the furnace heat balance. Pressure levels will dictate the extent of air entrained and its subsequent removal through the off-gas with other gases generated in the furnace. The furnace entrains air, then heats it to a higher temperature only to remove it with the off-gas, thus incurring energy losses; these can be significant for negative pressures. On the other hand maintaining a positive pressure will lead to the release of hazardous gases into the furnace work area, exposing the workers to health risks. Therefore a tradeoff must be made. The ideal would be to operate the furnace at zero pressure, but in practice, a slight negative pressure is adopted. An alternative is to use a secondary gas extraction system that is located in the roof of the furnace work area. This system rapidly removes gas fumes in the vicinity of the furnace. It is particularly useful when positive pressures cannot be avoided as during the early melting stage, foaming and when cave-ins occur.

The parameters that are directly responsible for the behaviour of the furnace pressure are the gas masses, the pressure constants (k_U and k_{PR}) and the off-gas mass extraction rate u_1. The latter is constant, based on the estimated volume flow rate of the off-gas - this is given as 66000 Nm^3/h [22] (see also section 4.3).

The pressure measurements respond only to peaks in furnace pressure. The instrument is not sensitive to pressures below a certain (unknown) level. A pressure that is expected to equal atmospheric pressure is not registered, neither are negative pressures[11]. On the

[11] Various stages of operation in the furnace will have a marked effect on the pressure. The opening and

other hand, a distinct response is observed to a large positive pressure as a result of foaming. Therefore the model fit for pressure will only attempt to fit to these peaks, while other pressure levels will be verified based on physical insight. The results of the pressure fit are shown in figure 5.9.

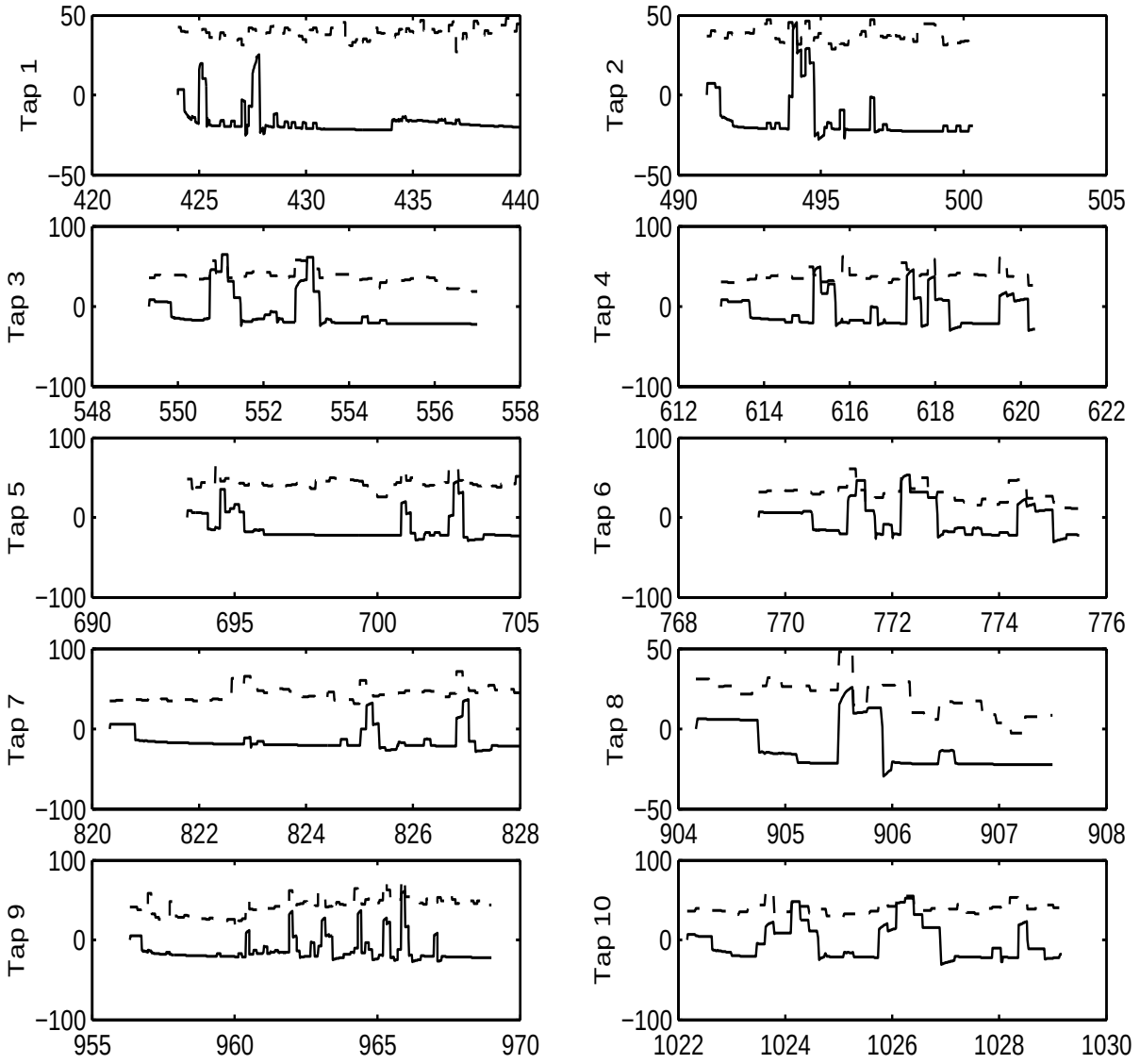

Figure 5.9: The model fitting to measured furnace pressure [Pa]. The original reported units of the measured pressure are mmH_2O. The multiplicative factor of 9.8 Pa/mmH_2O was applied to the measured data. The result was relatively high positive pressure values with an unrealistic offset: the mean pressure was at least 2000 Pa. This necessitated the use of yet another gain factor of K=0.01, to result in the pressure values shown. Solid line - model pressure; dashed line - measured pressure.

The preceding fit for pressure cannot be considered conclusive. Errors in the fit will

closing of the slag door and furnace roof should display a consistent effect on the pressure measurement. The same should apply in the case of refining where negative pressure conditions will prevail throughout except when graphite injection takes place - this does produce the expected response. It is possible the measuring instrument is only sensitive above a certain positive pressure.

have a negative effect on the energy balance when considering the heat loss to air entrainment. However, this effect will be negligible relative to the main energy sources and other heat loss routes such as loss through refractories, radiation, water cooling and furnace side walls. The error can be absorbed into other system parameters e.g. a higher arc efficiency (or a lower heat loss coefficient) when the entrainment losses are exaggerated and vice versa.

5.6 Analysis of parameter estimates

5.6.1 The error norm

The error norm used throughout the foregoing estimation is the least squares norm. It is given by

$$V_{_N} = \frac{\lambda_T}{N_T}\sum_{t=1}^{N_T}\varepsilon_{_T}^2(t) + \frac{\lambda_C}{N_C}\sum_{t=1}^{N_C}\varepsilon_{_C}^2(t) + \frac{\lambda_{\mathrm{FeO}}}{N_{\mathrm{FeO}}}\sum_{t=1}^{N_{\mathrm{FeO}}}\varepsilon_{_{\mathrm{FeO}}}^2(t), \tag{5.10}$$

t is the time at which a measurement is available and $\varepsilon(t) = y(t) - \widehat{y}(t)$. The plant relative pressure is sampled at regular intervals of 10 seconds; other outputs such as temperature, carbon and FeO are available at arbitrary time instants with no fixed sampling time. λ_x is an appropriate weight - it can be chosen to place an arbitrary weight on an output and its contribution to the penalty function $V_{_N}$. Here, the outputs are assigned equal weight, leading to

$$\begin{aligned} \lambda_T &= 1 \\ \lambda_C &= 9\cdot 10^5 \\ \lambda_{\mathrm{FeO}} &= 0.405 \end{aligned} \tag{5.11}$$

5.6.2 The method of influence functions

This section evaluates the influence function method (of section 3.6.1) applied to the model fit. In each case, the data set from one tap was omitted from the overall data. Then a parameter estimate was obtained in the same manner as in section 5.5. The results are shown in table 5.2; the tap number refers to the tap data that was omitted from the data set in order to obtain the corresponding estimate.

The absence of tap 1 results in the highest arc efficiency and lowest η_{FeO}, compared to the other 9 cases. This is the only tap in the data set for which oxygen injection makes the largest heat contribution: arc input occurs for a comparatively short period throughout the entire refining stage, while high levels of oxygen are injected to remove the bath carbon (see the appendix section A.2.3 for input profiles). Inclusion of tap 1 in the data set results in values of $\eta_{_{ARC}}$ and $\eta_{_{OXF}}$ that are generally confined to a small

range. The large change in the values of these parameters (from tap 1 onwards) indicates that tap 1 has a large influence on the entire data set. (These are also the parameters to which the model is most sensitive.) As a result, tap 1 should be eliminated from the data set as it does not fall within the typical operating range of the refining stage. k_{dC} is relatively unchanged for all taps - this points to a greater consistency of the process carbon relationships i.e. decarburization is not unduly influenced by any one tap, including tap 1. On the other hand, k_{VT} and k_{gr} fluctuate significantly.

Table 5.2: Influence function results with the corresponding tap skipped.

Tap #	ε_{Temp}	ε_{C}	$\varepsilon_{\mathrm{FeO}}$	k_{VT}	η_{ARC}	η_{FeO}	k_{dC}	k_{gr}
1	2.702	0.008	2.316	5.785	0.851	0.581	53.819	0.300
2	7.018	0.002	2.021	0.400	0.488	0.703	55.552	0.300
3	2.451	0.008	6.488	2.354	0.519	0.848	51.889	0.986
4	1.550	0.002	5.889	1.781	0.494	0.794	54.077	0.366
5	13.516	0.013	5.281	3.062	0.574	0.896	54.665	2.108
6	2.382	0.005	1.173	1.411	0.500	0.759	54.688	0.489
7	6.766	0.006	3.201	1.425	0.509	0.765	56.502	0.880
8	4.489	0.003	3.060	1.522	0.499	0.768	54.283	0.456
9	8.000	0.011	3.915	0.400	0.465	0.743	53.865	0.714
10	1.761	0.004	4.552	0.400	0.420	0.844	54.815	3.528

5.6.3 Parameter error bounds

So far the parameter estimation has been carried out with the view to obtain a single point estimate. While this does deliver an estimate that minimizes the error on average, it does not give sufficient information about the parameters or the resulting model. Other methods or tools exist for obtaining both the value of the parameters and other information that relates to them i.e. the variance in the parameters, the asymptotic properties of the parameters, and importantly a measure of the confidence in the estimates - this will indicate the range over which the parameters allow the model to represent the data satisfactorily.

The error bounds or confidence intervals on the parameters can be calculated from the covariance matrix as discussed in section 3.7. Using equation (3.24) to calculate P_N gives

$$P_N = \begin{bmatrix} 0.09116 & 0.01156 & 0.007380 & -0.0009926 & -0.001058 \\ 0.01156 & 0.03796 & -0.02401 & 0.002883 & -0.0007672 \\ 0.007380 & -0.02401 & 0.03378 & -0.004042 & 0.002731 \\ -0.0009926 & 0.002883 & -0.004042 & 0.01841 & -0.00008065 \\ -0.001058 & -0.0007672 & 0.002731 & -0.00008065 & 0.09225 \end{bmatrix} \tag{5.12}$$

Then, the covariance is obtained using equation (3.22):

$$\mathrm{Cov}\,\widehat{\theta}_N = \frac{1}{N}P_N = \begin{bmatrix} 0.03039 & 0.003852 & 0.002460 & -0.0003309 & -0.0003526 \\ 0.003852 & 0.01265 & -0.008004 & 0.0009611 & -0.0002557 \\ 0.002460 & -0.008004 & 0.01126 & -0.001347 & 0.0009102 \\ -0.0003309 & 0.0009611 & -0.001347 & 0.006137 & -0.00002688 \\ -0.0003526 & -0.0002557 & 0.0009102 & -0.00002688 & 0.03075 \end{bmatrix} \tag{5.13}$$

where $N = 3$ was used, based on the average number of data points per tap.

The corresponding error bounds on the parameters are obtained from the variance of each parameter which is the diagonal element of $\mathrm{Cov}\,\widehat{\theta}_N$. Then the 95 % confidence interval on the parameters can be calculated using equation (3.21). The results are presented in table 5.3; θ_N is the single-point estimate of the parameters.

Table 5.3: Confidence interval on parameters.

Parameter	Lower bound	θ_N	Upper bound
k_{VT}	1.73	2.08	2.42
η_{ARC}	0.29	0.51	0.73
η_{FeO}	0.54	0.75	0.96
k_{dC}	54.74	54.90	55.05
k_{gr}	0.08	0.42	0.76

The above bounds on the parameters were used to generate the model output plots of the previous sections where the model outputs at the upper and lower parameter bound were shown along with the output at the single-point estimate.

The final parameter estimate is:

$$\begin{aligned} k_{VT} &= 2.0761 \text{ kW/K} \\ \eta_{ARC} &= 0.5063 \\ \eta_{\mathrm{FeO}} &= 0.74774 \\ \beta &= 0 \\ k_{dC} &= 54.895 \text{ kg.s}^{-1} \\ k_{dSi} &= 0 \text{ kg.s}^{-1} \\ k_{gr} &= 0.42019 \text{ kg}^{-2} \\ k_{PR} &= 0.5 \text{ kg/(s.Pa)} \\ k_{U} &= 8.43 \\ h_{d} &= 2.1 \text{ m} \end{aligned}$$

No improvement in the temperature fit was achieved by incorporating the effect of foaming into the calculation for arc efficiency. Hence the value of $\beta = 0$. Both k_{gr} and β have a direct effect on the furnace heat energy: k_{gr} controls the effect of graphite injection on the furnace heat (and masses); and β also controls the effect of graphite on the furnace heat via arc efficiency. As far as furnace heat is concerned, the two parameters control the same effect: it is possible for k_{gr} to be set to such a value that it sufficiently captures the

effect of foaming on furnace heat without the need for adjusting arc efficiency in response to graphite injection (via β). Therefore β is redundant.

5.7 Furnace heat balance

This section gives a summary of the various heat sources and sinks and their relative contributions during refining and for the entire tap. This final step provides a preliminary check on the validity of the obtained model. Table 5.4 presents a summary of the various heat sources and sinks. The results are normalized to the total mass of steel being used i.e. in units of kWh/ton.

Table 5.4: Furnace energy contribution for refining [kWh/ton].

Source/sink	Tap1	Tap2	Tap3	Tap4	Tap5	Tap6	Tap7	Tap8	Tap9	Tap10
Decarburization	-13.16	-4.68	-6.63	-4.65	-6.13	-4.24	-7.64	-2.83	-14.42	-3.37
Theoretical bath oxidation	261.65	128.87	137.89	115.04	157.49	89.62	160.70	57.31	200.53	110.36
Effective bath oxidation (η_{FeO})	195.64	96.36	103.10	86.02	117.76	67.01	120.16	42.86	149.94	82.52
CO combustion by air	60.25	27.73	23.87	19.86	39.61	15.28	29.32	10.04	49.65	17.64
Desiliconization	2.11	0.47	1.25	0.68	1.08	0.87	1.48	0.60	2.19	0.99
Heating loss: injected O_2	-26.86	-13.28	-14.05	-11.56	-15.72	-8.84	-15.94	-5.54	-20.48	-11.12
Heating loss: $O_{2,\mathrm{air}}$	-5.65	-2.71	-2.29	-1.83	-3.65	-1.40	-2.71	-0.93	-4.57	-1.63
Heating loss: $N_{2,\mathrm{air}}$	-20.59	-9.86	-8.33	-6.65	-13.31	-5.10	-9.86	-3.37	-16.66	-5.94
Heating loss to slag input	0.00	0.00	0.00	0.00	0.00	0.00	0.00	0.00	0.00	0.00
Heating loss to DRI input	0.00	0.00	0.00	0.00	0.00	0.00	0.00	0.00	0.00	0.00
Melting of steel and slag	-0.12	-0.10	-0.09	-0.07	-0.10	-0.06	-0.09	-0.04	-0.13	-0.07
Graphite injection	-0.76	-1.56	-3.08	-2.86	-2.53	-3.70	-1.75	-0.54	-3.29	-2.90
Oxyfuel energy	12.86	7.50	7.03	5.85	8.63	4.71	8.42	3.09	11.99	5.57
Total Arc input	210.32	164.00	172.86	200.60	280.58	164.73	270.61	102.02	274.10	189.80
Effective Arc input (η_{ARC})	106.48	83.03	87.52	101.56	142.06	83.40	137.01	51.65	138.77	96.10
Heat loss via k_{VT}	-40.77	-26.59	-22.94	-18.37	-29.84	-15.16	-26.88	-10.17	-41.89	-17.76
Water loss	-0.04	-0.02	-0.02	-0.02	-0.03	-0.01	-0.03	-0.01	-0.04	-0.02

The above results are dependent on the parameter estimates: the effective arc power input depends on η_{ARC}, energy from bath oxidation on η_{FeO}, heat loss by graphite injection on k_{gr}, etc. Also, the total arc power is shown along with the effective power input that results from use of the efficiency parameter η_{ARC} - some of the input power is lost through various routes such as radiation and inefficiency of the electrical distribution. Of the refining oxygen injected, some oxidizes the bath while the rest is retained in the slag or lost with the off-gas, hence the listing of the theoretical (that would result had bath oxidation been 100 % efficient) and effective (through the parameter η_{FeO}) bath oxidation - the latter is used in the model as contribution from oxygen injection.

Only a small contribution results from the oxyfuel subsystem. This is mainly due the fact that during refining, the injection of fuel gas only serves to cool the lances and that most of the injected oxygen is used for bath oxidation - this is the main route by which the oxyfuel system contributes to the energy input during refining. Furthermore, the contribution of bath oxidation is comparable to that of arc input. This only occurs since the refining stage has the highest volume of injected oxygen; the arc energy input

dominates when the energy input is considered over the entire tap - these results are shown in table 5.5.

Table 5.5: Furnace energy contribution for the entire tap [kWh/ton].

Source/sink	Tap1	Tap2	Tap3	Tap4	Tap5	Tap6	Tap7	Tap8	Tap9	Tap10
Decarburization	-37.63	-35.99	-31.14	-34.98	-35.91	-38.56	-42.71	-38.13	-40.19	-42.54
Theoretical bath oxidation	582.26	423.03	404.36	328.60	356.63	277.19	354.25	278.47	388.82	324.37
Effective bath oxidation	435.38	316.31	302.36	245.71	266.66	207.27	264.89	208.23	290.74	242.54
CO combustion by air	314.20	183.14	181.37	82.68	104.93	314.96	237.04	242.81	178.17	225.58
Desiliconization	103.02	99.00	93.37	91.11	94.94	87.86	95.80	92.80	99.32	86.34
Heating loss: injected O_2	-54.40	-39.07	-35.84	-26.60	-28.37	-25.77	-31.88	-27.73	-33.22	-27.41
Heating loss: $O_{2,\text{air}}$	-23.74	-13.30	-12.88	-4.75	-6.11	-18.94	-16.27	-17.01	-12.90	-14.25
Heating loss: $N_{2,\text{air}}$	-86.49	-48.46	-46.91	-17.29	-22.26	-68.99	-59.27	-61.98	-46.99	-51.93
Heating loss: slag input	0.00	0.00	0.00	0.00	0.00	0.00	0.00	0.00	0.00	0.00
Heating loss: DRI input	0.00	0.00	0.00	0.00	0.00	0.00	0.00	0.00	0.00	0.00
Melting of steel and slag	-742.94	-730.06	-730.51	-741.55	-743.53	-721.53	-741.85	-730.86	-721.49	-750.79
Graphite injection	-3.80	-5.27	-7.93	-6.41	-5.16	-5.92	-3.89	-1.79	-7.93	-6.52
Oxyfuel energy	143.74	115.31	112.94	100.31	105.29	127.48	111.90	111.15	126.11	107.90
Total Arc input	1277.79	1191.37	1180.11	1077.17	1173.36	1119.15	1229.37	1216.45	1265.87	1181.52
Effective Arc input	646.94	603.19	597.49	545.37	594.07	566.62	622.42	615.88	640.90	598.20
Heat loss via k_{VT}	-24.97	-20.76	-18.70	-14.53	-15.48	-20.28	-17.28	-17.85	-19.32	-15.60
Cooling water loss	-0.14	-0.12	-0.11	-0.10	-0.11	-0.14	-0.11	-0.11	-0.13	-0.11

5.8 Conclusion

Due to the nonlinearity of the process, the parameter estimation will be highly dependent on the operating conditions. These will in turn be dependent on the initial conditions and the magnitude of the inputs. It is possible to obtain values for the parameters for which there will be relatively high confidence. This has been demonstrated by the small parameter variance of some taps; however, other taps had values that are too large to be practical. The main threat to the applicability of the model is the high variability of the process: in some operating regions it is possible to have highly accurate process depiction (with a high confidence), while other operating regions may compromise the accuracy of the model. A serious drawback is the inability to accurately infer these operating regions, in which case a clear distinction could be made for when the model can be used with high confidence and when it cannot.

Chapter 6

Model validation

The model validation process will test the performance of the model against data on which it was previously not fitted - the parameters obtained in the previous chapter will be used. In addition to data from 10 taps, data from an additional 8 taps were collected - this will be used for the validation. For the validation set of data, only the analysis obtained at the end of tap is available for the slag; and less bath carbon and silicon data are available.

6.1 Bath temperature

The results for the model performance on validation data are shown in figure 6.1. The error performance is poorer than in the case of the test data - this is expected. Tap 14 is of has the longest duration and the largest final temperature error. But the responses to heat input are well matched. The source of the significant error is likely that the increase in the model temperature begins well before the measured temperature, possibly due to incorrectly recorded measurement times. There is also a significant delay of at least 10 minutes in between measurements. Tap 15 has a large error mainly due to the occurrence of a cave-in between the first and last measurement. The response of the other taps is generally acceptable. The corresponding residual plot is shown in figure 6.2. Tap 16 has the least error mainly due to its short duration (of 2 minutes) relative to the other taps. The model generally performs better on the shorter duration taps.

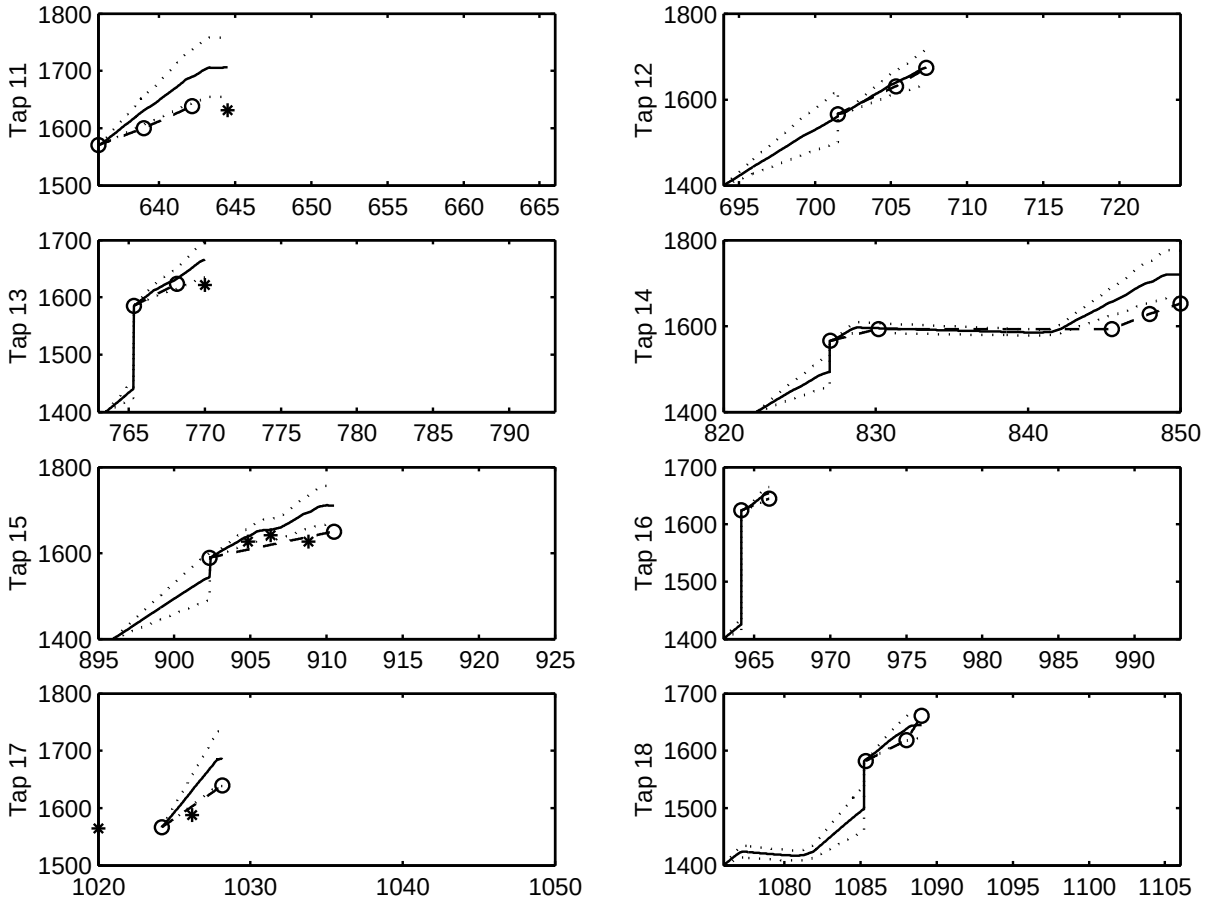

Figure 6.1: Model temperature output compared to the measured values [°C] for the validation data. o - measured temperature; * - rejected temperature measurement. The line – – – represents the interpolated temperature between valid measurement points; the solid line —— depicts the model temperature output. The 95 % confidence interval is shown with the line (· · ·).

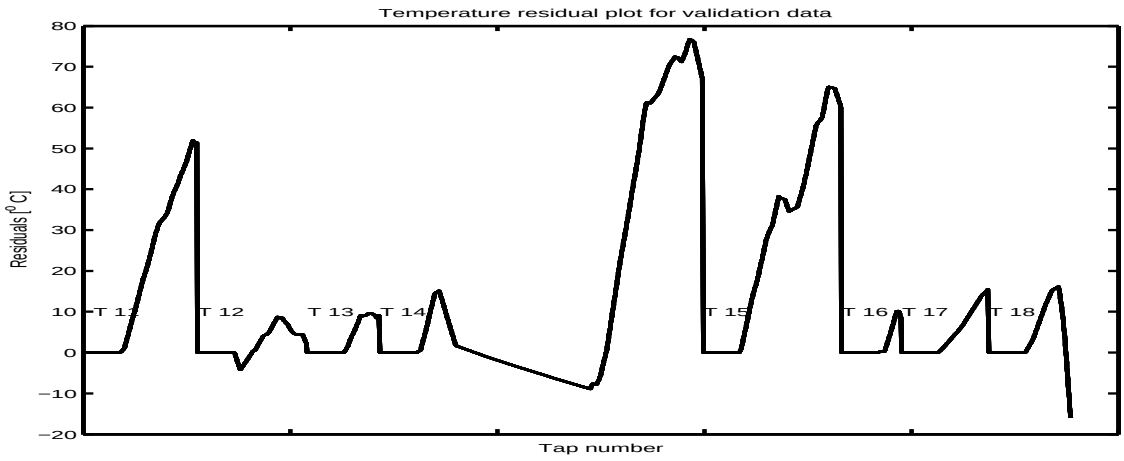

Figure 6.2: Residuals of temperature for the validation data.

6.2 Bath carbon

This section presents the results of the model carbon output performance against validation data. The model carbon output error is significantly lower than the temperature output error for tap 14. This is generally the case for the other taps where, overall, the model performance for carbon is significantly better than for temperature. As expected, the cave-in during tap 15 increased the bath carbon content, but the final model carbon error was relatively accurate. The worst carbon error is in tap 16, mainly because of the short duration between measurements and possible error in measurement - the rate of decrease in carbon for tap 16 is the largest in all the collected data.

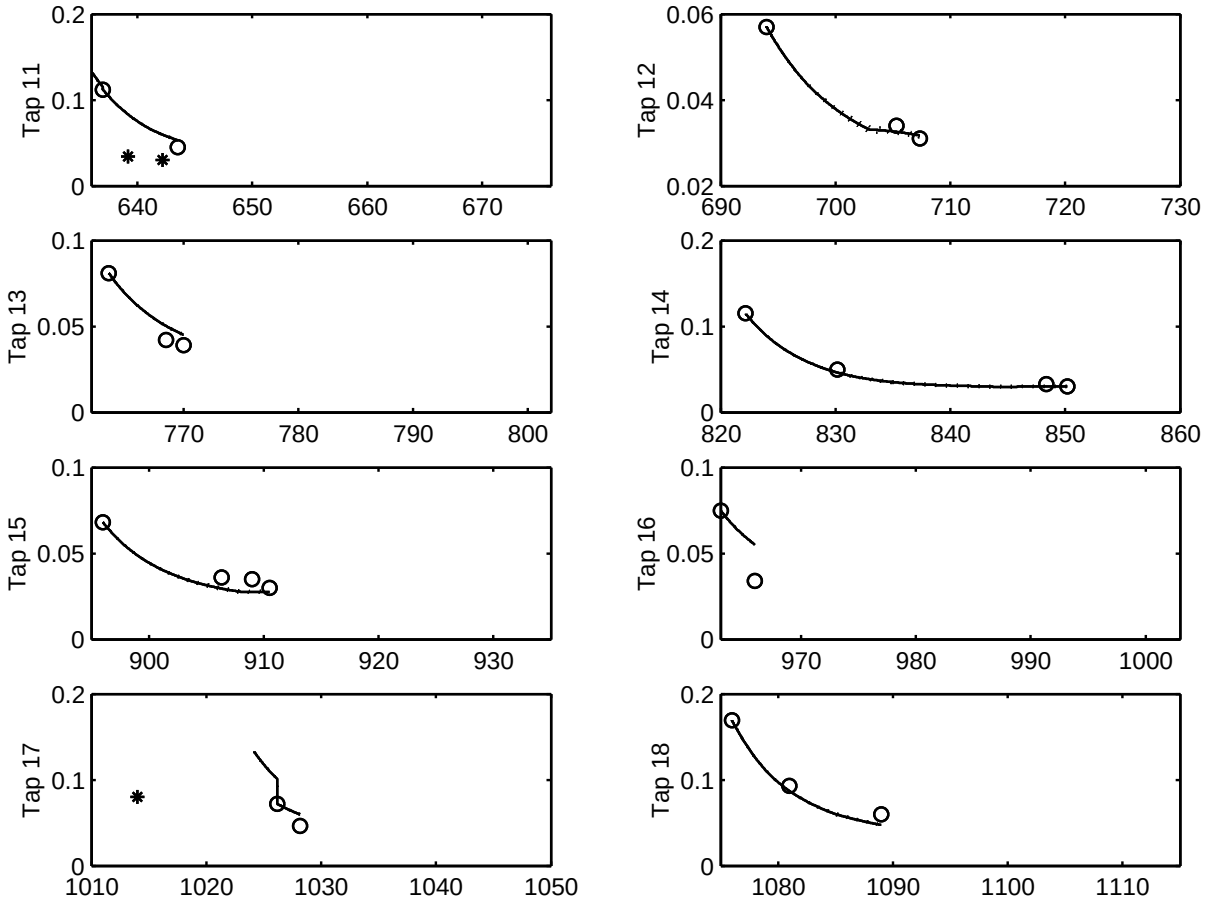

Figure 6.3: Comparison of model carbon output and measured bath carbon. The model fitting to measured carbon data [wt %]. o - measured carbon; * - rejected carbon measurement. The model is initialized to an arbitrary bath carbon level (0.1 %) - the carbon level is updated as soon as a valid measurement is made available, hence the instantaneous rise or drop in carbon near the first valid measured carbon. The model 95 % confidence interval is also shown as the dotted line ($\cdots$). It is only slightly visible in tap 1 - it is too narrow to be visible on the other taps.

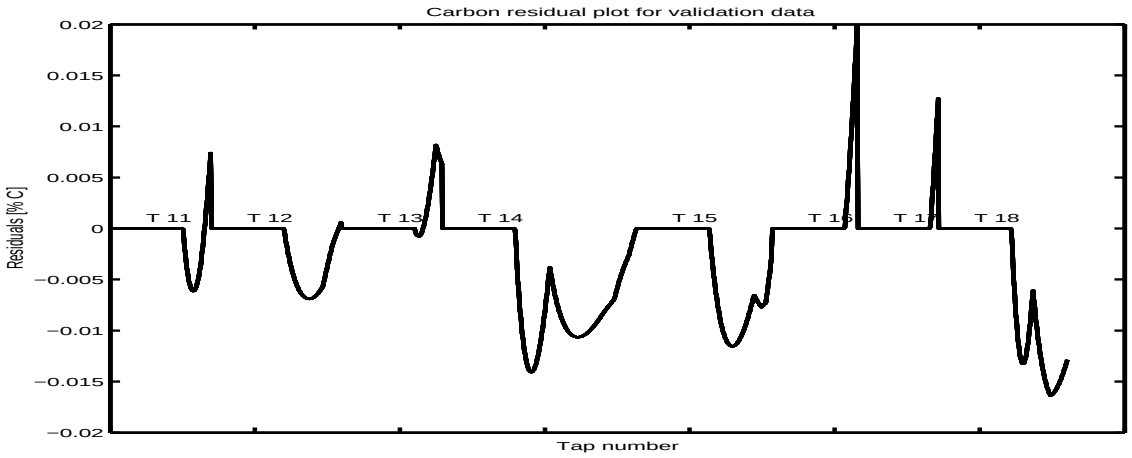

Figure 6.4: Residuals of the carbon output [wt %].

6.3 Bath oxygen activity

Comparison of the model oxygen output to measured oxygen is shown in figure 6.5. This is accompanied by a plot of the residuals in 6.6. The oxygen errors for all the taps closely resemble the carbon errors, except tap 11. This can be expected (for tap 11) since the largest errors in oxygen occur at the measurement points for which data were rejected - the same data were rejected in the carbon measurement. The results for taps 16 and 17 have large errors for oxygen as they did for carbon. The results are relatively accurate for taps 14 and 15.

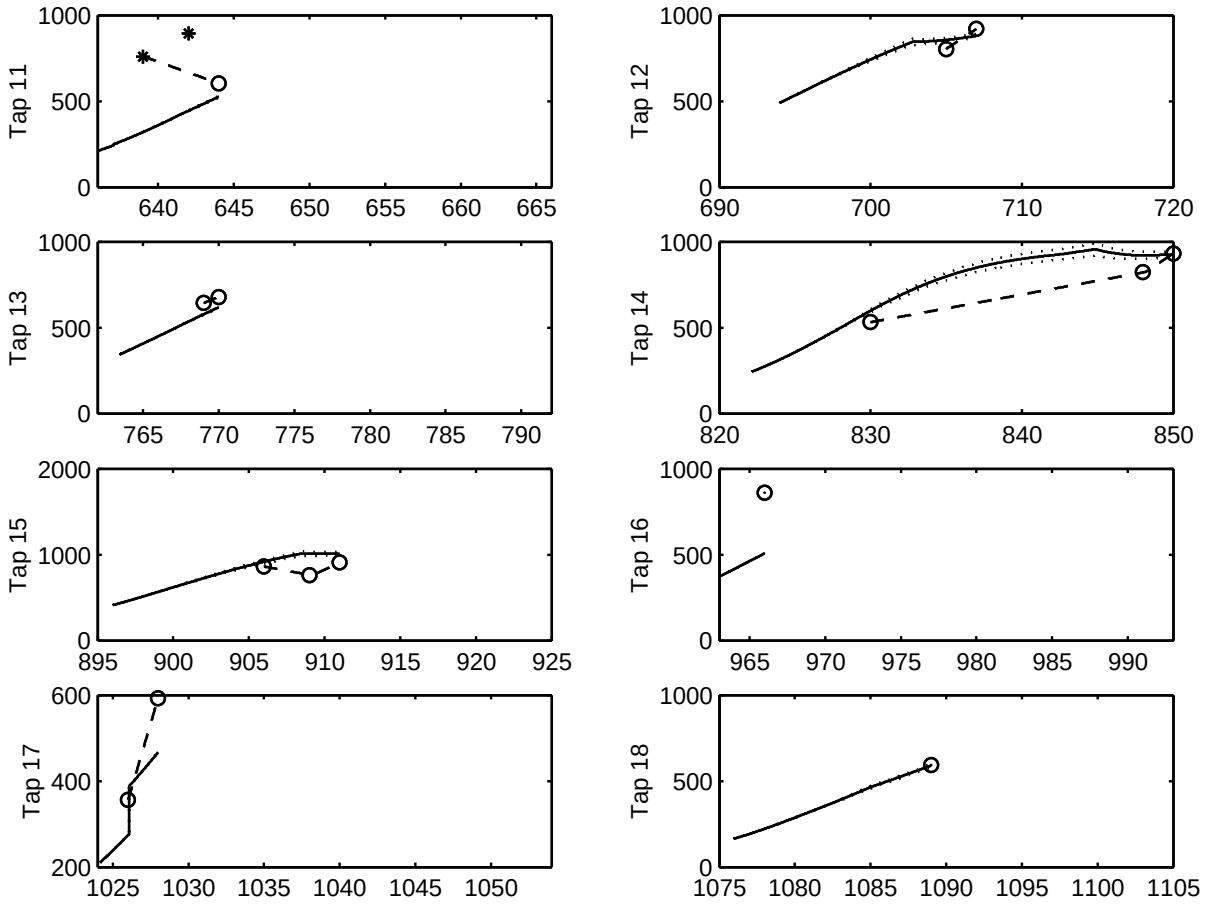

Figure 6.5: Comparison of model oxygen activity output [ppm] to measured validation data. o - measured oxygen; * - correspond to rejected carbon measurements. Not every measurement of oxygen activity has a corresponding bath carbon measurement - some carbon measurements were reported from the bath sample analysis for which O_2 activity measurements are not available, hence the fewer data points for oxygen activity compared to the carbon.

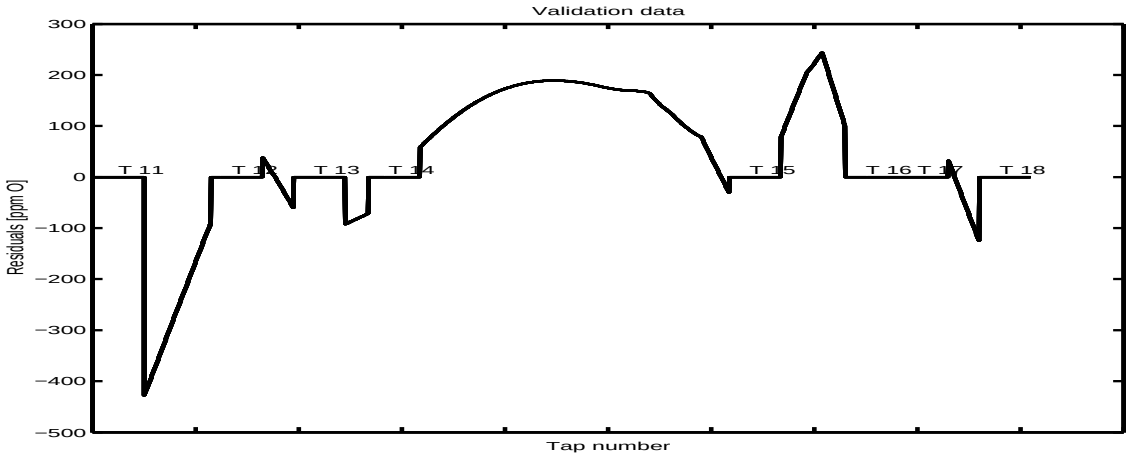

Figure 6.6: Residuals of the oxygen output [ppm].

6.4 Conclusion

The model performance against validation data is comparable to the performance against test data in the previous chapter. An important factor is the duration over which the model output is compared to the measured data - a short measurement duration results in accurate temperature predictions while the opposite is true for carbon. Overall, the results for the carbon output are better than for temperature.

Chapter 7

Conclusion and recommendations

7.1 Summary of dissertation results

The main focus of the dissertation was to deliver a model that is able to depict an actual EAF process as well as possible, first by updating an existing model to accommodate current EAF practice and by fitting the resulting model to process data. A large part of the modelling exercise was carried out by Bekker *et al.* [39]. The effect of gas evolution on the slag foam height was later studied by Oosthuizen *et al.* [6]. The focus of the modelling in the current dissertation was to incorporate the oxyfuel subsystem into the existing EAF model. The effect of the oxyfuel subsystem on the energy balance and the refining operations were studied. Model reduction was carried out, resulting in a simpler model that is valid only for the refining stage while significantly reducing the computational burden that is otherwise introduced by simulation with the complete model. Several modifications were also introduced to depict the effect of charging on the furnace mass balance. Chapter 2 also presented a description of EAF operation with several observations from EAF practice.

Chapter 3 presented an overview of the system identification process as well as some tools that are commonly used to carry out parameter estimation and to evaluate the quality of the resulting parameter estimates (and hence the model as a whole). The model fitting problem of the current dissertation was solved using these tools.

The main aim of chapter 4 was to identify the important process variables that must be measured, first to obtain a successful realistic simulation of the process and then to enable parameter estimation. The conditions under which these measurements could be most informative were also considered. This is essentially a problem of experiment design, though the application of the results were highly constrained by the limited obtainable plant data and the need to maintain normal operating conditions while measurements were being obtained. The identifiability results form an important contribution as they are well correlated with what can be expected from process operation. An analysis of

slag data was also presented and shown to correspond well with results from similar experiments.

Part of chapter 4 consisted of the collection and analysis of process data. Important data collected includes bath temperature and composition, and slag analysis results. Ancillary data such as the freeboard temperature and the cooling water temperature were also collected - these help to establish an improved freeboard heat balance, albeit with limited impact on the overall furnace heat balance since it (the freeboard heat contribution) is comparatively smaller. A complete record of measured relative pressure was also collected, however, its integrity is questionable for most operating stages of the furnace. An analysis of the freeboard gases is a desirable set of data as it would, in addition to pressure, allow a reliable estimate of the oxyfuel subsystem overall performance and efficiency.

The main results of the dissertation were presented in chapter 5. The practical implementation of the parameter estimation process was outlined together with discussions of the various threats to model validity that arise from the EAF process operation and the data from which it is collected. An initial model fit was carried out over the melting stage of the furnace. This resulted in the parameter values required to satisfactorily depict the progress of melting and the changes in the temperatures of the solid and liquid phases.

The effect of the high variability in the process was outlined by the wide range of parameter values obtained. This was revealed by the comparison of the overall model fit and the model fit on a tap-for-tap basis. Highly accurate estimates were obtained for the latter case while some taps exhibited large errors when the overall estimate was obtained.

A raw record of the measured data as well as comments on the practical model simulation and parameter estimation are given in the appendix.

7.2 Conclusions

The accuracy of the model is easier to verify at refining: most of the assumptions in the original model derivation hold at this stage of the process. This is also the stage where the behaviour of the various states is understood with better accuracy; much research and insight gained in the study of the oxygen furnace applies to the EAF during refining with little modification.

The temperature response during refining should be easier to predict since the superheat required to raise the bath temperature to a given level is more predictable. However, several unmeasured disturbances have an obviously negative impact on the accuracy of the temperature modelling. These range from unmeasured variations in material mass and composition to the effect of pressure on air entrainment. The effects of deslagging,

cave-in and late melt-in on the bath temperature are too critical to ignore. Despite these disturbances, the final accuracy was reasonable.

Refining presents a more predictable response of bath carbon to decarburization. Unlike temperature, carbon is susceptible to fewer disturbances, with the result that its modelling proved to be more accurate. The effect of deslagging, cave-in and late melt-in is less detrimental on the bath carbon: despite intermittent deslagging, sufficient slag FeO is maintained and the unmelted scrap is generally low in carbon so that only a limited increase in bath carbon will occur.

The collected furnace slag and bath data is a good contribution to EAF research [1]. Their analysis and the ability of the model to reproduce them in general, is a further contribution as it provides a first successful step in the effort to control the EAF process.

Much improvement in the model accuracy can be achieved by a more consistent furnace operation or measurement of disturbances. The current EAF practice is highly variable from one tap to the next. This exacerbates the effect of unmeasured disturbances since it is likely to change as unpredictably.

7.3 Recommendations for future work

The work carried out in this dissertation includes off-line estimation of parameters. If the model is installed at a plant, a crucial problem will be the need for the model to adapt to changes in the plant conditions. The model can implicitly take into account changes in inputs and initial conditions. Changes in physical parameters such as furnace dimension can be made as part of user input. On the other hand changes in the furnace such as refractory properties, energy efficiency, heat losses and reaction rates will change the inherent input-output relationships. The problem is therefore to adjust the model parameters online in response to the changes in the furnace. In this way the model can respond to changes in the furnace (within practical limits) without expert intervention. This may not be necessary when the model is used in a feedback control system where modelling errors will be compensated for by feedback.

In practice, the information on the bath analysis has a substantial delay associated with it. The process of obtaining an analysis of the bath chemistry involves acquiring the bath sample, cooling it (a short duration) and transferring it to the laboratory where it can be analysed. The total duration of this process can range from 4 to 9 minutes[2], or even longer, depending on the availability of sample analyser. This can have serious consequences implications for controller design.

[1] It has been reported that most EAF melt shops are reluctant to release their analysis results [18]!

[2] Based on the times recorded for the actual extraction of the sample and when the analysis data is reported.

7.3.1 Controller design

The aim of the controller design is to demonstrate the benefits of control on the process. Previous authors have designed controllers for the process, however, their main focus was on the use of the off-gas variables as the primary manipulated variables. While the success of this approach has been demonstrated, the off-gas variables have only an indirect or secondary effect on the main process variables such as decarburization, bath temperature, and iron yield.

Inputs with a direct influence on the process are fuel gas and oxygen injection, power input, graphite injection. Efficient control of power input is a well-established technique that is able to transfer maximum power to the process. Due to the high powers that are involved and the switching constraints enforced by the power system, and the transformer tap changing that allows for only discrete levels of power transfer, power input - as it is currently applied in most EAFs - may not lend itself easily to continuous control. The number of times a transformer changes tap positions has a direct influence on its operating life, therefore it is done only when necessary.

Depending on the level of bath carbon, oxygen injection will have serious implications for the iron yield and chemical energy input. With low bath carbon excessive oxygen injection will generate large volumes of FeO that cannot be restored into the bath - since very little bath carbon is available. In this case graphite injection can be used while at the same time foaming the bath. Conditions of high bath carbon call for less graphite injection to allow for effective decarburization. The control problem is then to regulate the oxygen injection and graphite injection to maintain a healthy balance between foaming, yield and decarburization.

Feedback control of foaming presents many opportunities for successful control of the furnace temperature. Sustaining a stable slag foam for long periods will increase the furnace heat efficiency: deslagging will only occur when bath measurements are required[3]. Control will better maintain the foam within values that are known to produce optimal results. On the other hand, the challenge is the instrumentation to measure the slag height which can be used as a feedback variable [4].

Foaming control can be accompanied by the control of slag FeO. Successful control of the FeO is achieved by maintaining a balance between bath oxidation (by oxygen injection) and FeO reduction by graphite injection (and decarburization): excessive oxygen injection will generate high levels of FeO which will be disposed of with the slag unless sufficient graphite is injected to restore some of the FeO to the bath. (The graphite injection is directly responsible for foaming.) The main advantage of FeO control will be the ability

[3] And the first deslagging to remove phosphorus.
[4] Other alternatives are the use of furnace audible signals to infer the state of foaming operations.

to limit material losses such as overuse of oxygen and yield losses. Control of both foaming and FeO can be simultaneously achieved by accurate knowledge of bath carbon, and control of oxygen and graphite injection, provided a reliable method exists to either measure or reasonably infer the slag foam conditions.

Given a highly accurate model, the number of bath measurements can be reduced to just the first bath analysis and temperature. These can be used to initialize the model after which it will be able to accurately predict the temperature and composition. This will eliminate the serious delays and energy losses required to obtain bath measurements.

Bibliography

[1] "World steel in figures," International iron and steel institute, Tech. Rep., 2003.

[2] D.E. Seborg, T.F. Edgar, and D.A. Mellicamp, *Process Dynamics and Control*. New York: John Wiley & Sons, 1989.

[3] N.S. Nise, *Control Systems Engineering*. John Wiley & Sons, 2000.

[4] J.G. Bekker, I.K. Craig, and P.C. Pistorius, "Model predictive control of an electric arc furnace off-gas process," *Control Engineering Practice*, vol. 8, no. 4, pp. 445–455, 2000.

[5] J.G. Bekker, *Modeling and Control of an Electric Arc Furnace Off-gas Process*. South Africa: Master's dissertation, University of Pretoria, 1998.

[6] D.J. Oosthuizen, J.H. Viljoen, I.K. Craig, and P.C. Pistorius, "Modeling of the off-gas exit temperature and slag foam depth of an electric arc furnace process," *ISIJ International*, vol. 41, no. 4, pp. 399–401, 2001.

[7] D.J. Oosthuizen, *Economic Evaluation and Design of an Electric Arc Furnace Controller Based on Economic Objectives*. South Africa: Master's dissertation, University of Pretoria, 2001.

[8] R.D. Morales, H. Rodriguez-Hernández, and A.N. Conejo, "A mathematical simulator for the EAF steelmaking process using direct reduced iron," *ISIJ International*, vol. 41, no. 5, pp. 426–435, 2001.

[9] R.D. Morales, R. Lule, F. López, J. Camacho, and J.A. Romero, "The slag foaming practice in EAF and its influence on the steelmaking shop productivity," *ISIJ International*, vol. 35, no. 9, pp. 1054–1062, 2001.

[10] R.D. Morales, A.N. Conejo, and H.H. Rodriguez, "Process dynamics of electric arc furnace during direct reduced iron melting," *Metallurgical and Materials Transactions B*, vol. 33B, pp. 187–199, 2002.

[11] C. Vercruyssen, P. Wollants, J.R. Roos, D.G.C. Robertson, and L. Bertels, "Mathematical modeling of refining of stainless steel in MRPA converter," *Iron and Steelmaking*, vol. 32, no. 4, pp. 287–296, 1994.

[12] H.G. Oltmann and E.B. Pretorius, "Simulation of the EAF refining stage," *AISE Steel Technology*, pp. 25–33, March 2003.

[13] P. Nyssen, C. Marique, C. Prüm, P. Bintner, and L. Sivini, "A new metallurgical model for the contol of EAF operations," in *Proceedings of the* 6^{th} *European Electric Steelmaking Conference*, Düsseldorf, June 1999, pp. 43–50.

[14] P. Nyssen, R. Colin, S. Knoops, and J.L. Junque, "On-line EAF control with a dynamic metallurgical model," in *Proceedings of the* 7^{th} *European Electric Steelmaking Conference*, Venice, May 2002, pp. 293–304.

[15] D.J. Oosthuizen, I.K. Craig, and P.C. Pistorius, "Economic evaluation and design of an electric arc furnace controller based on economic objectives," *Control Engineering Practice*, vol. 12, pp. 253–265, 2004.

[16] B.J. deVos, *Optimization of Raw Material Additions for an Oxygen-blowing Arc Furnace*. South Africa: Master's dissertation, University of Pretoria, 1993.

[17] C.R. Taylor, Ed., *Electric Furnace Steelmaking*. Iron and Steel Society, 1985.

[18] E.T. Turkdogan, *Fundamentals of Steelmaking*. London: Institute of Materials, 1989.

[19] R.F. Fruehan, Ed., *The Making, Shaping and Treating of Steel: Steelmaking and Refining Volume*, 11th ed. Association of Iron and Steel Engineers, 1998.

[20] B. Deo and R. Boom, Eds., *Fundamentals of Steelmaking Metallurgy*. Prentice Hall International, 1993.

[21] G. Holmes and F. Memoli, "Operational improvements achieved in Davsteel, utilizing the new Techint KT Injection system and TDR digital regulation: a case study," in *Electric Furnace Conference Proceedings*. Iron and Steel Society, 2001, pp. 527–537.

[22] F. Bellingan, *Private communication*. Vanderbijlpark: Cape Gate, 2003.

[23] C. Marique, P. Nyssen, and P. Salamone, "On-line control of the foamy slag in EAF," in *Proceedings of the* 6^{th} *European Electric Steelmaking Conference*, Düsseldorf, June 1999, pp. 154–161.

[24] M.J. Thomson, N.G. Kournetas, E. Evenson, I.D. Sommerville, A. McLean, and J. Guerard, "Effect of oxyfuel burner ratio changes on energy efficiency in electric arc furnace at Co-Steel Lasco," *Ironmaking and Steelmaking*, vol. 28, pp. 267–272, 2001.

[25] A. Pujadas, J. McCauley, and M. Iacuzzi, "EAF energy optimization at nucor yamato steel," in *ISSTech 2003 Conference Proceedings*. Iron and Steel Society, 2003, pp. 391–402.

[26] M.H. Khan, E.J. Evenson, and O.I. Negru, "Results of the Goodfellow EFSOP^{TM} at Birmingham Steel Corp., Seattle, WA, USA," in *Electric Furnace Conference Proceedings*. Iron and Steel Society, 2003, pp. 415–428.

[27] R.K. Galgali, P. Datta, A.K. Ray, K.K. Prasad, and H.S. Ray, "Reduction and foaming of FeO containing slag," *Ironmaking and Steelmaking*, vol. 28, pp. 321–327, 2001.

[28] I. Kimihisa and R.J. Fruehan, "Slag foaming in electric furnace steelmaking," in *Electric Furnace Proceedings*. Iron and Steel Society, 1987, pp. 345–351.

[29] I. Kimihisa and R.J. Fruehan, "Study on the foaming of CaO-SiO_2-FeO slags: Part 1. Foaming parameters and experimental results," *Metallurgical and Materials Transactions B*, vol. 20B, pp. 509–514, 1989.

[30] I. Kimihisa and R.J. Fruehan, "Study on the foaming of CaO-SiO_2-FeO slags: Part 2. Dimensional analysis and foaming in iron and steelmaking processes," *Metallurgical and Materials Transactions B*, vol. 20B, pp. 515–521, 1989.

[31] R. Jiang and R.J. Fruehan, "Slag foaming in bath smelting," *Metallurgical and Materials Transactions B*, vol. 22B, pp. 481–489, 1991.

[32] P.E. King and M.D. Nyman, "Modeling and control of an electric arc furnace using a feedforward artificial neural network," *Journal of Applied Physics*, vol. 80, pp. 1872–1877, 1996.

[33] D. Raisz, M. Sakulin, H. Renner, and Y. Tehlivets, "Recognition of operational states in electric arc furnaces," in *Proceedings of the Ninth International Conference on Harmonics and Quality of Power*, vol. 2. IEEE, October 2000, pp. 475–480.

[34] S.A. Billings and H. Nicholson, "Modelling a three-phase electric arc furnace: comparative control strategies," *Applied Mathematical Modelling*, vol. 1, pp. 355–361, 1977.

[35] S.A. Billings, F.M. Boland, and H. Nicholson, "Electric arc furnace modeling and control," *Automatica*, vol. 15, pp. 137–148, 1979.

[36] F. Oeters, Ed., *Metallurgy of Steelmaking*. Düsseldorf: Verlag Stahleisen mbH, 1994.

[37] L. Ljung, *System Identification, Theory for the User*, 2nd ed. Prentice Hall, 1999.

[38] J.P. Norton, *An Introduction to Identification*. London: Academic Press, 1986.

[39] J.G. Bekker, I.K. Craig, and P.C. Pistorius, "Modeling and simulation of an electric arc furnace process," *ISIJ International*, vol. 39, no. 1, pp. 23–32, 1999.

[40] L. Gmelin, Ed., *Gmelin Handbook of Inorganic Chemistry*, 8th ed. Springer-Verlag, 1985, vol. 8a.

[41] R.J. Fruehan, "Potential benefits of gas stirring in an electric arc furnace," *ISS Transactions*, vol. 12, no. 1, pp. 33–40, 1991.

[42] W.T Lankford, Ed., *The Making, Shaping and Treating of Steel: Steelmaking and Refining Volume*, 10th ed. Pittsburgh: Association of Iron and Steel Engineers, 1985.

[43] K.-C Chou, U.B. Pal, and E. R.G. Reddy, "A general model for BOP decarburization," *ISIJ International*, vol. 33, no. 8, pp. 862–868, 1993.

[44] P.L. Rathaba, I.K. Craig, and P.C. Pistorius, "Influence of the oxyfuel burner subsystem on the eaf process," in *to appear in Proceedings of the IFAC workshop on Automation in Mining, Mineral and Metal Processing*, Nancy, September 2004.

[45] M.W. Chase, Ed., *NIST-JANAF thermochemical tables*. National Institute of Standards and Technology, 1998.

[46] B. Bowman, "Major developments in arc furnace technology over the last four decades," in *Proceeding of Aceria, 11 Seminaro*. Buenos Aires: Inst. Argentino de Siderurgia, November 1997.

[47] C.M. Bishop, *Neural Networks for Pattern Recognition*. Oxford: Oxford University Press, 1995.

[48] J.A. Snyman, C. Frangos, and Y. Yavin, "Penalty function solutions to optimal control problems with general constraints via a dynamic optimization method," *Computers, Mathematics and Applications*, vol. 23, pp. 47–55, 1992.

[49] P. Lindskog, *Methods, algorithms and tools for system identification based on prior knowledge*. Lingköping: Lingköping University, 1996.

[50] MathWorks, *Matlab Optimization Toolbox*. MathWorks, 2001.

[51] P.M. Mäkilä, "Squared and absolute errors in optimal approximation of nonlinear systems," *Automatica*, vol. 39, pp. 1865–1876, 2003.

[52] D.C. Montgomery, G.C. Runger, and N.F. Hubele, *Engineering statistics*. John Wiley & Sons, 1998.

[53] X. Xia and C.H. Moog, "Identifiability of nonlinear systems with application to HIV/AIDS models," *IEEE Transactions on Automatic Control*, vol. 48, no. 2, pp. 330–336, 2002.

[54] P.L. Rathaba, I.K. Craig, X. Xia, and P.C. Pistorius, "Identifiability of an electric arc furnace model," in *Proceedings of the IFAC workshop on Automation in Mining, Mineral and Metal Processing*, Shanghai, October 2003, pp. 86–91.

[55] L. Ljung and T. Glad, "On global identifiability for arbitrary model parameterizations," *Automatica*, vol. 30, no. 2, pp. 265–276, 1994.

[56] M.S. Grewal and K.G. Glover, "Identifiability of linear and nonlinear dynamical systems," *IEEE Transactions on Automatic Control*, vol. AC-21, pp. 833–837, 1976.

[57] E.T. Tunali and T.J. Tarn, "New results for identifiability of nonlinear systems," *IEEE Transactions on Automatic Control*, vol. 32, no. 2, pp. 146–154, 1987.

[58] S. Auduloy, G. Bellu, L. D'Angio, M.P. Saccomani, and C. Cobelli, "Global identifiability of nonlinear biological systems," *IEEE Transactions on Biomedical Engineering*, vol. 48, no. 1, pp. 55–65, 2001.

[59] M.P. Saccomani, S. Audoly, and L. D'Angiò, "Parameter identifiability of nonlinear systems: the role of initial conditions," *Automatica*, vol. 39, pp. 619–632, 2003.

[60] X. Xia, "Estimation of HIV/AIDS parameters," *Automatica*, vol. 39, no. 11, pp. 1983–1988, 2003.

[61] J.A. Jacques, *Compartmental Analysis in Biology and Medicine*, 2nd ed. The University of Michigan Press and John Wiley & Sons, 1988.

[62] M. Kirschen, H. Pfeifer, F.-J. Wahlers, and H. Mees, "Off-gas measurements for mass and energy balances of a stainless steel EAF," in *59th Electric Furnace Conference Proceedings*. Iron and Steel Society, 2001, pp. 737–745.

[63] J.J. Eksteen, S.J. Frank, and M.A. Reuter, "Towards predictive control of ferroalloy furnaces: combining thermochemistry, inventory modelling and systems engineering," in *Proceedings: Tenth International Ferroalloy Congress*, Cape Town, February 2004, pp. 648–658.

[64] J.J. Eksteen, S.J. Frank, and M.A. Reuter, "Distributed compositional and temperature nature of melts in submerged and open arc furnaces in high carbon ferrochrome production," in *Proceedings: Tenth International Ferroalloy Congress*, Cape Town, February 2004, pp. 83–93.

[65] J.H. Mathews, *Numerical Methods for Computer Science, Enigineering and Mathematics*, 2nd ed. Prentice-Hall, 1992.

Appendix A

Appendix

A.1 Nomenclature

Below is a list of all variables and parameters used throughout the dissertation.

List of abbreviations

BOF	Basic oxygen furnace
DRI	Direct reduced iron
EAF	Electric arc furnace
LS	Least square(s)
ODE	Ordinary differential equation
OXF	Oxyfuel
ppm	Parts per million
RHS	Right hand side
SID	System identification
$\mathcal{M}$	Main nonlinear model
$\mathcal{M}_{\mathcal{L}}$	Linearised model
$\mathcal{M}_{\mathcal{R}}$	Reduced nonlinear model

Model states

x_1 solid steel [kg]
x_2 liquid steel [kg]
x_3 dissolved carbon [kg]
x_4 dissolved silicon [kg]
x_5 solid slag mass [kg]
x_6 liquid slag mass [kg]
x_7 FeO mass in slag [kg]
x_8 SiO_2 mass in slag [kg]
x_9 CO in freeboard [kg]
x_{10} CO_2 in freeboard [kg]
x_{11} nitrogen in freeboard [kg]
x_{12} bath and molten slag temperature [K]
x_{13} scrap and solid slag temperature [K]
x_{14} relative furnace pressure [Pa]
x_{15} [kg.s^2]
x_{16} [kg.s]
x_{17} mass flow through the off-gas system [kg]
x_{18} mass of water vapour in the freeboard [kg]
x_{19} mass of methane in the freeboard [kg]
x_{20} mass of propane in the freeboard [kg]
x_{21} mass of hydrogen in the freeboard [kg]
x_{22} mass of oxygen in the freeboard [kg]

Inputs

u_1 off-gas turbine flow [kg/s]
u_2 slip gap width [m]
d_1 rate of oxygen injection [kg/s]
d_2 rate of DRI input [kg/s]
d_3 rate of slag input [kg/s]
d_4 average arc power input [kW]
d_5 rate of graphite injection [kg/s]

Outputs

y_1 Bath temperature [°C]
y_2 Percentage carbon [wt %]
y_3 Bath oxygen activity [ppm]
y_4 Percentage FeO [wt %]
y_5 Relative pressure [Pa]

Parameters

$C_p(k)$	heat capacity of element/compound k [kJ/(mol.K)]
M_k	molar mass of element/compound k [kg/mol]
X_k	mole fraction of element/compound k
X_k^{eq}	equilibrium mole fraction of element/compound k
$\lambda(k)$	latent heat of fusion of element/compound k [kJ/mol]
ΔH_k	enthalpy of formation of compound k [kJ/mol]
T_k	initial temperature of element/compound k [K]
k_{air_1}	mole fraction of oxygen in air [mol/kg]
k_{air_2}	mole fraction of nitrogen in air [mol/kg]
k_{XC}	equilibrium concentration constant for carbon
k_{XSi}	equilibrium concentration constant for silicon
k_{dC}	decarburization rate constant [kg/s]
k_{dSi}	desiliconization rate constant [kg/s]
k_{gr}	graphite reactivity constant
k_{therea_1}	melting rate constant of metallic charge [kW/(K.kg)]
k_{therea_5}	melting rate constant of solid slag [kW/(K.kg)]
k_{VT}	heat loss coefficient [kW/K]]
k_{PR}	furnace pressure constant
h_d	pressure distribution constant
η_{FeO}	efficiency of bath oxidation
η_{ARC}	efficiency of arc power input
$\%_{met}$	percentage metallization of DRI

A.2 Tap data

A.2.1 Analysis results

The following table summarizes the analysis results for the slag and bath chemistry. The time at which each sample was extracted is also shown; here, the actual time of day at which the data was recorded is used, with units [hh:mm]. The data relates to tap data collected from 7h00 to 17h10 on 18 November 2003 - taps 1 to 10, and 10h00 to 18h10 on 19 November 2003 - taps 11 to 18. The results of the slag mass calculations of section 4.3.4 are shown in table A.3.

For the first 10 taps, extensive measurement were carried out - 3 slag samples, additional steel analyses and temperature readings. For the other taps, normal operation and measurement occurred with only one slag sample extracted at tap time. Under normal operation, at least one temperature and carbon measurement is taken.

Table A.1: Measured bath and slag data.

Tap #	Time	% C	% Si	O_2[ppm]	Time	Temp °C	Time	% FeO	% SiO_2	% CaO	% MgO	% Al_2O_3
1	7.05	0.199	0.03	-	7.15	1619	7.04	17.70	18.2	50.53	3.53	5.10
	7.15	0.125	-	219	7.16	1630	7.16	31.55	10.5	43.45	3.33	3.07
	7.16	0.119	-	229	7.20	1678	7.20	36.53	9.08	37.57	3.47	2.73
	7.20	0.043	-	658								
2	8.14	0.082	0.01	-	8.14	1598	8.11	27.04	13.7	43.74	5.08	3.69
	8.16	0.060	-	448	8.16	1618	8.16	30.25	12.5	43.09	5.42	3.51
	8.18	0.054	-	504	8.18	1638	8.18	39.20	10.3	34.41	5.43	3.01
	8.21	0.039	-	704	8.21	1640						
3	9.10	0.111	0.03	-	9.13	1597	9.10	31.50	13.4	40.13	5.04	4.13
	9.14	0.053	-	514	9.15	1636	9.14	26.21	12.6	46.07	6.38	3.90
	9.17	0.043	-	623	9.18	1631	9.17	31.82	11.4	40.48	6.14	3.48
4	10.14	0.078	0.02	-	10.14	1594	10.13	32.13	11.6	41.14	5.46	4.32
	10.20	0.043	-	648	10.20	1610	10.18	29.80	10.7	43.12	5.77	4.13
					10.21	1658	10.20	31.65	10.1	41.13	5.77	3.78
5	11.36	0.060	0.02	-	11.37	1586	11.33	37.80	9.85	36.39	5.14	3.48
	11.42	0.056	-	466	11.42	1602	11.43	38.25	7.58	36.15	5.11	2.72
	11.44	0.040	-	699	11.44	1658	11.45	38.12	8.10	39.83	5.69	2.91
6	12.51	0.060	0.03	-	12.53	1615	12.50	43.95	10.8	29.38	5.25	4.14
	12.55	0.048	0.03	-	12.55	1647	12.53	43.65	10.1	30.32	5.43	3.84
	12.55	0.026	-	1048			12.56	45.29	9.61	30.21	5.38	3.68
7	13.43	0.088	0.03	-	13.43	1571	13.40	34.52	11.7	37.95	5.41	5.00
	13.45	0.071	0.03	-	13.47	1546	13.44	34.81	11.6	37.65	5.49	5.03
	13.47	0.065	-	376	13.49	1601	13.48	36.35	9.41	32.00	5.71	3.96
	13.49	0.054	-	481	13.51	1615						
	13.55	0.046	-	572								
8	15.05	0.056	0.03	-	15.07	1630	15.04	37.33	8.96	38.27	8.07	3.81
	15.07	0.051	0.03	-	15.08	1643	15.06	35.64	9.24	37.74	7.81	3.92
	15.08	0.037	-	738			15.08	35.06	8.57	34.60	7.30	3.62
9	16.02	0.157	0.03	-	16.05	1540	15.56	26.96	11.7	40.20	7.23	4.58
	16.06	0.106	0.03	-	16.08	1615	16.06	26.57	10.6	43.41	7.05	4.22
	16.08	0.062	-	481	16.10	1636	16.09	27.05	10.2	39.16	6.34	4.00
	16.09	0.072	0.03	-	16.13	1660						
	16.10	0.093	-	293								
	16.13	0.033	-	845								
10	17.03	0.078	0.03	-	17.05	1579	17.02	24.57	14.8	42.47	5.31	4.36
	17.05	0.085	0.03	-	17.07	1614	17.05	23.91	15.0	44.46	5.98	4.57
	17.09	0.044	-	624	17.09	1647	17.09	25.08	15.2	43.29	6.50	4.64
	17.09	0.059	0.03	-								
11	10.37	0.112	0.02	-	10.36	1570	10.43	35.69	11.1	36.17	5.59	3.83
	10.39	0.034	-	760	10.39	1600						
	10.42	0.030	-	894	10.42	1638						
	10.44	0.045	-	604	10.44	1631						
12	11.34	0.057	0.02	-	11.41	1566	11.47	36.34	11.6	34.72	6.96	3.89
	11.45	0.034	-	804	11.45	1631						
	11.47	0.031	-	920	11.47	1673						
13	12.43	0.081	0.02	-	12.45	1585	12.50	34.91	10.2	37.55	5.68	3.59
	12.48	0.042	-	642	12.48	1623						
	12.50	0.039	-	678	12.50	1621						
14	13.42	0.115	0.04	-	13.47	1594	14.10	36.18	10.8	34.39	5.48	3.78
	13.50	0.050	-	531	13.50	1610						
	14.08	0.033	-	823	14.05	1658						
	14.10	0.030	-	930	14.08	1621						
					14.10	1652						
15	14.56	0.068	0.03	-	15.02	1589	15.09	41.95	10.2	34.43	6.04	3.57
	15.06	0.036	-	861	15.05	1626						
	15.09	0.035	-	757	15.06	1641						
	15.11	0.030	-	907	15.08	1626						
					15.10	1650						
16	16.03	0.075	0.03	-	16.04	1624	16.05	37.33	10.2	37.51	5.83	3.47
	16.06	0.034	-	861	16.06	1645						
17	16.54	0.080	0.03	-	17.00	1564	17.10	31.93	12.4	39.96	4.31	4.53
	17.06	0.036	-	356	17.04	1566						
	17.08	0.035	-	592	17.06	1588						
					17.08	1639						
18	17.56	0.169	0.03	-	18.05	1582	17.10	31.93	11.2	39.96	6.76	4.20
	18.01	0.093	0.02	-	18.08	1618						
	18.09	0.060	-	592	18.09	1661						

Table A.2: Detailed slag analysis data (showing the tap number and analysis (in wt %) for each of the samples per tap).

ID	SiO_2	Al_2O_3	Fe(tot)	Fe(met)	FeO	Fe_2O_3 [5]	TiO_2	CaO	MgO	K_2O	MnO	P	Cr
Tap1/1	18.2	5.10	14.5	0.72	11.7	6.70	0.70	50.5	3.53	< 0.02	5.45	0.53	0.08
Tap1/2	10.5	3.07	27.3	2.79	14.2	19.3	0.45	43.5	3.33	< 0.02	4.66	0.40	0.13
Tap1/3	9.08	2.73	33.0	4.61	18.2	20.4	0.39	37.6	3.47	< 0.02	4.35	0.29	0.13
Tap2/1	13.7	3.69	23.2	2.16	16.0	12.3	0.55	43.7	5.08	< 0.02	4.49	0.34	0.10
Tap2/2	12.5	3.51	25.1	1.62	18.1	13.5	0.51	43.1	5.42	< 0.02	4.09	0.30	0.09
Tap2/3	10.3	3.01	33.4	2.92	25.9	14.7	0.43	35.4	5.43	< 0.02	3.56	0.25	0.08
Tap3/1	13.4	4.13	25.5	1.00	18.2	14.8	0.55	40.1	5.04	< 0.02	4.37	0.30	0.09
Tap3/2	12.6	3.90	22.7	2.28	14.8	12.7	0.54	46.1	6.38	< 0.02	3.89	0.28	0.07
Tap3/3	11.4	3.48	28.1	3.35	17.7	15.7	0.49	40.5	6.14	< 0.02	3.60	0.23	0.07
Tap4/1	11.6	4.32	26.0	1.04	16.5	17.3	0.58	41.1	5.46	< 0.02	4.13	0.24	0.14
Tap4/2	10.7	4.13	26.0	2.82	17.2	14.0	0.56	43.1	5.77	< 0.02	3.71	0.23	0.13
Tap4/3	10.1	3.78	28.4	3.76	17.2	16.1	0.50	41.1	5.77	< 0.02	3.45	0.20	0.12
Tap5/1	9.85	3.48	31.8	2.40	24.4	14.9	0.50	36.4	5.14	< 0.02	3.86	0.21	0.09
Tap5/2	7.58	2.72	36.5	6.78	19.6	20.8	0.40	36.1	5.11	< 0.02	2.83	0.18	0.07
Tap5/3	8.10	2.91	31.1	1.46	21.4	18.5	0.42	39.8	5.69	< 0.02	3.10	0.17	0.07
Tap6/1	10.8	4.14	34.6	0.47	31.4	13.9	0.55	29.4	5.25	< 0.02	4.63	0.20	0.09
Tap6/2	10.1	3.84	35.1	1.13	29.9	15.3	0.51	30.3	5.43	< 0.02	4.09	0.19	0.09
Tap6/3	9.61	3.68	36.1	0.87	29.2	17.9	0.49	30.2	5.38	< 0.02	3.98	0.17	0.08
Tap7/1	11.7	5.00	28.1	1.31	21.7	14.2	0.60	38.0	5.41	< 0.02	4.28	0.22	0.11
Tap7/2	11.6	5.03	27.9	0.80	23.2	12.9	0.59	37.6	5.49	< 0.02	4.51	0.21	0.11
Tap7/3	9.41	3.96	31.1	2.83	21.7	16.3	0.50	32.0	5.71	< 0.02	4.31	0.17	0.09
Tap8/1	8.96	3.81	30.3	1.32	25.2	13.5	1.34	38.5	8.07	< 0.02	3.54	0.20	0.08
Tap8/2	9.24	3.92	29.4	1.68	19.6	17.8	1.35	37.7	7.81	< 0.02	3.52	0.19	0.08
Tap8/3	8.57	3.62	34.3	7.01	18.6	18.3	1.23	34.6	7.30	< 0.02	3.28	0.18	0.07
Tap9/1	11.7	4.58	22.5	1.59	16.0	12.2	1.76	40.2	7.23	< 0.02	4.26	0.23	0.18
Tap9/2	10.6	4.22	23.5	2.86	12.8	15.3	1.82	43.4	7.05	< 0.02	3.40	0.16	0.14
Tap9/3	10.2	4.00	27.6	6.60	12.9	15.8	1.54	39.2	6.34	< 0.02	3.06	0.17	0.12
Tap10/1	14.8	4.36	20.9	1.75	15.4	10.2	0.89	42.5	5.31	< 0.02	4.51	0.28	0.11
Tap10/2	15.0	4.57	20.1	1.49	14.2	10.8	0.89	44.5	5.98	< 0.02	4.40	0.27	0.11
Tap10/3	15.2	4.64	20.7	1.25	12.8	13.6	0.90	43.3	6.50	< 0.02	4.17	0.25	0.11
Tap11	11.1	3.83	29.4	1.68	21.6	15.7	3.10	36.2	5.59	< 0.02	3.37	0.15	0.08
Tap12	11.6	3.89	29.2	0.94	23.0	14.8	2.38	34.7	6.96	< 0.02	3.17	0.14	0.08
Tap13	10.2	3.59	32.2	5.03	18.6	18.1	1.15	37.6	5.68	< 0.02	3.21	0.18	0.07
Tap14	10.8	3.78	33.1	5.00	21.9	15.8	0.83	34.8	5.48	< 0.02	3.13	0.19	0.06
Tap15	10.2	3.57	33.8	1.22	22.6	21.5	0.65	34.4	6.04	< 0.02	3.08	0.21	0.08
Tap16	10.2	3.47	30.7	1.63	21.8	17.2	0.59	37.5	5.83	< 0.02	3.29	0.20	0.08
Tap17	12.4	4.53	27.8	2.93	18.1	15.4	0.70	40.0	4.31	< 0.02	3.42	0.23	0.07
Tap18	11.2	4.20	25.4	2.38	16.1	15.0	0.61	41.7	6.76	< 0.02	3.42	0.24	0.06

A.2.2 Initial slag masses

The slag masses in table A.3 were calculated based on the mass of the known charge input and the slag composition. That is, given the mass and composition (see table 2.3) of the slag additives and the analysis results of the slag, the total liquid slag (CaO, MgO and other components), FeO and SiO_2 can be determined. For instance, tap 1: $\%\,\mathrm{CaO} = 50.53\,\%$ corresponds to a mass of $m_{\mathrm{CaO}} = 0.905 \times 4.51 + 0.63 \times 1.02 = 4.72$ ton; with $\%\,\mathrm{FeO} = 17.7\,\%$, $m_{\mathrm{FeO}} = \frac{m_{\mathrm{CaO}} \times \%\,\mathrm{FeO}}{\%\,\mathrm{CaO}} = \frac{4.72 \times 17.7}{50.53} = 1.65$ ton. Other slag components such as SiO_2 and the total slag itself can be calculated in a similar fashion. Note that since SiO_2 lies within a relatively small range, the average SiO_2 composition of 11.17 % was used.

[5] Calculated as $\mathrm{Fe_2O_3} = 1.43\left(\mathrm{Fe(tot)} - \mathrm{Fe(met)} - \frac{\mathrm{FeO}}{1.286}\right)$, with units of percentages.

Table A.3: Initial slag mass estimates (in [ton]) from analysis data.

Tap #	Liquid slag	FeO	SiO_2	Lime	Dololime
1	6.65	1.65	1.04	4.51	1.02
2	6.96	3.05	1.26	4.61	1.20
3	6.83	3.75	1.33	4.42	1.24
4	6.65	3.77	1.31	4.51	1.19
5	6.71	4.97	1.47	4.50	1.13
6	7.23	7.08	1.80	4.45	1.12
7	6.91	4.39	1.42	4.52	1.16
8	6.48	4.70	1.41	4.55	1.16
9	7.35	3.20	1.33	4.47	1.16
10	7.45	2.85	1.30	4.40	1.50
11	7.02	4.72	1.48	4.52	1.09
12	7.23	5.01	1.54	4.56	1.04
13	6.85	4.44	1.42	4.53	1.06
14	7.32	5.03	1.55	4.59	1.09
15	6.55	5.86	1.56	4.55	1.09
16	6.58	4.77	1.43	4.51	1.12
17	6.67	3.74	1.31	4.47	1.01
18	7.08	3.53	1.33	4.59	1.30

A.2.3 Furnace inputs

This subsection provides a record of the inputs used to obtain the results throughout the dissertation. The inputs were collected online during the measurement trials. These include arc power input, graphite injection, fuel gas and oxygen injection. The oxygen consists of two components: the burner oxygen - used in burner mode and to cool the lances - and refining oxygen that is injected for decarburization. The slip gap width and the off-gas flow are constant at 0.5 m and 0.5 kg/s throughout. Furthermore, there are no continuous feeds of DRI and slag - the plots of these constant inputs will therefore not be shown.

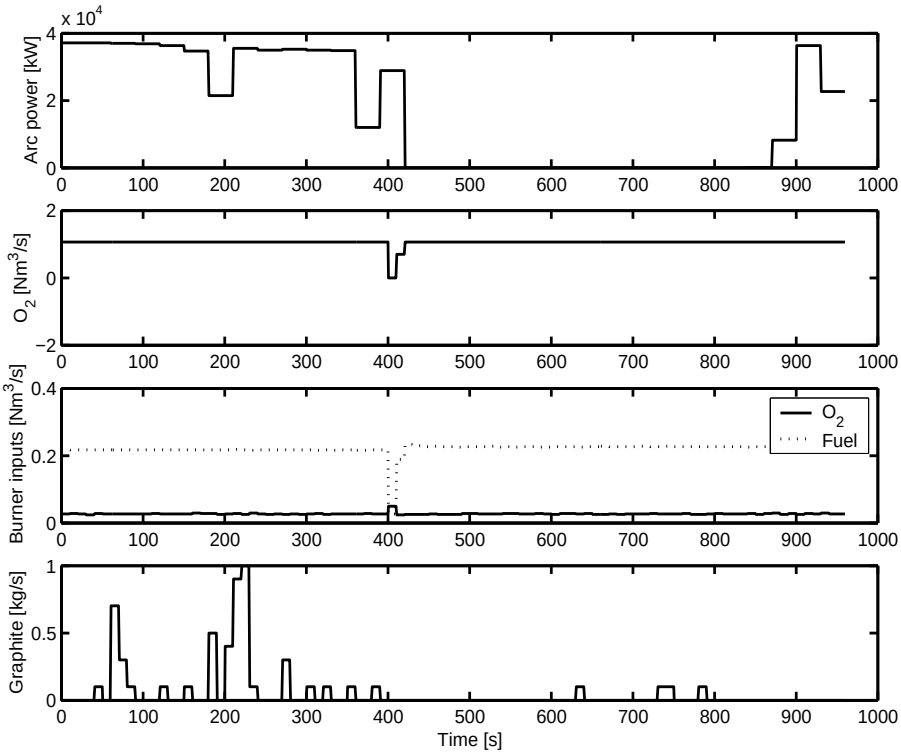

Figure A.1: Furnace inputs for tap 1.

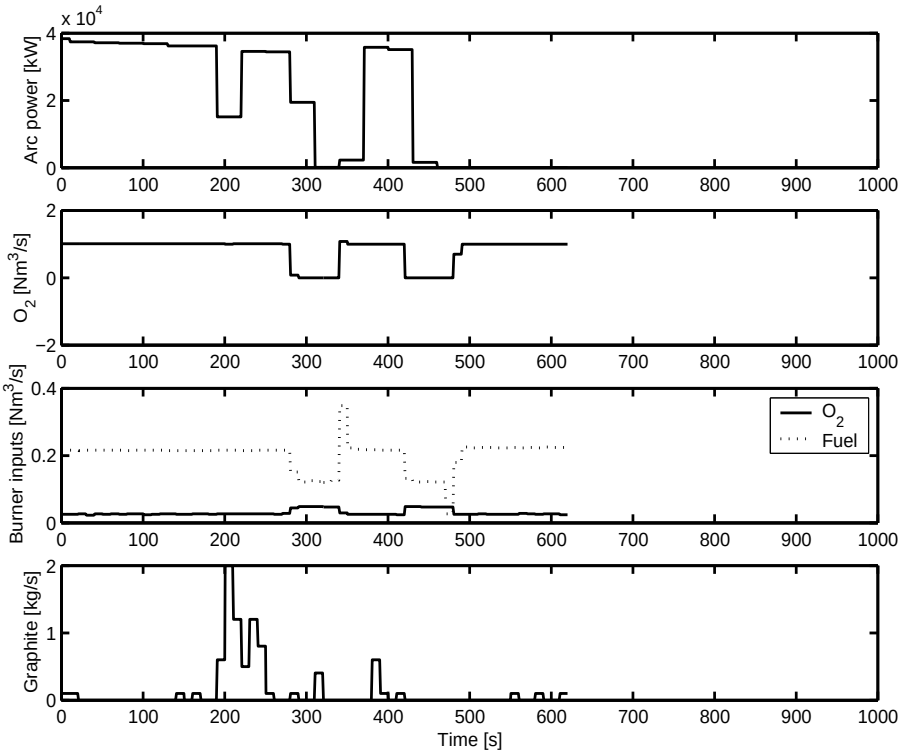

Figure A.2: Furnace inputs for tap 2.

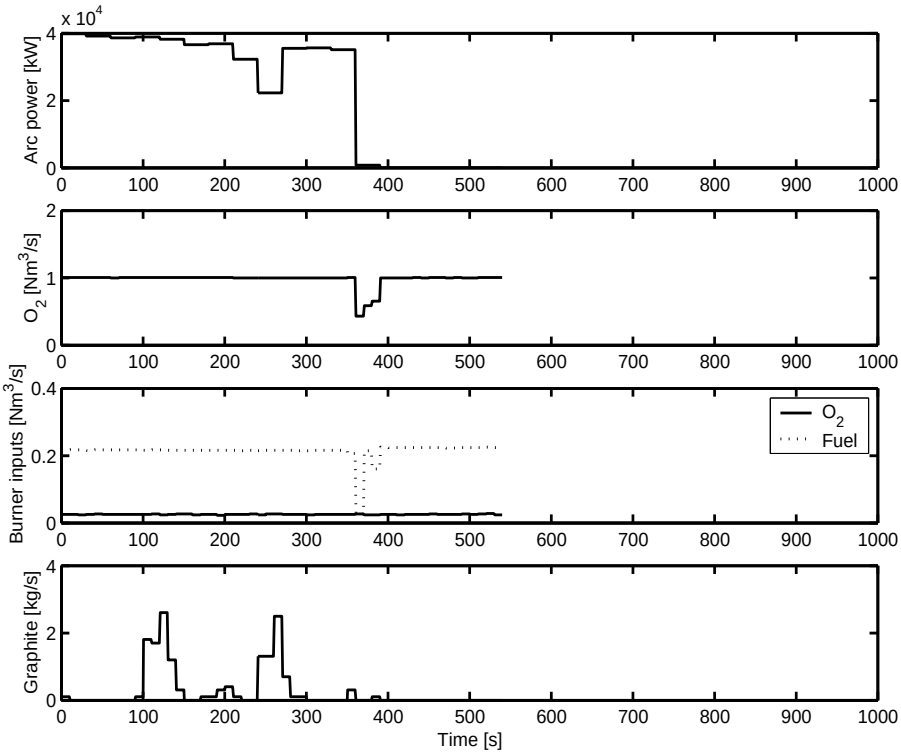

Figure A.3: Furnace inputs for tap 3.

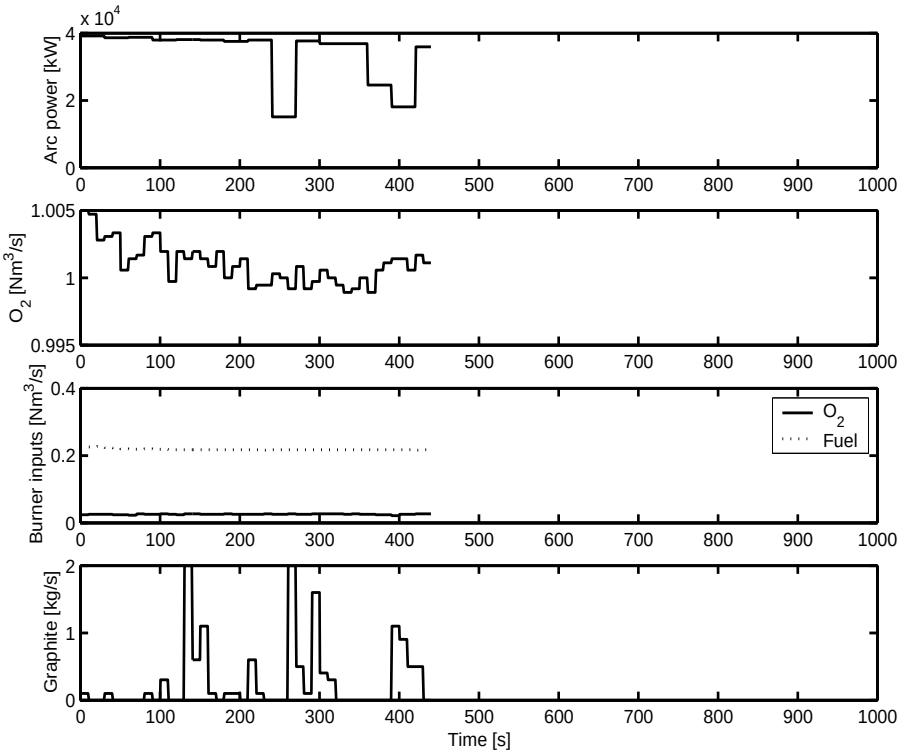

Figure A.4: Furnace inputs for tap 4.

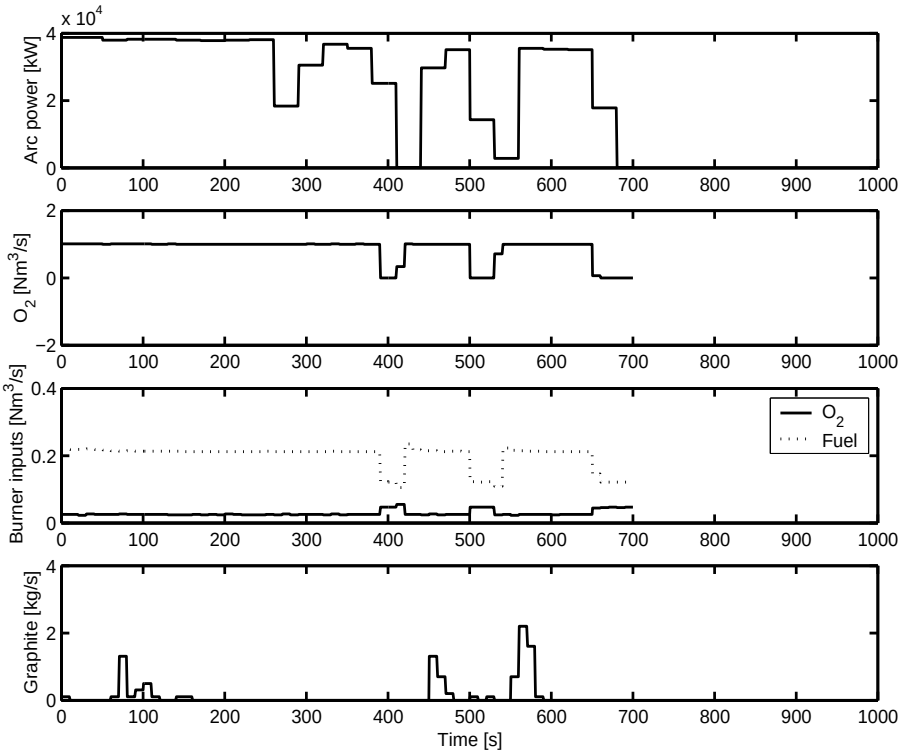

Figure A.5: Furnace inputs for tap 5.

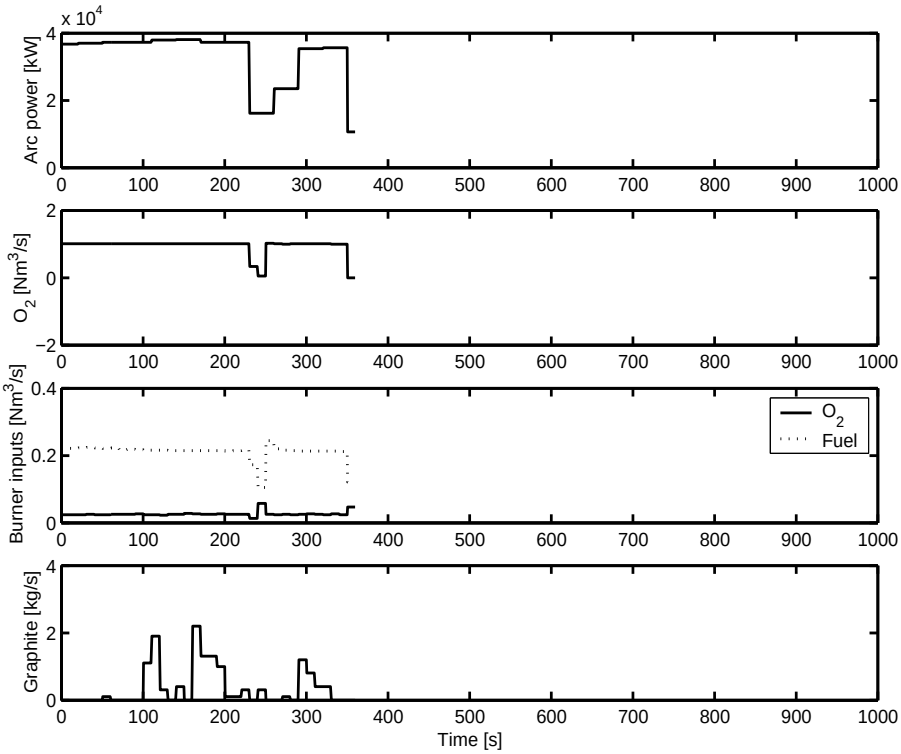

Figure A.6: Furnace inputs for tap 6.

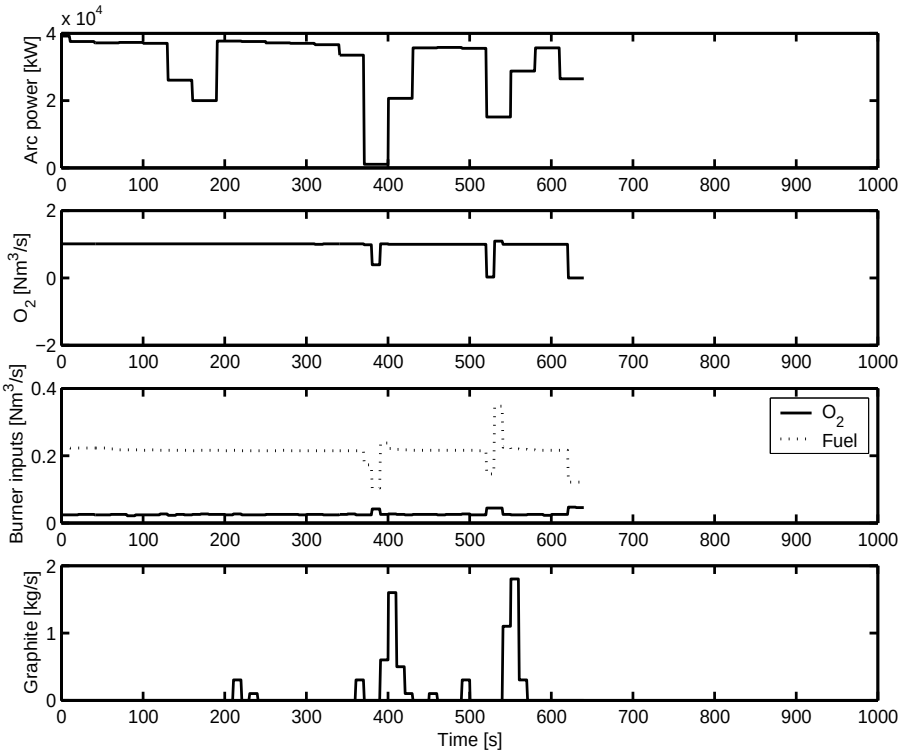

Figure A.7: Furnace inputs for tap 7.

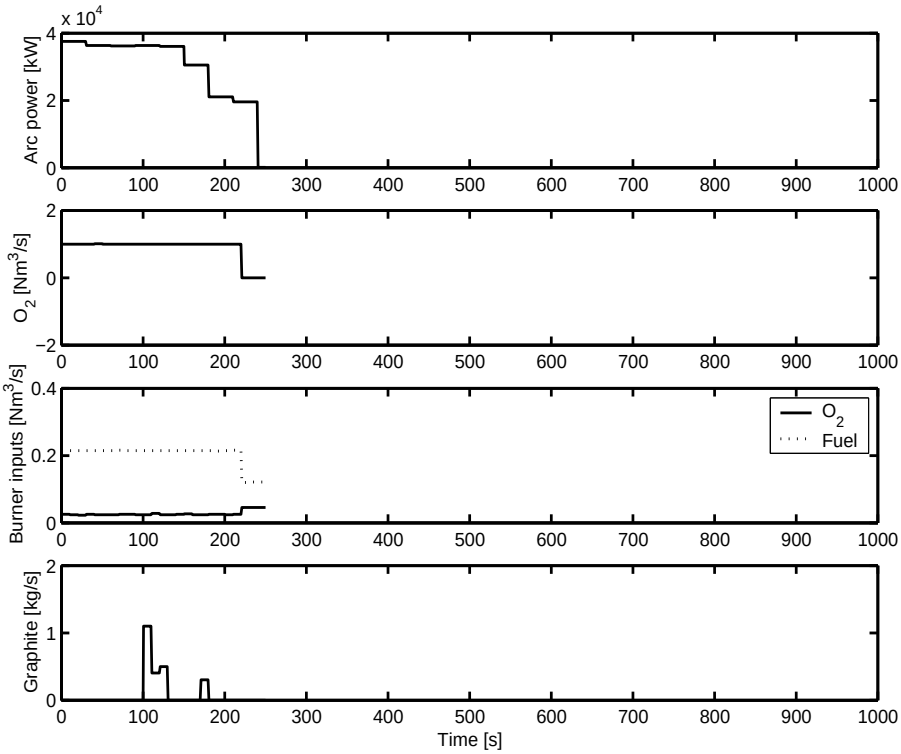

Figure A.8: Furnace inputs for tap 8.

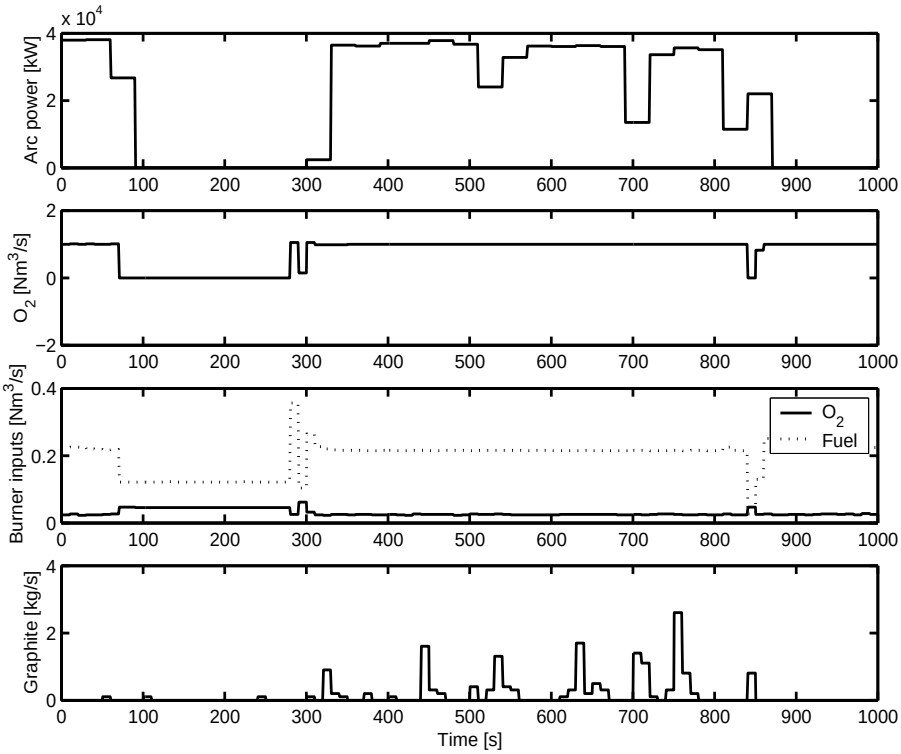

Figure A.9: Furnace inputs for tap 9.

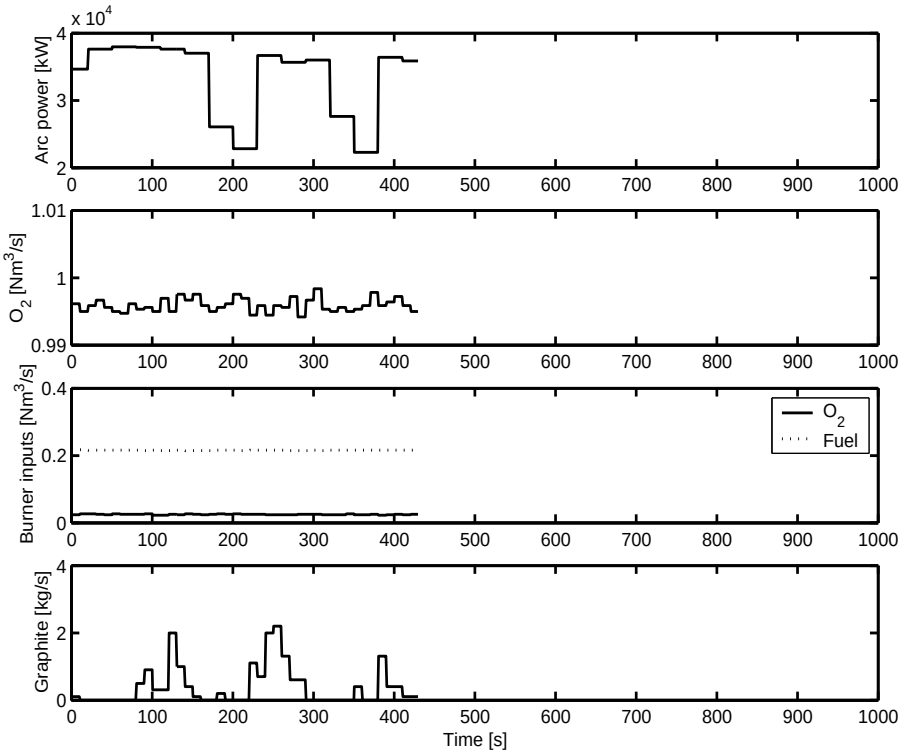

Figure A.10: Furnace inputs for tap 10.

A.3 EAF pressure

This section analyses the plant data relating to the measured furnace pressure, the results obtained in practice and its expected behaviour based on the knowledge of furnace operation. The furnace pressure is a good reflection of the changes that take place in freeboard masses and general furnace openings. Increasing the size of the openings will have a marked effect on the pressure, with a tendency towards lower pressure values.

Particular examples are the furnace roof and slag door; other openings such as electrode ports and openings between furnace panels are permanent and will have no effect on the changes in the pressure. Given a perfect instrument for measuring pressure, the following scenarios should result.

- **Open roof**
  When the furnace roof is open, the relative pressure will be zero. Any value recorded will mark the point of zero relative pressure and it should always be the same (within practical limits) for all conditions when the roof is open. It can be expected that furnace pressure readings will be relative to this constant offset.

- **Early meltdown**
  During early meltdown the scrap will prevent any air entrainment [19], and the combustion of volatile materials will generate high gas volumes, both these mechanisms will increase the furnace pressure (hence the blowing out of flames from all furnace openings at the onset of arcing).

- **Opening of slag door**
  The refining stage involves the injection of oxygen into the bath and high levels of foaming. For the duration of foaming the slag door is kept open so that excess slag can flow out of the slag door and measurement probes can be inserted into the furnace. With no graphite injection the pressure should be negative. However, instantaneous pressure spikes will coincide with graphite injection as rapid gas evolution takes place in the slag.

- **Burner and lancing modes**
  In burner operation, with the furnace sealed, significant gas volumes are generated with the effect that pressure increases occur. Oxygen injection will, despite the large volume of O_2, lead to little or no pressure increases since the main product is FeO, not a gas.

The above scenarios are reflected in the following figure where the results of two typical heat cycles are presented. Some correlation can be noted between the pressure and

graphite injection. However very little sensible pressure changes occur in response the onset of burner mode, lancing or opening of the roof or slag door. As a result, the pressure record cannot be considered reliable for model fitting.

A.4 Model simulation

The model simulation is computationally intensive. This is due to the subsampling that is used to accommodate the gas phases and pressure which have very short time constants. In the solution of the main model differential equations (using Runge-Kutta methods [65]), the slowly varying states such as masses are sampled at a longer time interval e.g. $\Delta t = 1$ second. To carry out the subsampling, the differential equations are further solved within the interval Δt from t_i to t_{i+1} at a much smaller sampling time of $\Delta t_s = (t_{i+1} - t_i)/N$, where N is the number of subsamples and interval $i = 0$ at the beginning of the model simulation and $i = M$ at the end of the entire tap simulation. Therefore, the model equations are effectively solved $M \times N$ times - the smaller the N and/or M, the faster the model simulation. Decreasing the number of subsamples will significantly shorten the model simulation time as these subsamples are typically chosen to be 300 to 1000 - a significant computational expense when a long model simulation is required. It is possible to decrease the subsamples to $N = 1$, but this must be accompanied by an equal decrease (by the same factor) in the pressure constant k_{PR}. The pressure will be exaggerated (since the furnace is made significantly air tight) and the gas phase equally decreased. Except for these states (gases and pressure), the model response will be the same as with the higher number of subsamples. This shortened simulation time is advantageous particularly for parameter estimation when hundreds and even thousands of function evaluations are required. It can be used to obtain an initial parameter set that can subsequently be applied to the model with with higher N, since these parameters are close to the solution. This approach has been successfully used to shorten the parameter estimation process in this dissertation.

A.5 Measurement considerations

A.5.1 Discrepancy between carbon measurements

A problem experienced in the data analysis is the discrepancy between carbon measurements obtained using two different methods: extracting a bath sample for laboratory analysis with a mass spectrometer and using a composite lance which reports temperature, oxygen activity and bath carbon. Table A.4 shows the results recorded from several taps and the corresponding measurement times (these values are derived from table A.1).

In all the measurements shown no cave-in was detected.

Table A.4: Comparison of carbon measurements.

	Sample analysis		Composite probe	
Tap #	Time	% C	Time	% C
6	12:55	0.048	12:55	0.028
8	15:07	0.051	15:08	0.037
9	16:09	0.072	16:08	0.062
	16:09	0.072	16:10	0.093
10	17:09	0.059	17:09	0.044

Tap 6 is a clear example of the difference between the carbon content reported from the analysis and a reading from the composite probe. The results are within one minute of each other but the analysis results are twice as much as the probe readings. For taps 8 and 10, the analysis results are also higher. A major cause of the discrepancy could be the inaccuracy of the bath carbon estimate that is obtained from the measured bath oxygen when using the composite lance or factors such as undetected late melt-ins (or cave-ins) or inhomogeneous bath conditions.